



This is to certify that the thesis entitled

A Study of the Pion-Nucleus Optical Potential

presented by

Karen Sue Stricker

has been accepted towards fulfillment of the requirements for

Ph.D. degree in Physics

Major professor

Date October 23, 1979

O-7639



RETURNING MATERIALS:
Place in book drop to remove this checkout from your record. FINES will be charged if book is returned after the date stamped below.

FEB 2 (2 200)	

A STUDY OF THE PION-NUCLEUS OPTICAL POTENTIAL

Ву

Karen Sue Stricker

A DISSERTATION

Submitted to
Michigan State University
in partial fulfillment of the requirements
for the degree of

DOCTOR OF PHILOSOPHY

Department of Physics

1979

ABSTRACT

A STUDY OF THE PION-NUCLEUS OPTICAL POTENTIAL

By

Karen Sue Stricker

The optical potential model is a convenient means of characterizing the interaction of the pion with the nucleus. Its simplicity makes it practical for the calculation of elastic scattering and pion distorted waves for more complicated processes. Its success in reproducing the early pion data and the existence of new, higher quality data motivate the present investigation.

An optical potential for pion-nucleus interactions in the energy range 0-250 MeV pion kinetic energies is constructed with the Watson multiple scattering series and the πN transition amplitude as starting point. The pion-nucleon to pion-nucleus center of mass transformation is calculated to first order in the ratio of total pion energy to nucleon mass. Multiple scattering corrections in low energy approximation are included to second order in the s-wave and to all orders in the p-wave (the Lorentz-Lorenz or Ericson-Ericson effect). True pion absorption terms, proportional to the square of the nuclear density, are included in both s and p-wave parts of the potential. Pauli blocking is approximated, and an energy shift due to the Coulomb interaction is incorporated.

The potential parameters are taken from the experimental πN phase shifts and theoretical calculations. The potential, of Kisslinger type, is incorporated in coordinate space computer codes which calculate pionic atom level shifts and widths, elastic scattering differential cross sections, and total and partial cross sections. These calculations are compared to the current experimental data. It is found that at low energies (0-50 MeV) the potential produces elastic cross sections which fit the data provided the s-wave repulsion is increased. The pionic atom level data require more absorptive strength than that given by current calculations, as well as increased repulsion consistent with the scattering results. The general features of the resonance region elastic scattering and total cross sections are well reproduced.

ACKNOWLEDGMENTS

My thesis advisor, Professor Hugh McManus, deserves much credit and many thanks for his constant guidance and encouragement throughout this work. I also wish to thank James A. Carr, whose research on a related thesis topic afforded numerous opportunities for productive collaboration, and Professor Dan O. Riska, for many helpful discussions. The various experimental groups whose data are included in this work were most generous in providing their results prior to publication. I am also indebted to several other theorists in the field of pion physics who freely shared their ideas and calculations.

Most of the computations for this thesis were performed on the MSU Cyclotron Laboratory computer, the staff of which gave much valuable assistance. The MSU Physics Department provided time on the main University computer for some of these calculations. I also wish to acknowledge the dedicated, courageous, and expert typing of the rough draft by Mrs. Shari Conroy and the final copy by Mrs. Carol Cole.

Finally, I am pleased to acknowledge my parents, whose support and encouragement were invaluable through my academic life, and my friends at MSU, whose concern and cheerful camaraderie smoothed many rough spots. To Daniel Bauer especially I owe more than I can say for a friendship which has become something much greater.

TABLE OF CONTENTS

							Page
LIST	OF T	ABLES	•	•		•	V
LIST	OF F	IGURES		•	•		vi
Chapt	ter						
I.	INT	RODUCTION					1
II.	THE	FIRST ORDER OPTICAL POTENTIAL		•			9
	1. 2. 3. 4.	The Pion-Nucleon Interaction	•	•	•	•	9 15 19 26
III.	THE	FULL OPTICAL POTENTIAL	•		•	•	31
	1. 2. 3. 4. 5.	Kinematics	•	•	•	•	32 45 61 77 83
IV.	PIO	NIC ATOM LEVELS		•	•	•	87
	1. 2. 3.	General Features					88 91 93
٧.	ELA	STIC SCATTERING CROSS SECTIONS	•		•		102
	1. 2. 3. 4. 5.	General FeaturesLow Energy Scattering General FeaturesResonance Region Scattering Details of the Calculations CalculationsLow Energy Region	•	•	•	•	103 109 112 114 133

Chapt	ter	Page
VI.	TOTAL AND PARTIAL CROSS SECTIONS	147
	1. Extraction of Total Cross Sections and Scattering Amplitudes	148
	2. Total Cross Section and Scattering Amplitude	
	Calculations	153
	Sections	156 167
VII.	CONCLUSIONS	173
Apper	ndix	
Α.	THE PION-NUCLEON SCATTERING AMPLITUDE	178
В.	DETAILS OF THE DERIVATION OF THE MULTIPLE SCATTERING	100
	SERIES	183
С.	INTEGRATION OVER NUCLEON MOMENTA	187
D.	RELATIVISTIC POTENTIAL THEORY	200
LIST	OF REFERENCES	206

LIST OF TABLES

Tabl	e	Page
1.	Symbols used throughout this work and their interpretation	8
2.	The Coulomb energy shift E_{ζ} , evaluated at the nuclear surface, for various nuclei	82
3.	The forms and parameters of the matter and charge density distributions for various nuclei	86
4.	Experimental pionic atom energy level shifts and widths in keV from Refs. 59 and 60	89
5.	Parameters used in the pionic atom calculations	99
6.	Parameters used in the low energy elastic scattering calculations	116

LIST OF FIGURES

Figure		Page
1.	The quantities w_i and w_{ij} as a function of pion lab kinetic energy	12
2.	The optical potential parameters b_0 , b_1 , c_0 , and c_1 as a function of pion lab kinetic energy	13
3.	Comparison of calculations with the Kisslinger (solid curve) and Laplacian (dashed curve) optical potentials .	35
4.	Comparison of calculations with no kinematic corrections (dashed curve), full kinematics (solid curve), and alternative choices for the kinematic corrections (dotted and dot-dashed curves)	46
5.	The integral I as a function of pion lab kinetic energy, and the approximation $Im(I) = k_0 \dots \dots$	51
6.	The first order s-wave optical potential parameter b_0 , and the same parameter but with the second order correction included, \overline{b}_0 , as a function of pion lab kinetic energy	52
7.	The effect of the second order s-wave term (solid curve) compared to calculations with the first order term only (dashed curve) and with the second order term in zero energy approximation (dotted curve)	54
8.	The parameter c' compared to the first order p-wave parameter \mathbf{c}_0 as a function of pion lab kinetic energy .	59
9.	The effect of the Ericson-Ericson correction to the p-wave, λ = 1.6 (solid curve) and λ = 1.0 (dotted curve), compared to calculations with no correction (dashed curve) and with the correction included to second order only, λ = 1 (dash-dotted curve)	60
10.	The effect of the c' term (solid curve) compared to calculations without this term (dashed curve)	62
11.	Diagrams of the s and p-wave processes included in the calculation (50) of the absorption parameters	71

Figure		Page
12.	The absorptive parameters ${\bf B}_0$ and ${\bf C}_0$ as a function of pion lab kinetic energy	74
13.	The effect of the absorption terms (solid curve) compared to calculations without these terms (dashed curve) and with the absorption terms included to first order only (dotted curve)	76
14.	The Pauli factor Q as a function of pion lab kinetic energy	79
15.	Comparison of calculations with (solid curve) and without (dashed curve) Pauli corrections	80
16.	Comparison of calculations of π^+ and π^- scattering on 160 and ^{208}Pb at 162 MeV with (solid curve) and without (dashed curve) the Coulomb shift. The references for the π^- data are the same as for the corresponding π^+ data	84
17a.	Calculations of the s-wave shift as a function of Z compared to the experimental data, with the parameters of set 1 of Table 5 with λ = 1 (dashed line), λ = 1.6 (dotted line), and with the parameters of set 2 (solid line). Data are from Ref. 59	94
17b.	Calculations of the s-wave width. Data are from Ref. 59	95
17c.	Calculations of the p-wave shift. Data are from Ref. 60	96
17d.	Calculations of the p-wave width. Data are from Ref. 60	97
18.	Amplitudes and corresponding cross sections for the first order real optical potential in Born approximation. The vertical scales are arbitrary	106
19.	Elastic scattering cross sections for 50 MeV π^+ on 12 C with (a) the full Born amplitude and (b) the full optical model calculation, for Re(\overline{b}_0) = 0., -0.04 fm, -0.08 fm, and -0.12 fm	107
20.	Elastic scattering cross sections for 50 MeV π^- on ^{12}C with curves same as in previous figure	108
21.	Comparison of black disk model calculation (dashed curve) and full optical potential calculation (solid curve) for π^+ and π^- scattering from 160 and 208 Pb at 162 MeV	111
	TOT LICE	111

Figure		Page
22a.	Elastic scattering of π^+ from 12 C at 30, 40, and 50 MeV with the optical potential parameters of set 1 (dashed curves) and set 2 (solid curves). Data are from Refs. 32 (diamonds), 34, 69, 70 (triangles), and 68 (circles)	117
22b.	Elastic scattering of π^+ from 16 O. Data from Refs. 32 (diamonds), and 33, 34, and 69 (triangles)	118
22c.	Elastic scattering of π^+ from 40 Ca. Data from Refs. 34, 69	119
22d.	Elastic scattering of π^+ from 90 Zr. Data from Refs. 34, 69	120
22e.	Elastic scattering of π^+ from ²⁰⁸ Pb. Data from Refs. 34, 69	121
22f.	Elastic scattering of π^- from ^{12}C and ^{208}Pb at 30 MeV. Data from Refs. 71 and 72	122
23a.	Elastic scattering of π^+ from ^{12}C at 30, 40, and 50 MeV, with the optical potential parameters from set 2 of Table 5 (solid curves), set 3 of Table 6 (dotted curves), and set 3 but with $\text{Im}(B_0)$ and $\text{Im}(C_0)$ from set 2 of Table 5 (dashed curves)	124
23b.	Elastic scattering of π^+ from $^{16}0$	125
23c.	Elastic scattering of π^+ from ^{40}Ca	126
23d.	Elastic scattering of π^+ from ^{90}Zr	127
23e.	Elastic scattering of π^+ from ^{208}Pb	128
23f.	Elastic scattering of π^- from ^{12}C and ^{208}Pb at 30 MeV .	129
24.	Comparison of elastic scattering calculations for π^+ on ^{12}C with two values of Re(B ₀) (solid and dashed curves) and a series of values for Re(b_0)	132
25a.	Elastic scattering of π^+ and π^- from 16 O. Optical potential parameters are taken from the RSL phase shifts and Riska calculations with $\lambda = 1.6$ (solid curves) and $\lambda = 1.0$ (dashed curves). Also shown are first order Kisslinger potential calculations (dotted curves). Data are from Refs. 35, 74	135

igure		Page
25b.	Elastic scattering of π^+ and π^- from 40 Ca. Data are from Ref. 35	136
25c.	Elastic scattering of π^+ and π^- from ^{208}Pb . Data are from Refs. 36 (162 MeV) and 75 (all other energies)	137
26.	Imaginary absorption parameters extrapolated from pionic atom values (dashed curves) compared to those of Ref. 50 (solid curves)	141
27a.	Elastic scattering of π^+ and π^- from 16 O. Absorption parameters are taken from Ref. 50 (solid curves) and extrapolated from pionic atom values (dashed curves) with other parameters from the RSL phase shifts and $\lambda = 1.6$	143
27b.	Elastic scattering from ⁴⁰ Ca	144
	Elastic scattering from ²⁰⁸ Pb	145
28.	Total cross section calculations using the absorption parameters of Ref. 50 (solid curves) and extrapolated pionic atom parameters (dashed curves) compared to the data of Carroll et al. (78)	155
29a.	The amplitude $\frac{4\pi}{k}$ Re[f _N (0)] for π^+ (circles) and π^- (x's) on ²⁷ Al, as a function of energy. Curves are same as in Figure 28. Data are from Jeppeson et al. (79)	157
29b.	The amplitude $\frac{4\pi}{k}$ Im[f _N (0)] for π^+ and π^- on ²⁷ Al	158
30a.	The amplitude $\frac{4\pi}{k}$ Re[f _N (0)] for π^+ and π^- on ²⁰⁸ Pb. Curves are same as in Figure 28. Data are from Ref. 79	159
30b.	The amplitude $\frac{4\pi}{k}$ Im[f _N (0)] for π^+ and π^- on ²⁰⁸ Pb	160
31a.	The amplitude $\frac{4\pi}{k}$ Re[f _N (0)] for π^+ and π^- as a function of A at 165 MeV. Curves are same as in Figure 28. Data are from Ref. 79	161
31b.	The amplitude $\frac{4\pi}{k}$ Im[f _N (0)] as a function of A	162
32.	Partial cross section calculations for π^+ on ^{12}C as a function of energy compared to the data of Navon et al. (81). Curves are same as in Figure 28	169
33.	Partial cross section calculations as a function of A for π^+ at 165 MeV, compared to the data of Ref. 81. Curves are same as in Figure 28	171

CHAPTER I

INTRODUCTION

In the past few years the field of pion-nucleus interactions has advanced rapidly. A large amount of excellent quality data has come out of the intermediate energy laboratories; LAMPF at Los Alamos, New Mexico, USA; TRIUMF in Vancouver, Canada; and SIN in Switzerland. This data includes not only elastic and inelastic differential cross sections, but also total and partial cross sections and single and double charge exchange measurements as well as more complicated reactions. Much progress has also been made in the theoretical description of the pion-nucleus interaction, with characterizations which vary from the phenomenological to the fundamental and microscopic. The present work will focus on the optical potential model, which takes a middle ground between these two approaches and has had a fair amount of success in the description of the early pion-nucleus data.

The concept of an optical potential, that is, a complex potential describing the interaction between the projectile and the nucleus as a whole, and in which the imaginary part accounts for flux lost to other channels from the elastic channel, is due to Bethe (1). An optical model for scattering of high energy particles by nuclei was first introduced by Fernbach, Serber, and Taylor (2) to describe

the scattering of 90 MeV neutrons. They proposed a constant complex potential inside the nucleus, the imaginary part of which can be related to the mean free path λ of the nucleon in nuclear matter (3),

$$Im(U_{opt}) = \frac{k_0}{2M} \frac{1}{\lambda} , \qquad (I-1)$$

where \mathbf{k}_0 is the particle momentum and M its mass. The mean free path can, in turn, be expressed in terms of the total collision cross section and the nuclear density,

$$\frac{1}{\lambda} = \sigma_{\mathsf{T}} \rho \quad . \tag{I-2}$$

The optical model was first applied to low energy scattering by Feshbach, Porter, and Weisskopf (4) in the analysis of resonances in 0-3 MeV neutron total cross sections. A theoretical basis for the optical model was provided by Watson (5), who derived the optical potential from a multiple scattering theory. A simplification of the theory, due to the antisymmetry of the target states, was given by Kerman, McManus, and Thaler (6).

The study of the pion-nucleus interaction began with the discovery of the pion in 1947, since early pion experiments usually involved nuclear targets in cloud chambers and emulsions. An optical model for pion-nucleus elastic scattering which included both s- and p-wave terms was first given by Kisslinger (7), and used in the analysis of differential cross section data (8) for 62 MeV π^+ and π^-

on ¹²C. The analysis of the measured energy shifts and widths of pionic atoms made clear the necessity of including higher order terms in the optical potential. The inclusion of true pion absorption terms, first suggested by Brueckner (9), and the calculation of the Lorentz-Lorenz effect were made by Ericson and Ericson (10) and greatly improved the agreement between calculated and measured levels.

The emphasis shifted to the resonance region with the appearance of $\pi^{-12}C$ elastic scattering cross sections at 120, 200, and 280 MeV from CERN (11), followed by data on other nuclei. Although the Kisslinger potential was originally derived for low energy scattering, it was found to give reasonable results in the resonance region also (12). A local optical potential form, the Laplacian model, gave similar results for scattering near resonance (13). Glauber theory (14) was also successfully applied to scattering data in this region (15).

Very little was known of the low energy (0-50 MeV) pion scattering cross sections, and few calculations beyond first order existed for these energies (16) until about 1975, when more accurate data of 50 MeV π^+ elastic scattering from ^{12}C appeared (17). Thies (18) showed that the inclusion of kinematic effects, higher order multiple scattering terms, and s-wave absorption greatly improved the agreement between the calculated and measured cross sections.

Since 1975 the theoretical activity in pion-nucleus interactions has been intense. The most successful microscopic calculations have been the isobar-hole calculations (19) which treat the dominant channel, with Δ_{33} intermediate states, by means of a spreading potential, the parameters of which are fitted to the data. The phenomenological input is small, and the results are encouraging; however, calculations for nuclei larger than 16 0 are impractical.

The phenomenological optical model has also received a great deal of attention. It has been shown (20) that a first order Kisslinger potential with four free parameters can be fitted to the elastic scattering data for pion kinetic energies around 50 MeV. Four parameters are also sufficient to describe the pionic atom data for a wide range of nuclei (21). The elastic scattering cross sections in the resonance region can also be fit by optical model calculations, requiring, however, a somewhat more sophisticated potential with more than four parameters (22).

The phenomenological approach, although successful in describing various classes of data, has almost no predictive power and is most unsatisfying to a theorist. The microscopic theories have a strong theoretical base and a minimum of approximations but are extremely complicated, tedious calculations and have been made for only a few light nuclei at a few energies. Thus the need at present for a simpler approach based on theoretical considerations but with a simple optical potential form. Such a model, if carefully constructed, should be valid over a fairly wide energy range, say

0-250 MeV, and for all nuclei large enough to justify the optical model assumptions, certainly carbon and all heavier nuclei. The theoretical basis gives the model predictive power; its simplicity makes it a useful tool in calculations of more complicated processes. The important physical content of the theory appears in the optical potential in a straightforward way, not buried in vast computer calculations, giving a feel for the important features of the problem. It is to be hoped that the microscopic calculations will eventually become sufficiently tractable and accurate to be applicable to most nuclei and energies. However, an optical potential type model, taking input from the more sophisticated theories with suitable approximations, will almost certainly be the basis of most practical calculations.

The early work on theoretically based optical potentials by the Ericsons (10) and Thies (18) has already been mentioned. Pieces of the problem have been much discussed by various authors. A review of all such research will not be attempted in this brief introduction; the interested reader is referred to the proceedings of the several recent pion conferences (23). The purpose of this dissertation is to bring together all aspects of the problem in a coherent framework, to construct an optical potential with a broad range of validity. The form chosen for the potential is a coordinate space form of Kisslinger type, local in the sense of depending on only one pion coordinate. Previous investigations suggest that the essential physics survives the approximations necessary to obtain

such a form, which is chosen for its simplicity. The more important test of the validity of the theory is, of course, the accuracy with which it predicts the experimental results, hence the inclusion in this work of calculations of pionic atom level shifts and widths, differential elastic scattering cross sections, and total and partial cross sections for a variety of nuclei and energies.

The reason usually given for the study of the pion-nucleus interaction is the hope that the pion can be used as a probe of nuclear structure once the pion-nucleus dynamics are understood. The nature of the pion, with three isospin states and no spin, and the fact that pions can be absorbed on nucleons, make the pion a unique tool in, for example, the determination of neutron and proton distributions and perhaps the study of correlations between nucleons. There is a growing interest, however, in the pion-nucleus problem itself. The field of intermediate energy physics, of which pion physics is an important part, has become a meeting ground for the nonrelativistic many-body theories of low energy nuclear physics and the relativistic field theories developed in elementary particle physics. Although the present study does not delve deeply into these questions, the development of the potential indicates where these elements enter and provides a base for more detailed calculations. Any improvements to the optical potential model discussed here will almost certainly involve a more careful synthesis of these two aspects of the problem.

The dissertation is divided into six main parts. In the first of these, Chapter II, the information is presented which forms the basis of the optical potential theory: the pion-nucleon interaction, the form of the pion wave equation, and the multiple scattering formalism. From these the first order Kisslinger optical potential is constructed. In Chapter III, the optical potential is refined with the addition of kinematic effects, multiple scattering corrections, true absorption terms, and Pauli and Coulomb effects. This completes the construction of the optical potential; the comparisons to data are discussed in the following three chapters. The first of these, Chapter IV, is a discussion of the optical potential applied to the analysis of pionic atom shifts and widths. Chapter V presents the calculations of elastic differential cross sections, compared to a selection of the available data. In Chapter VI a discussion is given of the calculation of total and partial cross sections, with the results compared to the data. In Chapters V and VI, two different approaches are taken to the choice of parameters for the optical potential. The first is to adopt the parameters as calculated theoretically in the earlier chapters. The second is to extrapolate by simple means the information gained from the pionic atom analysis discussed in Chapter IV to non-zero energies, extending the work of reference 24. The major conclusions of this work are discussed in the final chapter.

The symbols used for some common quantities are given in Table 1. These will be used throughout, unless otherwise noted.

Table 1. Symbols used throughout this work and their interpretation.

Symbol	Meaning	
(κ,ω)	Momentum and energy of incoming pion	
(κ',ω')	Momentum and energy of outgoing pion	
(p,E)	Momentum and energy of incoming nucleon	
(p̞',E')	Momentum and energy of outgoing nucleon	
(P,E _A)	Momentum and energy of incoming nucleus	
m	Mass of pion	
M	Mass of nucleon	
MA	Mass of nucleus	
ţ	Isospin operator for pion	
τ	Isospin operator for nucleon	
σ	Spin operator for nucleon	
cm subscript	Quantities in pion-nucleon center of mass	
2cm subscript	Quantities in pion-two nucleon center of mass	
no subscript	Quantities in pion-nucleus center of mass (Subscripts are often dropped when only one frame is being considered.)	

CHAPTER II

THE FIRST ORDER OPTICAL POTENTIAL

The optical model provides a method by which the pion-nucleus many body problem can be reduced to a one particle equation for the pion, interacting with an optical potential which describes the nucleus. The optical potential can be derived from knowledge of the measured pion-nucleon scattering amplitude and a multiple scattering formalism which relates the pion-nucleon amplitude to the pion-nucleus interaction. In Section 1 of this chapter the pion-nucleon interaction is described. The pion wave equation is discussed in Section 2. The development of the multiple scattering series for the optical potential is given in Section 3, and the first order coordinate space optical potential is given in Section 4.

1. The Pion-Nucleon Interaction

The most prominent feature of pion-nucleon scattering in the energy region 0-300 MeV pion lab kinetic energy is the effect of the πN resonance, denoted Δ_{33} , at 1236 MeV total center of mass energy or about 180 MeV pion kinetic energy. The subscripts 33 refer to the isospin and total angular momentum of the resonance, both of which have the value 3/2. The orbital angular momentum of the state is L = 1. This channel dominates the πN interaction

at these energies, giving rise to a large p-wave term in the scattering amplitude.

The most general scattering amplitude for this problem can be expanded in orbital angular momentum, isospin, and total angular momentum. The s- and p-wave terms of this expansion are

$$f_{\pi N} = (b_0 + b_1 t \cdot \tau) + (c_0 + c_1 t \cdot \tau) k_{cm} \cdot k'_{cm}$$

$$+ (s_0 + s_1 t \cdot \tau) \sigma \cdot (k_{cm} \times k'_{cm}) . \qquad (II-1)$$

The relationships between the coefficients b_i , c_i , and s_i and the measured pion-nucleon phase shifts are derived in Appendix A, and are given by

$$b_{0} = \frac{1}{k_{cm}} \frac{1}{3} (2w_{3} + w_{1})$$

$$b_{1} = \frac{1}{k_{cm}} \frac{1}{3} (w_{3} - w_{1})$$

$$c_{0} = \frac{1}{k_{cm}^{3}} \frac{1}{3} (4w_{33} + 2w_{31} + 2w_{13} + w_{11})$$

$$c_{1} = \frac{1}{k_{cm}^{3}} \frac{1}{3} (2w_{33} + w_{31} - 2w_{13} - w_{11})$$

$$s_{0} = \frac{1}{k_{cm}^{3}} \frac{1}{3} (2w_{33} - 2w_{31} + w_{13} - w_{11})$$

$$s_{1} = \frac{1}{k_{cm}^{3}} \frac{1}{3} (w_{33} - w_{31} - w_{13} + w_{11})$$

$$(II-2)$$

The $\mathbf{w_i}$ and $\mathbf{w_{i\,j}}$ are related to the $\mathbf{\alpha_{2I,2J}}$ of Appendix A by

$$w_{i} = k_{cm}^{0} \alpha_{i1}^{0}$$

$$w_{ij} = k_{cm}^{1} \alpha_{ij}^{1}$$
(II-3)

where

$$\alpha_{2I,2J}^{L} = \frac{\exp(2i\delta_{2I,2J}^{L}) - 1}{2i k_{cm}}$$
 (II-4)

Here I, L, and J are respectively the isospin, orbital angular momentum, and total angular momentum of the system.

The first two terms of equation II-1, referred to as the sand p-wave terms, are the most important terms for the calculation
of pion-nucleus scattering. The third term, also a p-wave term,
is usually negligible for pion-nucleus calculations since the nucleon
spin is summed over, and will not be discussed further. The d-wave
and higher partial waves do not contribute appreciably until energies well above resonance.

The w_i and w_{ij} and the s- and p-wave parameters are shown in Figures 1 and 2, as a function of pion lab kinetic energy T_{π} . They are computed from the parametrization of the π -nucleon phase shifts given by Rowe, Salomon, and Landau (25), in which an analytic function of energy is fitted to the quantity $k_{cm}^{-(2L+1)} \tan \delta_{2I,2J}^{L}$. over the energy range 0-400 MeV. The advantage of such a parametrization is that the scattering parameters derived from it vary

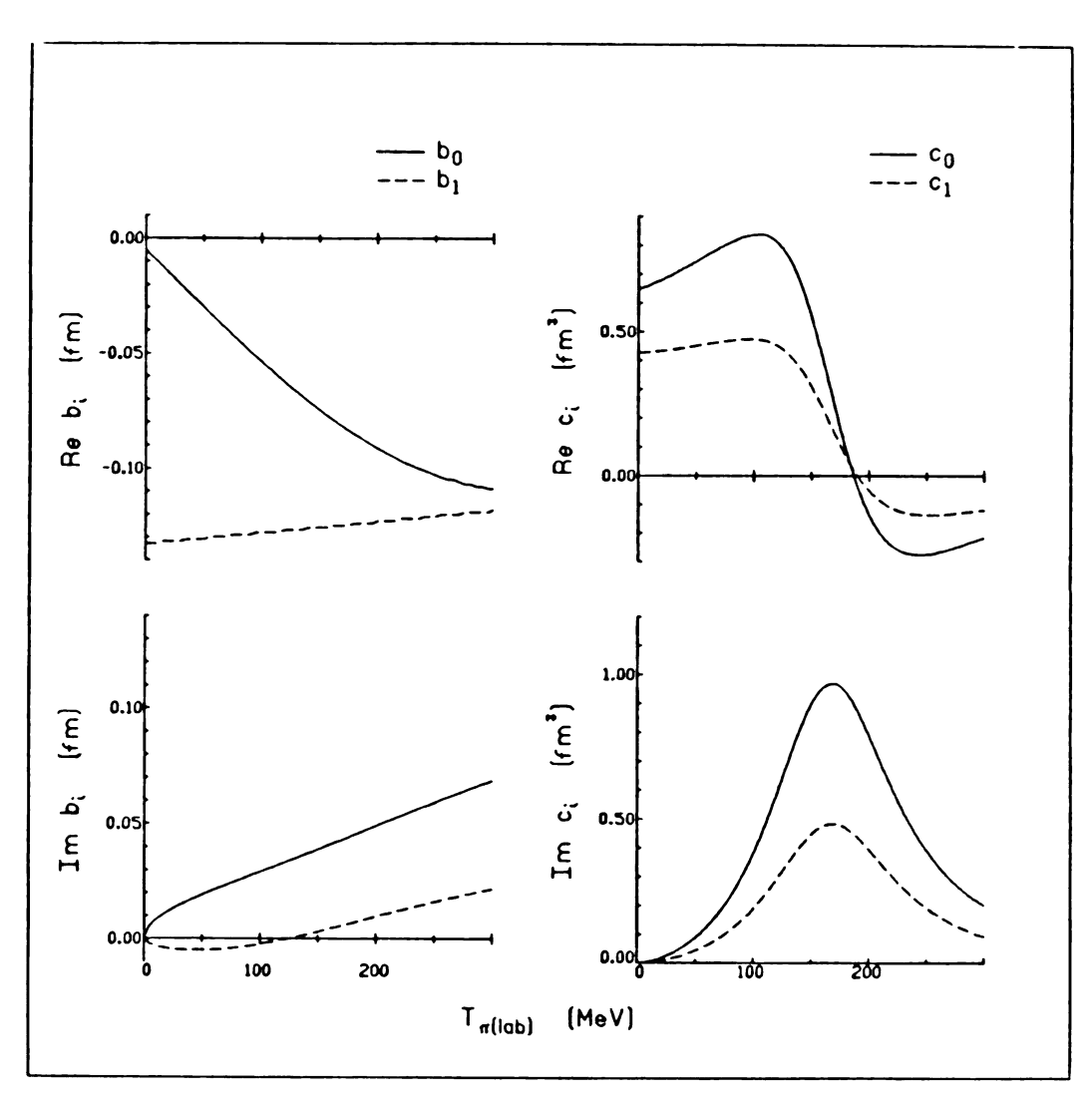


Figure 1. The quantities $\mathbf{w_i}$ and $\mathbf{w_{ij}}$ as a function of pion lab kinetic energy.

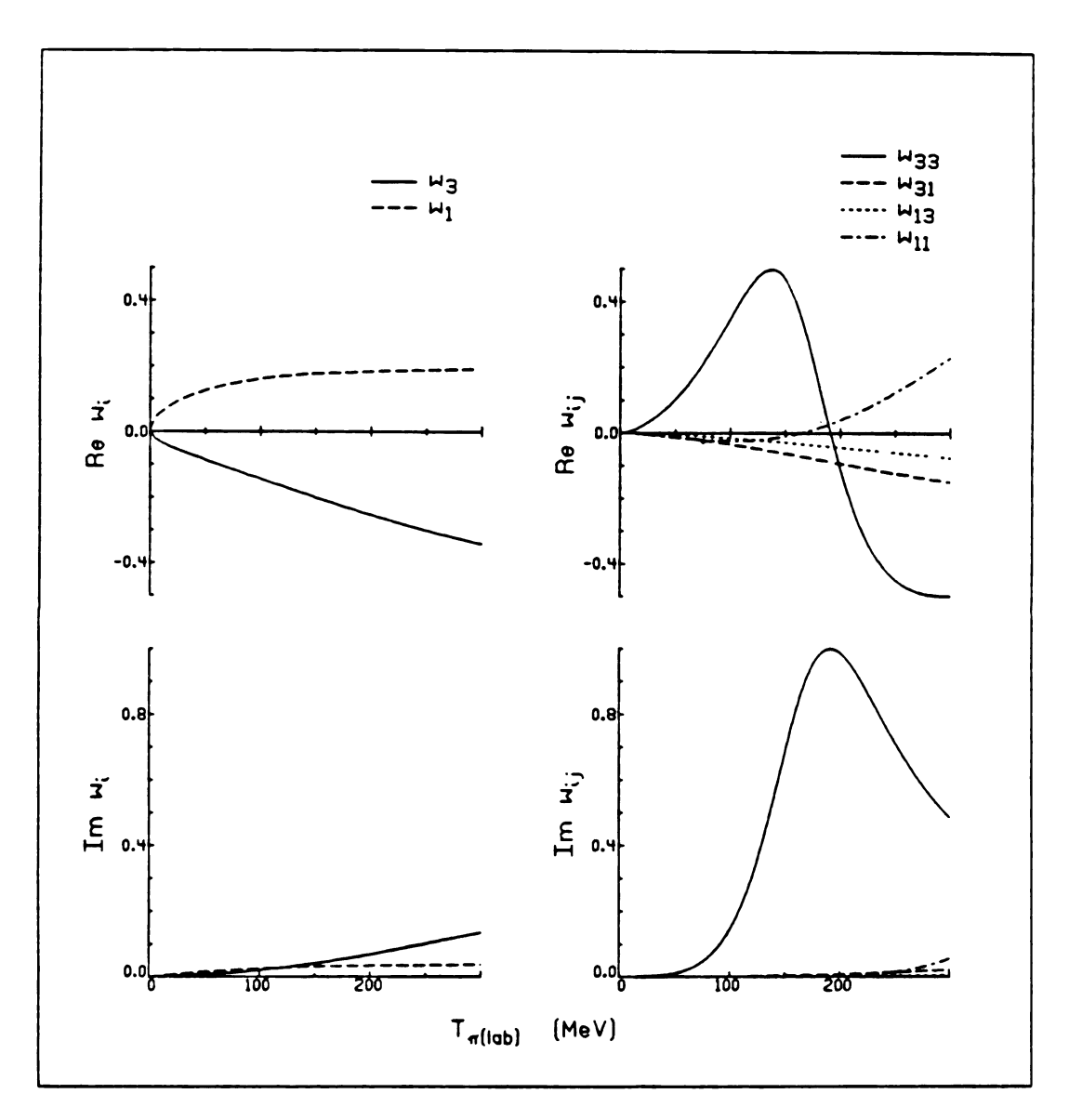


Figure 2. The optical potential parameters b_0 , b_1 , c_0 , and c_1 as a function of pion lab kinetic energy.

smoothly with energy, even at low energies, whereas the scattering parameters calculated directly from phase shifts, even those that have been smoothed, such as the CERN Theoretical set (26), are quite noisy below about 80 MeV.

Several things may be noted. Although the phase shifts $\delta^L_{2I,2J}$ are purely real below the threshold for pion production, ω_{cm} + E_{cm} = 2m + M, the scattering parameters are not; the imaginary parts are zero only at zero pion kinetic energy. The real part of the isoscalar s-wave parameter b_0 is negative in this energy region, corresponding to a repulsive s-wave interaction, and is nearly zero at low energies due to a near cancellation of the two terms w_1 and $2w_3$. The p-wave parameters c_0 and c_1 are dominated by the δ^1_{33} phase shift and display characteristic resonant behavior, the real part crossing zero at the resonance energy and the imaginary part reaching a maximum at this point. The parameter $Re(c_0)$ is positive below resonance, hence an attractive p-wave interaction in this region.

The quantity required for the pion-nucleus calculations is the pion-nucleon transition amplitude $t^{\pi N}$. This is related to the pion-nucleon potential v by a Lippmann-Schwinger type equation,

$$t^{\pi N} = v + v2\overline{\omega}_{cm}g^{0}t^{\pi N} , \qquad (II-5)$$

where $\mathbf{g}^{\mathbf{0}}$ is the propagator for a free pion; in momentum space

$$g^0 = \frac{1}{-k^2 + k_0^2 + i\varepsilon}$$
 (II-6)

The factor $2\overline{\omega}_{\rm cm}$, where $\overline{\omega}_{\rm cm}$ is the relativistic equivalent of the reduced mass

$$\overline{\omega}_{\rm cm} = \frac{\omega_{\rm cm}^{\rm E}_{\rm cm}}{\omega_{\rm cm} + E_{\rm cm}} , \qquad (II-7)$$

is a result of the use of the Klein-Gordon equation rather than the Schrödinger equation for the pion. This point will be considered in more detail in the discussion of the pion-nucleus scattering equation. Matrix elements of $\mathbf{t}_{\pi N}$ between momentum states of the pion and nucleon can be written

$$\langle \underline{k}', \underline{p}' | \underline{t}^{\pi N} | \underline{k}, \underline{p} \rangle = (2\pi)^3 \delta(\underline{k} + \underline{p} - \underline{k}' - \underline{p}') \underline{t}^{\pi N} (\underline{k}_{cm}, \underline{k}'_{cm})$$
 (II-8)

The transition amplitude and scattering amplitude can then be shown (27) to be related in the πN center of mass by

$$t^{\pi N}(k_{cm},k_{cm}') = -\frac{4\pi}{2\overline{\omega}_{cm}} f_{\pi N}(k_{cm},k_{cm}')$$
 (II-9)

Thus, the required pion-nucleon T-matrix is related in a simple way to the experimental phase shifts.

2. The Pion Wave Equation

Before discussing the multiple scattering series expansion for the optical potential, it is necessary to consider what form the wave equation for the pion will take. The nucleus is quite massive and can be treated nonrelativistically. However, the rest mass of the pion is not large compared to its momentum at the energies considered here and must be treated relativistically. Thus, the Hamiltonian for the system must include rest masses and can be written

$$H = (k^2 + m^2)^{\frac{1}{2}} + M_A + \frac{P^2}{2M_A} + V$$
 (II-10)

where $\frac{P}{c}$ and $\frac{M}{A}$ are the momentum and mass of the nucleus, and V characterizes the interaction between the nucleons in the target and the pion. The part of the Hamiltonian which describes the internal dynamics of the nucleus has been neglected, assuming that the excitation energies of the various nuclear states do not play an important role. The Schrödinger equation for the system is then

$$[(k^2 + m^2)^{\frac{1}{2}} + M_A + \frac{p^2}{2M_A} + V]\Psi = E_T\Psi$$
 (II-11)

Goldberger and Watson (27) have shown that for |V| << m and $\frac{|\nabla V|}{|V|} << k_0$ $\equiv (\omega^2 - m^2)^{\frac{1}{2}}$, this equation is equivalent to a Klein-Gordon-like equation for Ψ ,

$$(k^2 + m^2)\Psi = (E_T - V - M_A - \frac{P^2}{2M_A})^2\Psi$$
 (II-12)

In the pion-nucleus center of mass system

$$k^2 = P^2 \tag{II-13}$$

and equation II-12 can be written

$$[k^{2}(1 + \frac{E_{T} - M_{A}}{M_{A}}) + m^{2}]\Psi = (E_{T} - M_{A} - V)^{2}\Psi$$
 (II-14)

where the terms $(\frac{P^2}{2M_A}V)$ and $(\frac{P^2}{2M_A})^2$ have been dropped. Replacing k^2 by $-\nabla^2$ and rearranging gives

$$\{\nabla^2 + [(E_T - M_A)^2 - m^2] \frac{M_A}{E_T} - 2(E_T - M_A) \frac{M_A}{E_T} V + \frac{M_A}{E_T} V^2\} \Psi = 0$$
(II-15)

The quantity $(E_T - M_A)$ can be evaluated by considering the pion far from the nucleus, in which case the total energy of the system is

$$E_{T} = \omega + M_{A} + \frac{k_{0}^{2}}{2M_{A}}. \qquad (II-16)$$

Thus, equation II-15 can be written

$$(\nabla^2 + k_0^2 - 2\overline{\omega} V + \frac{\overline{\omega}}{\omega} V^2)\Psi = 0$$
 (II-17)

where $\overline{\omega}$ is the reduced energy for the pion-nucleus system,

$$\overline{\omega} = \frac{\omega E_{A}}{\omega + E_{A}}. \qquad (II-18)$$

A similar equation can be written for the bound state case, but with k_0^2 replaced by $-\kappa^2$. It is seen that equation II-17 is very similar

to the usual Schrödinger equation but with (-2mV) replaced by $(-2\overline{\omega}V + \frac{\overline{\omega}}{\omega}V^2)$.

Because the potential V depends on the coordinates of the nucleons as well as the pion, $V = V(r_1, r_2, ... r_A; r)$, equation II-17 is still an A + 1 particle equation. The formalism and approximations required to reduce this to a one-body equation for the pion are discussed in the next section. Some simplification can be made at this point by dividing the pion-nucleus potential into two components,

$$V = V_S + V_{EM} . (II-19)$$

The potential V_{EM} , describing the electromagnetic interaction between the pion and various nucleons, can be approximated by the Coulomb potential V_C due to a smooth charge distribution corresponding to the measured proton distribution of a given nucleus. With this approximation $V_{EM} = V_C(r)$ depends only on the pion coordinate measured relative to the nuclear center. The strong potential V_S is assumed to be of the form

$$V_{S} = \sum_{i} v_{i}(r_{i}, r)$$
 (II-20)

with \underline{r}_i the coordinate of the ith nucleon, \underline{r} that of the pion. Note that \mathbf{v}_i is just the strong part of the potential \mathbf{v} of equation II-5.

The strategy of the next section will be to ignore the Coulomb potential and manipulate the wave equation with potential $V = V_S$ in such a way that the nucleon coordinates can be integrated out. The resulting potential, known as the optical potential, can then be put in a wave equation for the pion that includes the Coulomb potential. This procedure is an approximation, the effect of which is discussed in a later section.

One more approximation is made at this point; the V_SV_C and V_S^2 parts of V^2 are dropped as they are small compared to the ωV_C and ωV_S terms. Then equation II-17 becomes

$$(-k^2 + k_0^2 - 2\overline{\omega}V_S - 2\overline{\omega}V_C + \frac{\overline{\omega}}{\omega}V_C^2)\Psi = 0$$
 (II-21)

where, in preparation for the calculations of the next section, the momentum space form has been given.

3. The Multiple Scattering Series

The multiple scattering formalism (5) has as its starting point the Lippmann-Schwinger equation (28),

$$T = V + VG^{0}T, \qquad (II-22)$$

which is equivalent to the Schrödinger equation for a scattering problem. Here the Hamiltonian is given by

$$H = H_0 + V$$
, (II-23)

 $\boldsymbol{\mathsf{G}}^0$ is the propagator for the noninteracting pion-nucleus system,

$$G^{0} = \frac{1}{E - H_{0} + i\varepsilon}, \qquad (II-24)$$

and T, the transition matrix, is defined by

$$V\psi = T\phi , \qquad (II-25)$$

where ψ is the wavefunction which is the solution to the full Schrödinger equation,

$$H\psi = E\psi , \qquad (II-26)$$

and ϕ is the solution to the equation without interaction,

$$H_0 \Phi = E \Phi . \tag{II-27}$$

An equation similar to the Lippmann-Schwinger equation can be derived from equation II-17 by defining

$$\hat{V} = 2\overline{\omega}V_{S}$$

$$\hat{T} = 2\overline{\omega}T$$

$$\hat{G}^{0} = \frac{1}{-k^{2} + k_{O}^{2} + i\varepsilon}$$
(II-28)

Then equation II-17 can be written

$$\hat{T} = \hat{V} + \hat{V}\hat{G}^{0}\hat{T}$$
 (II-29)

and manipulated in the same way as the conventional Lippmann-Schwinger equation. Note that \hat{T} , \hat{V} , and \hat{G} are (A+1) particle operators. In this section equation II-29 will be rearranged in order to make use of the knowledge of the pion-nucleon T-matrix and in order to group all the largest terms together in such a way that the nucleon coordinates can be integrated over, reducing the problem to a one particle equation. By defining an optical potential which includes these largest terms and solving the corresponding wave equation, they can be treated exactly.

To derive the optical potential the infinite series implicit in the Lippmann-Schwinger equation,

$$\hat{T} = \hat{V} + \hat{V}\hat{G}^{0}\hat{V} + \hat{V}\hat{G}^{0}\hat{V}\hat{G}^{0}\hat{V} + \dots$$
 (11-30)

is rearranged in two ways. The derivation given here roughly follows that of Eisenberg (29).

The first rearrangement groups together all interactions which do not have the nuclear ground state as an intermediate state into the subseries

$$\hat{U} = \hat{V} + \hat{V}\hat{G}^{0}(1 - P_{0})\hat{V} + \hat{V}\hat{G}^{0}(1 - P_{0})\hat{V}\hat{G}^{0}(1 - P_{0})\hat{V} + \dots$$

$$= \hat{V} + \hat{V}\hat{G}^{0}(1 - P_{0})\hat{U}$$
(II-31)

where P_0 is the ground state projection operator |0><0|; $(1-P_0)$ projects onto all other states. It is to be hoped that the ground state expectation value of this series converges rapidly, since the matrix elements of V between the ground state and an excited state are assumed to be much smaller than the ground state to ground state matrix elements. Using the first result of Appendix B, equation II-29 can be written

$$\hat{T} = \hat{U} + \hat{U}\hat{G}^{0}P_{0}\hat{T} . \qquad (II-32)$$

This series contains all the large terms, i.e. those with ground state intermediate states, and therefore is not expected to converge rapidly. The ground state expectation value of equation II-32 gives

$$\hat{T}_{00} = \hat{U}_{00} + \hat{U}_{00} \hat{G}_{00}^{0} \hat{T}_{00}$$
 (II-33)

where

$$\hat{U}_{00} = \langle 0 | \hat{U} | 0 \rangle$$
, (II-34)

with similar definitions for \hat{T}_{00} and \hat{g}_{00}^0 . Note that \hat{g}^0 is diagonal in the nuclear states,

$$< n |\hat{G}^{0}|_{m}> = \hat{G}_{n}^{0} \delta_{mn}$$
 (II-35)

Equation II-33 is now a one particle equation for the pion and can be written as a Schrödinger-like equation with $\rm U_{00}$ as potential. Thus the problem can be solved "exactly" (by computer), if $\rm U_{00}$ is known.

The second rearrangement is motivated by the fact that the πN T-matrix, not the potential, is the quantity closely related to the experimental data. The terms in the expansion for \hat{U} which involve only the potential of the ith nucleon can be grouped together to define a quantity similar to the free $t_{\pi N}$ of equation II-5. Writing

$$\hat{\mathbf{U}} = \sum_{i} \hat{\mathbf{U}}_{i} \tag{II-36}$$

and noting that

$$\hat{V} = \sum_{i} \hat{v}_{i} , \qquad (II-37)$$

equation II-31 can be rewritten using the second result of Appendix B,

$$\hat{U} = \sum_{i} \hat{\tau}_{i} + \sum_{i} \sum_{j \neq i} \hat{\tau}_{i} \hat{G}^{0} (1 - P_{0}) \hat{\tau}_{j}$$

$$+ \sum_{i} \sum_{j \neq i} \sum_{k \neq j} \hat{\tau}_{i} \hat{G}^{0} (1 - P_{0}) \hat{\tau}_{j} \hat{G}^{0} (1 - P_{0}) \hat{\tau}_{k} + \dots$$
(II-38)

where τ_i is defined by

$$\hat{\tau}_{i} = \hat{v}_{i} + \hat{v}_{i} \hat{G}^{0} (1 - P_{0}) \hat{\tau}_{i} . \qquad (II-39)$$

In order to relate $\hat{\tau}_i$ to the free pion-nucleon T-matrix $t^{\pi N}$, define

$$\tau_{\mathbf{i}} = \frac{1}{2\omega} \hat{\tau}_{\mathbf{i}} \text{ and } \mathbf{v}_{\mathbf{i}} = \frac{1}{2\omega} \hat{\mathbf{v}}_{\mathbf{i}}$$
 (II-40)

Then

$$\tau_{i} = v_{i} + v_{i}[G^{0}(1 - P_{0})2\overline{\omega}]\tau_{i}$$
 (II-41)

The first result of Appendix B applied to equations II-41 and II-5 gives the relationship of τ_i and the free πN T-matrix for the ith nucleon $t_i^{\pi N}$,

$$\tau_i = t_i^{\pi N} + t_i^{\pi N} [G^0(1 - P_0)2\overline{\omega} - g^02\overline{\omega}_{cm}] \tau_i$$
 (II-42)

As was pointed out by Kerman, McManus, and Thaler (6), the antisymmetrization of the intermediate states can be exploited in order to simplify equation II-38 for \hat{U} . Let \mathbf{A} be a projection operator projecting onto completely antisymmetrized target states. Note that \mathbf{A} commutes with \mathbf{V} , \mathbf{P}_0 , and \mathbf{G}^0 since these are totally symmetric in the nucleon coordinates. Thus, assuming \mathbf{T} and \mathbf{U} will always be taken between properly antisymmetrized states, equations II-29 and II-31 can be written

$$\hat{T} = \hat{V} + \hat{V}\hat{G}^{0} \hat{A}\hat{T}$$
 (II-43)

$$\hat{U} = \hat{V} + \hat{V}\hat{G}^{0}(1 - P_{0})\hat{A}\hat{U}$$
 (II-44)

Equations II-38, II-39, II-41, and II-42 can be rederived with the operator Aincluded, yielding equations of the same form but with $\hat{\mathsf{G}}^0(1-\mathsf{P}_0)$ replaced by $\hat{\mathsf{G}}^0(1-\mathsf{P}_0)$ A. Note that the $\hat{\tau}_i$ thus defined are somewhat different than those defined in equation II-39. With this change the matrix elements of the $\hat{\tau}_i$ in the equivalent of equation II-38 are the same for all i, since with the antisymmetrization all nucleons are equivalent. Equation II-38 becomes

$$\hat{U} = A\hat{\tau}_{i} + A(A - 1)\hat{\tau}_{i}\hat{G}^{0}(1 - P_{0})\hat{A}\hat{\tau}_{j}$$

$$+ A(A - 1)^{2}\hat{\tau}_{i}\hat{G}^{0}(1 - P_{0})\hat{A}\hat{\tau}_{j}\hat{G}^{0}(1 - P_{0})\hat{A}\hat{\tau}_{k} + \dots$$
(II-45)

where i \neq j, j \neq k, and so on. The equation giving $\tau_{\textbf{i}}$ in terms of $t_{\textbf{i}}^{\pi N}$ is now

$$\tau_{i} = t_{i}^{\pi N} + t_{i}^{\pi N} [G^{0}(1 - P_{0})A2\overline{\omega} - g^{0}2\overline{\omega}_{cm}] \tau_{i}$$
 (II-46)

The difference between τ_i and $t_i^{\pi N}$ will be neglected; this is known as the impulse approximation (30).

The final result, equation II-45, is the multiple scattering series for \hat{U} . The first term describes the scattering to all orders from one nucleon, summed over all nucleons. The second term

describes scattering to all orders by one nucleon, propagation, and then scattering to all orders by a second nucleon. The third term describes three such scatterings, and so on. The optical potential is given by

$$2\overline{\omega}U_{\text{opt}} = \hat{U}_{00} \equiv \langle 0 | \hat{U} | 0 \rangle$$
 (II-47)

Writing equation II-33 in the form of a Schrödinger equation and including the Coulomb potential gives a wave equation much like equation II-17 but involving pion coordinates only,

$$(\nabla^2 + k_0^2 - 2\overline{\omega}) (U_{opt} + V_C) + \frac{\overline{\omega}}{\omega} V_C^2) \phi(r) = 0$$
 (II-48)

where ϕ is the pion wavefunction.

It is, of course, impossible to calculate all terms of the series for \hat{U} , equation II-45. However, the first two terms and a partial summation of the rest can be calculated if some approximations are made. This is the subject of the next chapter.

4. The Optical Potential--Simplest Assumptions

To see the general features of the pion-nucleus optical potential, it is useful to construct the first order potential, arising from the first term in equation II-45. The impulse approximation is made, and kinematic corrections due to the transformation of $\mathbf{t}^{\pi N}$ to the pion-nucleus center of mass, and to the difference between ω and $\overline{\omega}$, are ignored. Then

$$2\omega U_{\text{opt}}^{(1)} = A<0 |2\omega t_{i}^{\pi N}|0>$$
 (II-49)

which, by equations II-8 and II-9, is

$$2\omega U_{\text{opt}}^{(1)}(k,k') = A<0 | (2\pi)^{3} \delta(k + p_{1} - k' - p_{1}')(-4\pi) f_{\pi N}(k,k') | 0>$$
(II-50)

Here $|0\rangle$ represents $\psi_0(p_1,p_2...p_A)$ and $|0\rangle$ represents $\psi_0^*(p_1,p_2...p_A)$. The scattering amplitude $f_{\pi N}$ is given in equation II-1. Since $f_{\pi N}(k,k')$ is independent of the nucleon momenta in this approximation, equation C-10 of Appendix C can be used to write

$$2\omega U_{\text{opt}}^{(1)}(\mathbf{k},\mathbf{k}') = -4\pi A f_{\pi N}(\mathbf{k},\mathbf{k}')\rho(\mathbf{q})$$
 (II-51)

where $\rho(q)$ is the Fourier transform of the nuclear density $\rho(r)$, normalized to 1, and q is the momentum transfer, q = k' - k. Assuming a nucleus with N = Z and zero spin, isovector and spin dependent terms can be ignored, and the optical potential becomes

$$2\omega U_{\text{opt}}^{(1)}(k,k') = -4\pi A\{b_{0}\rho(q) + c_{0}\rho(q)k \cdot k'\}$$
 (II-52)

in momentum space or

$$2\omega U_{\text{opt}}^{(1)}(r) = -4\pi A\{b_0 \rho(r) - \nabla \cdot [c_0 \rho(r)] \nabla\}$$
 (II-53)

in coordinate space. The gradient operators act on all functions of \underline{r} to their right (see Appendix C). Equation II-53 is known as the Kisslinger potential (7). This is not the only choice for the form of $U_{opt}^{(1)}$, as will be discussed in the first section of Chapter III, but it is the form adopted in this work.

As might be expected, the Kisslinger potential has s-wave and p-wave parts which are respectively repulsive and attractive for energies below resonance. The imaginary parts of the potential reflect the flux lost from the elastic channel, which process is sometimes called absorption. However, it is important to make a distinction between this process, in which the pion is present in the final state with the nucleus in an excited state, and the process not included in the simple optical potential above, in which the pion is absorbed by the nucleus and does not reappear. The former process will be referred to as quasielastic, and the latter as true absorption. At zero pion kinetic energy there is no energy available for quasielastic processes, and the first order optical potential is purely real.

Due to the p-wave interaction the Kisslinger potential is "non-local" (more accurately, velocity dependent). The p-wave term acting on the pion wavefunction can be written

$$c_0 \nabla \cdot [\rho(r) \nabla \phi(r)] = c_0 [\nabla \rho(r)] \cdot [\nabla \phi(r)] + c_0 \rho(r) \nabla^2 \phi(r) . \qquad (II-54)$$

The first term contributes a surface peaked interaction. The second term is somewhat troublesome, as it has the same form as the kinetic

energy term but appears with opposite sign below resonance. The difficulty can be seen more clearly when the optical potential, equation II-53, is put in the wave equation II-48,

$$\{[1 - 4\pi c_0 \rho(r)] \nabla^2 + k_0^2 + 4\pi b_0 \rho(r) - 4\pi c_0 [\nabla \rho(r)] \cdot \nabla \nabla^2 - 2\omega V_C + V_C^2 \phi(r) = 0$$
(II-55)

When Re($4\pi c_0 \rho$) becomes greater than one, the $\nabla^2 \phi$ term changes sign, giving rise to an attractive "potential" in which an infinite number of bound states can exist, with the peculiar property that pion wavefunctions with more nodes correspond to more deeply bound pion states (31). The pion wavefunction can be shown to have a logarithmic singularity at the point where the $\nabla^2 \phi$ term changes sign. With $\rho(r) \approx .17 \text{ fm}^{-3}$ in the nuclear interior the requirement Re(4 $\pi c_0 \rho(r)$)>1 leads to $Re(c_0) > .47 \text{ fm}^3$, a condition satisfied by c_0 computed from phase shifts in the entire low energy region. Higher order corrections to be discussed in the next chapter, in particular the Ericson-Ericson effect, reduce the strength of the p-wave term. It is not clear, however, whether this reduction is sufficient to avoid difficulties. It is to be noted that although the pion wavefunction is singular in the interior, its exterior behavior is not anomalous, and the calculated scattering cross sections are perfectly reasonable.

The anomalous behavior of the Kisslinger potential is due, of course, to the approximations made, and in particular to the

off-shell extrapolation chosen. The introduction of form factors, which eliminate the high momentum components, is one possible remedy.

CHAPTER III

THE FULL OPTICAL POTENTIAL

As noted in the introduction, the first order treatment of the optical potential described in the previous chapter was found to be inadequate for the description of pion-nucleus processes, in particular the pionic atom level shifts and widths. This led to studies of kinematic and second order effects in the optical potential. In this chapter the various corrections to the first order optical potential which are incorporated into the calculations are derived.

The first section of this chapter deals with the kinematic transformation which was ignored in the simple optical potential of the last chapter, that is, the transformation of the pion-nucleon T-matrix from the pion-nucleon to the pion-nucleus center of mass. In the second section, the higher order multiple scattering terms are considered, in particular the second order s-wave term and a partial summation of the p-wave terms known as the Ericson-Ericson effect. Terms which arise from true absorption are discussed in Section 3. Other corrections, due to the Pauli exclusion principle and Coulomb distortion, are described in Section 4. Finally, the full optical potential is stated in Section 5.

In order to give some indication of the effect of the various kinematic and higher order corrections in pion-nucleus calculations, a representative set of differential elastic scattering calculations is shown where appropriate. Calculations for the nuclei 16 O and 208 Pb at 50 and 162 MeV are given to illustrate the nucleon number and energy dependence of the effects. Only π^+ scattering is shown in most cases, since the π^- scattering shows similar changes. The low energy data shown is that of Ref. 32 (diamonds), and Refs. 33 and 34 (triangles). The data at 162 MeV is from Ref. 35 (16 O) and Ref. 36 (208 Pb).

1. Kinematics

The pion-nucleon transition matrix $\tau_i \approx t_i^{\pi N}$ which is required for the optical potential is simply related to the experimentally measured scattering amplitude $f_{\pi N}$, defined in the πN center of mass, where $|\underline{k}| = |\underline{k}'|$. However, τ_i must be known for $\underline{k} + \underline{p} \neq 0$ as well. If one ignores the Fermi motion of the nucleons within the nucleus τ_i must be calculated in the pion-nucleus center of mass. This is sometimes referred to as the angle transformation, since it involves the transformation of the angle between \underline{k} and \underline{k}' in the p-wave term, among other things. When Fermi motion is included the transformation depends on \underline{p} as well as \underline{k} . It is a straightforward matter to relate $t^{\pi N}$ for $\underline{k} + \underline{p} = \underline{Q}$ to the πN center of mass amplitude for which $\underline{k} + \underline{p} = 0$. If, however, $|\underline{k}| \neq |\underline{k}'|$ in the frame in which $\underline{k} + \underline{p} = 0$, some assumption must be made about the off energy shell behavior of $t^{\pi N}$. An infinite number of such assumptions exist.

A complete theory of the pion-nucleon system would provide a unique off-shell extrapolation; however, such a theory does not yet exist.

The Kisslinger potential assumes that $t^{\pi N}$ is proportional to $b_0 + c_0 k \cdot k'$ for all k and k'. A different off shell amplitude can be obtained if the scattering amplitude

$$f_{\pi N} = b_0 + c_0 k \cdot k' \qquad (III-1)$$

is rewritten using

$$\underset{\sim}{\mathbf{k}} \cdot \underset{\sim}{\mathbf{k}}' = \frac{1}{2} (\mathbf{k}^2 - \mathbf{q}^2) , \qquad (III-2)$$

which gives

$$f_{\pi N} = b_0' + c_0' q^2$$
 (III-3)

where $b_0' = b_0 + \frac{1}{2} k^2 c_0$, $c_0' = -\frac{1}{2} c_0$, and q = k' - k. This leads to an optical potential, with the simplifying assumptions of the previous chapter,

$$2\omega U_{\text{opt}}(r) = -4\pi \{b_0' \rho(r) + c_0' [\nabla^2 \rho(r)]\}, \qquad (III-4)$$

which is generally called the Laplacian model. Note that the ∇^2 acts only on $\rho(r)$, making this a local potential. The Equation III-2

is only true on shell, therefore the off shell behavior of these two potentials is somewhat different.

Figure 3 shows a comparison of differential cross sections calculated with these two potentials. The differences are pronounced, especially at 50 MeV, where the two curves are of quite different character. At 162 MeV the curves have different magnitude but more or less the same shape. The partial cross sections also show large differences at 50 MeV. For ¹⁶0 the reaction cross section calculated with the Kisslinger potential is three times that for the Laplacian potential, with a corresponding inequality in the total cross sections; the elastic cross sections are about equal. For ²⁰⁸Pb the Kisslinger reaction cross section is also greater than the Laplacian; however, the total elastic scattering cross section for the Kisslinger potential is only about half that of the Laplacian, leading to a smaller total cross section. At 162 MeV the cross sections are much more similar; those of the Laplacian potential are slightly larger.

The Kisslinger and Laplacian potentials have been the most popular models for pion-nucleus scattering and are easily transformed to coordinate space. Another type of potential is known as the separable potential because the k and k' dependence of the pion-nucleon potential \mathbf{v} is assumed to be of the form $\pm \mathbf{g}(k)\mathbf{g}(k')$ in each channel, leading to a $\mathbf{t}^{\pi N}$ of the form $\pm \mathbf{g}(k)\mathbf{g}(k')\mathbf{D}(E)$ in each channel. The $\mathbf{g}'\mathbf{s}$, known as form factors, reflect the finite range of the πN interaction. This assumed form is quite useful in that the form factors and \mathbf{D} can be related to the πN phase shifts (37) and give

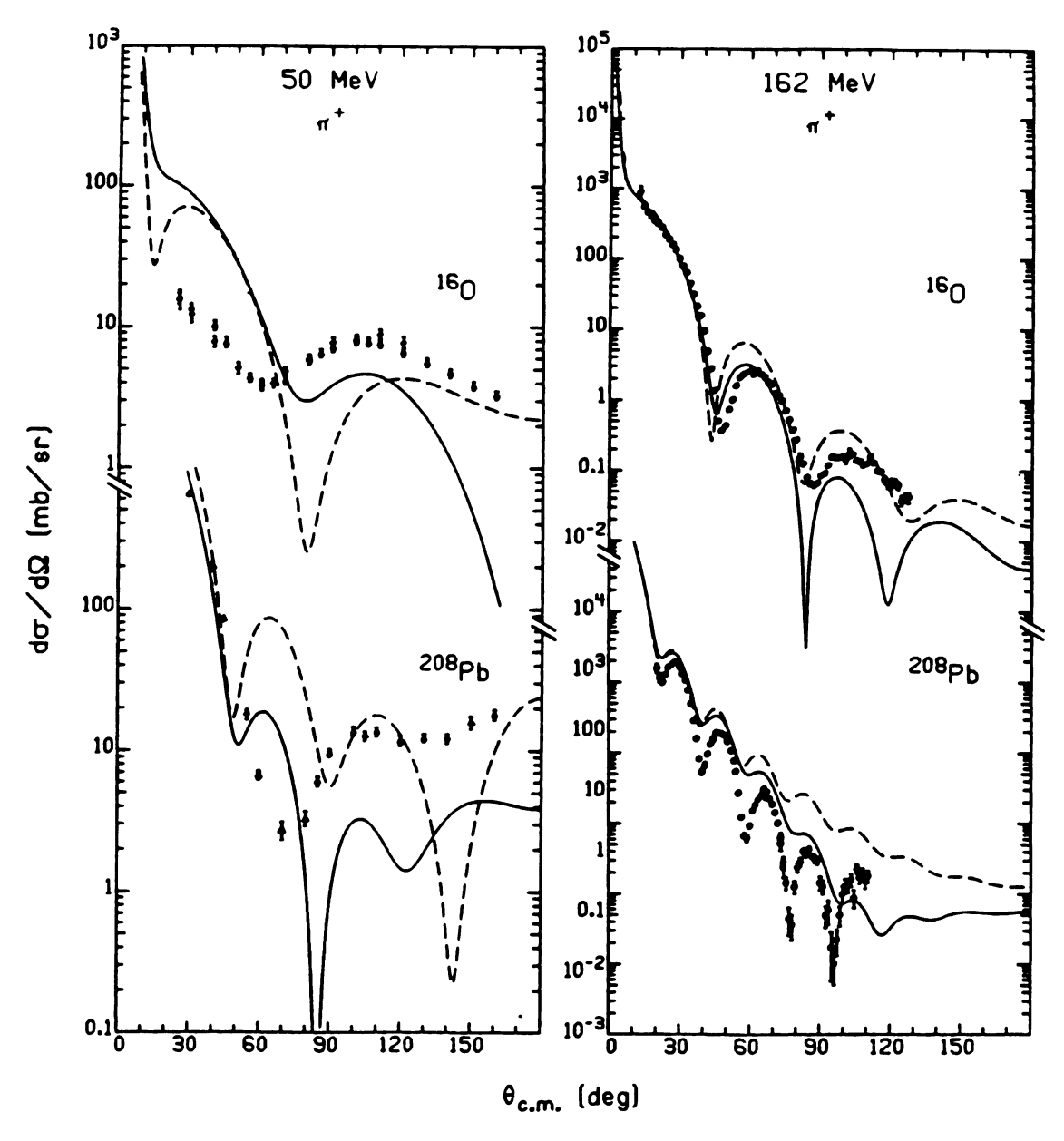


Figure 3. Comparison of calculations with the Kisslinger (solid curve) and Laplacian (dashed curve) optical potentials.

a more realistic off shell behavior for $\mathbf{t}^{\pi \mathbf{N}}$; however, the coordinate space potential derived from such a theory is of an awkward non-local form.

The Kisslinger form will be adopted for the optical potential in this work. Because it is explicitly separated into s- and p-wave parts it is best for pionic atom analysis and low energy scattering. The form is convenient, also, for the calculation of higher order terms. In the low energy region the Kisslinger potential parameters vary slowly with energy. This is not true in the resonance region, however. It has been shown that when higher order multiple scattering terms are included, taking account of the correlations between nucleons, Kisslinger and Laplacian potentials give similar results (30). This is true since the interaction is of short range and the correlations insure that nucleons are not close together, so that the potentials due to different nucleons are almost non-overlapping. Thus Beg's theorem (38) is applicable, which states that for non-overlapping potentials the scattering depends only on the on-shell part of the potential.

Once the off-shell behavior of the pion-nucleon T-matrix is chosen, all necessary T-matrix elements can be calculated. One method of doing this relativistically is given by relativistic potential theory (39). The process is more complicated than a Lorentz transformation, since the T-matrix does not have well-defined transformation properties (see Appendix D). The relativistic potential theory provides a prescription (40) for relating $\langle k', p' | t(E_T) | k, p \rangle$,

where E_T is the total energy of the pion-nucleon system, to t(w,q',q), where w is an energy parameter related to E_T . The momentum q is related to k and p, and q' is related to k' and p', by equation D-2 of Appendix D, which is equivalent to a Lorentz transformation to the two-particle center of mass frame. Thus $q = k_{cm}$ and $q' = k'_{cm}$. It is to be noted that the β for the transformation (k,p) + (q,-q) is not in general the same as the β for (k',p') + (q',-q'). The quantity t(w,q,q') with |q| = |q'| is just the on-shell T-matrix and with $|q| \neq |q'|$ is its off-shell extrapolation.

The exact expression for $\langle \underline{k}',\underline{p}'|t(E_T)|\underline{k},\underline{p}\rangle$ in terms of $t(w,\underline{q},\underline{q}')$ is given by equations D-5, D-6, and D-10, along with an expansion of the result in powers of Q^2 , where $Q=\underline{k}+\underline{p}=\underline{k}'+\underline{p}'$, given by equation D-11. Keeping only the first term in the expansion,

$$\langle \underline{k}', \underline{p}' | t(E_T) | \underline{k}, \underline{p} \rangle = (2\pi)^3 \delta(\underline{k}' + \underline{p}' - \underline{k} - \underline{p}) Nt(w, \underline{k}'_{cm}, \underline{k}_{cm})$$
(III-5)

where

$$N = \left[\frac{E\omega E'\omega'}{E_{cm}\omega_{cm}E'_{cm}\omega'_{cm}} \frac{(E_{cm} + \omega_{cm})(E'_{cm} + \omega'_{cm})}{(E + \omega)(E' + \omega')} \right]^{-\frac{1}{2}}$$
(III-6)

and

$$w = (E_T^2 - Q^2)^{\frac{1}{2}}$$
 (III-7)

Note that

$$E = (p^{2} + M^{2})^{\frac{1}{2}} \qquad E_{cm} = (k_{cm}^{2} + M^{2})^{\frac{1}{2}}$$

$$\omega = (k^{2} + m^{2})^{\frac{1}{2}} \qquad \omega_{cm} = (k_{cm}^{2} + m^{2})^{\frac{1}{2}}$$
(III-8)

are not the same as the on-shell values usually represented by these symbols.

The off-shell forms discussed previously were given for $\mathbf{f}_{\pi N}.$ Since $\mathbf{t}^{\pi N}$ is related to $\mathbf{f}_{\pi N}$ by

$$t^{\pi N}(w, k'_{cm}, k_{cm}) = -\frac{4\pi}{2\overline{\omega}_{cm}} f_{\pi N}(w, k'_{cm}, k_{cm})$$
 (III-9)

where

$$\overline{\omega}_{\rm cm} = \frac{\omega_{\rm cm} E_{\rm cm}}{\omega_{\rm cm} + E_{\rm cm}},$$

an off-shell form is needed for the reduced energy $\overline{\omega}_{\rm cm}$. This is chosen to be symmetric in incoming and outgoing particle energies,

$$\overline{\omega}_{cm} = \left[\frac{\omega_{cm} E_{cm}}{\omega_{cm} + E_{cm}} \frac{\omega_{cm}' E_{cm}'}{\omega_{cm}' + E_{cm}'} \right]^{\frac{1}{2}}.$$
 (III-10)

Taking the impulse approximation

$$\tau_i = t_i^{\pi N} \tag{III-11}$$

and recalling

$$\hat{\tau}_{i} = 2\overline{\omega}\tau_{i}$$
, (III-12)

it is seen that off-shell matrix elements of $\hat{\tau}_{\pmb{i}}$ also require an off-shell form for $\overline{\omega}$, taken as

$$\overline{\omega} = \left[\frac{\omega E_{A}}{\omega + E_{A}} \frac{\omega' E'_{A}}{\omega' + E'_{A}} \right]^{\frac{1}{2}}$$
(III-13)

with E_{A} and E_{A}^{\prime} the initial and final energies of the nucleus. Putting all these factors together gives

$$\langle \underline{k}', \underline{p}'_{i} | \tau_{i}(E_{T}) | \underline{k}, \underline{p}_{i} \rangle = -4\pi (2\pi)^{3}$$

$$\times \delta(\underline{k}' + \underline{p}'_{i} - \underline{k} - \underline{p}_{i}) = \frac{\overline{\omega}}{\overline{\omega}_{Cm}} N f_{\pi N}(w, \underline{k}'_{Cm}, \underline{k}_{Cm})$$
(III-14)

In order to simplify this result, the nucleons and nucleus are assumed nonrelativistic, so that

$$E = E' = E_{cm} = E'_{cm} = M$$
 and $E_{A} = E'_{A} = M_{A} = AM$. (III-15)

This is not sufficient to make equation III-14 usable in a coordinate space calculation, as ω and ω' still depend on \underline{k} and \underline{k}' . Therefore, ω and ω' are set equal to their on-shell values

$$\omega = \omega' = \omega_0 \equiv (k_0^2 + m^2)^{\frac{1}{2}}.$$
 (III-16)

With these approximations equation III-14 becomes

$$\langle \underline{k}', \underline{p}_{i}' | \tau_{i}(E_{T}) | \underline{k}, \underline{p}_{i} \rangle = -4\pi (2\pi)^{3}$$

$$\times \delta(\underline{k}' + \underline{p}_{i}' - \underline{k} - \underline{p}_{i}) \frac{1 + \varepsilon}{1 + \varepsilon/A} f_{\pi N}(w, \underline{k}'_{cm}, \underline{k}_{cm})$$
(III-17)

where

$$\varepsilon = \frac{\omega_0}{M} \tag{III-18}$$

and the difference between $\frac{\omega_0}{M}$ and $\frac{\omega_{0cm}}{M}$, of order ϵ^2 , has been neglected. At 50 MeV ϵ = .20; at 200 MeV ϵ = .36.

The arguments of $f_{\pi N}$, k_{cm} and k'_{cm} , must be expressed in terms of k, p, k', and p'. For this equation D-2 or equivalently the Lorentz transformation can be used. The latter gives

$$k_{\text{cm}} = k + \beta \gamma \left(\frac{\gamma}{\gamma + 1} \beta \cdot k - \omega \right)$$

$$k_{\text{cm}} = k' + \beta' \gamma' \left(\frac{\gamma'}{\gamma' + 1} \beta' \cdot k' - \omega' \right)$$
(III-19)

where

$$\beta = \frac{k + p}{E + \omega} \text{ and } \beta' = \frac{k' + p'}{E' + \omega'}$$
 (III-20)

To make these expressions tractable, only terms of first order in β will be kept. (This is nearly equivalent to expanding to first order in ϵ .) At T_{π} = 200 MeV $<\beta>$ \cong .25 and the error due to the

dropped terms is about 6%. With the additional approximations given in III-15 and III-16, equation III-19 becomes

$$k_{cm} = \frac{Mk - \omega_0 p}{M + \omega_0} = \frac{k - \epsilon p}{1 + \epsilon}$$

$$k'_{cm} = \frac{Mk' - \omega_0 p'}{M + \omega_0} = \frac{k' - \epsilon p'}{1 + \epsilon} ,$$
(III-21)

and the p-wave term in $f_{\pi N}$ is

$$k_{\text{cm}} \cdot k_{\text{cm}}' = \frac{1}{(1+\epsilon)^2} \left[k_{\text{c}} \cdot k_{\text{c}}' - \epsilon (k_{\text{c}} \cdot p_{\text{c}}' + k_{\text{c}}' \cdot p_{\text{c}}) + \epsilon^2 p_{\text{c}} \cdot p_{\text{c}}' \right]. \quad (III-22)$$

The last term is of order ϵ^2 and should be dropped. However, it is an induced s-wave term and, as noted by Brown, Jennings, and Rostokin (41), is important since the first order s-wave term is unusually small. A more careful calculation, too tedious to be given here, indicates that this is the only important ϵ^2 term.

Because the nucleon is part of a moving nucleus, the nucleon momentum should be separated into a part due to the momentum of the nucleus as a whole and a part due to the momentum of the nucleon relative to the nucleus,

$$\underline{p} = -\frac{1}{A} \underbrace{k}_{\infty} + \underline{p}_{0} \tag{III-23}$$

However, this separation complicates greatly the process of transforming from momentum space to coordinate space and only contributes terms of order ϵ/A which are negligibly small for all but the lightest nuclei. Therefore p and p₀ will be considered equivalent.

Let

$$\frac{p}{p} = \frac{p + p'}{2} \qquad \qquad K = \frac{k + k'}{2}$$

$$\overline{p} = p' - p \qquad \qquad q = k' - k$$
(III-24)

Then equation III-22 can be written

$$k_{\text{cm}} \cdot k'_{\text{cm}} = \frac{1}{(1+\epsilon)^2} k \cdot k' - \frac{2}{1+\epsilon} P \cdot K$$

$$-\frac{1}{2} \frac{1}{1+\epsilon} q^2 + (\frac{\epsilon}{1+\epsilon})^2 p \cdot p'$$
(III-25)

The T-matrix is now expressed in terms of pion-nucleus center of mass quantities, and the first order term of the optical potential,

$$2\overline{\omega}U_{\text{opt}}^{(1)} = A<0|\tau_{i}|0> \qquad (III-26)$$

can be calculated. Omitting the spin term this is

$$2\overline{\omega} U_{\text{opt}}^{(1)} = -4\pi A < 0 | (2\pi)^{3} \delta(\underline{p}_{i} + \underline{k} - \underline{p}_{i}' - \underline{k}') \{ (1 + \varepsilon) (b_{0} + b_{1} \underline{t} \cdot \underline{\tau}_{i})$$

$$+ (c_{0} + c_{1} \underline{t} \cdot \underline{\tau}_{i}) [\frac{1}{1 + \varepsilon} \underline{k} \cdot \underline{k}' - 2\underline{p} \cdot \underline{K} - \frac{1}{2} q^{2} + \frac{\varepsilon^{2}}{1 + \varepsilon} \underline{p} \cdot \underline{p}'] \} | 0 >$$
(III-27)

where it is assumed that $p_j' = p_j$ for $j \neq i$. The integrations over ground state nucleon momenta of the various terms are given in Appendix C. (This process is called Fermi averaging.) The result is

$$2\overline{\omega} U_{\text{opt}}^{(1)}(k,k') = -4\pi \{p_1[b_0\rho(q) + \varepsilon_{\pi}b_1(\rho_p(q) - \rho_n(q))]$$

$$+ p_1^{-1}[c_0\rho(q) + \varepsilon_{\pi}c_1(\rho_p(q) - \rho_n(q))]k \cdot k'$$

$$- \frac{1}{2}(1 - p_1^{-1})[c_0\rho(q) + \varepsilon_{\pi}c_1(\rho_p(q) - \rho_n(q))]q^2$$

$$+ \frac{(p_1 - 1)^2}{p_1}c_0\kappa(q) \}$$
(III-28)

where ε_{π} is the pion charge, ± 1 , $p_1 = 1 + \varepsilon$, and $\kappa(q)$ is the Fourier transform of 2M times the kinetic energy density of the nucleus, given in equation C-13. The transformation to coordinate space gives

$$2\overline{\omega} U_{\text{opt}}^{(1)}(\underline{r}) = -4\pi \{ p_1 [b_0 \rho(r) + \varepsilon_{\pi} b_1 (\rho_p(r) - \rho_n(r))]$$

$$- p_1^{-1} \underline{\nabla} \cdot [c_0 \rho(r) + \varepsilon_{\pi} c_1 (\rho_p(r) - \rho_n(r))] \underline{\nabla}$$

$$+ \frac{1}{2} (1 - p_1^{-1}) \underline{\nabla}^2 [c_0 \rho(r) + \varepsilon_{\pi} c_1 (\rho_p(r) - \rho_n(r))]$$

$$+ \frac{(p_1 - 1)^2}{p_1} c_0 \kappa(r) \} . \qquad (III-29)$$

The nucleon, neutron, and proton densities $\rho,~\rho_n,~$ and ρ_p are normalized to A, N, and Z, respectively.

This method of treating $k_{\text{cm}} \cdot k_{\text{cm}}'$ is, of course, not unique. One could, for example, replace q^2 by $2k_0^2 - 2k_0 \cdot k_0'$, leading to the optical potential

$$2\overline{\omega} U_{\text{opt}}^{(1)}(r) = -4\pi \{ p_1 b_0 \rho(r) - c_0 \nabla \cdot \rho(r) \nabla - c_0 \nabla - c_0$$

where isovector terms have been suppressed for simplicity. It should be noted that any choice of kinematics must treat k and k' symmetrically; otherwise the potential is not Hermitian and the results may violate unitarity.

The energy parameter w, given by equation III-7, is the energy at which the scattering parameters should be evaluated and should also be expressed in terms of p_i and p_i' before the integrals over nucleon momenta are performed. This is not practicable, however, and w^2 is evaluated with E_T and Q the total energy and momentum of the nucleon and pion before collision,

$$w^2 = (E + \omega)^2 - (p + k)^2$$
 (III-31)

This is just the total energy in the pion-nucleon center of mass.

It should be noted that the same results can be obtained from much simpler assumptions (see for example Ref. 24). It is instructive, however, to begin with a theory which claims to be relativistically correct and consistent. The approximations made are all explicit and the calculations required to improve the model are obvious, if not simple.

Figure 4 illustrates the effect on elastic scattering calculations of several choices for the kinematic transformation. The calculation with a first order optical potential with no kinematic terms, equation II-53 (dashed line), is compared to that with kinematics as in equation III-29 (solid line), equation III-30 (dashdotted line), and equation III-29 but without the κ (r) term (dotted line). It is clear that the choice of kinematics has a non-negligible effect on the scattering from both light and heavy nuclei, not only at low energies, but in the resonance region as well.

2. Multiple Scattering Corrections

Thus far only the first term of the multiple scattering series has been used in the construction of the optical potential. In this section the second and higher order terms of the series are considered. These modify both the s- and p-wave parts of the optical potential. As the s-wave parameter b_0 is nearly zero, the second order s-wave correction, first derived by Ericson and Ericson(10), is quite important. The p-wave parts of the multiple scattering series can be summed to all orders in the low energy limit, giving rise to what is termed the Ericson-Ericson or LLEE effect (10) first

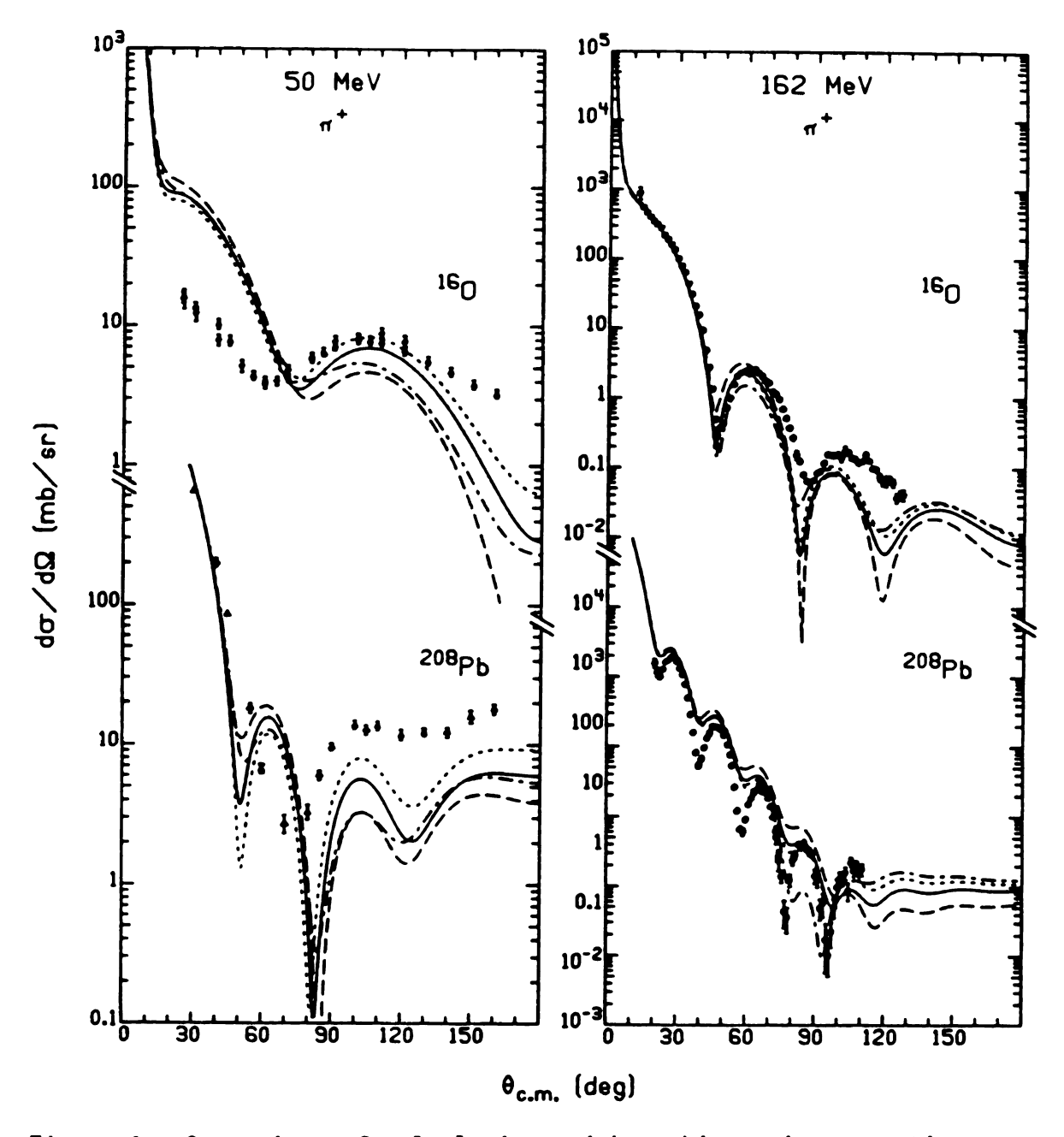


Figure 4. Comparison of calculations with no kinematic corrections (dashed curve), full kinematics (solid curve), and alternative choices for the kinematic corrections (dotted and dot-dashed curves).

discussed by M. Ericson (43), analogous to the Lorentz-Lorenz effect in electromagnetism (44).

The second term in the multiple scattering series for U, equation II-45, is

$$A(A-1)\hat{\tau}_{i}\hat{G}^{0}(1-P_{0})A\hat{\tau}_{i}$$
 (III-32)

Making the impulse approximation as before, the second order optical potential can be written

$$2\overline{\omega} \bigcup_{\text{opt}}^{(2)}(k,k') \equiv \langle 0 | \widehat{U}^{(2)} | 0 \rangle = \int \langle 0 | A(A-1)(2\pi)^3 \delta(\underline{p}_1' + \underline{k}' - \underline{p}_1 - \underline{k}'') \rangle$$

$$\times (-4\pi)\overline{f}(k',k'') \frac{1}{-k''^2 + k_0^2 + i\varepsilon} [1 - |0 \rangle \langle 0|]$$

$$\times (2\pi)^3 \delta(\underline{p}_2' + \underline{k}'' - \underline{p}_2 - \underline{k})(-4\pi)\overline{f}(\underline{k}'',\underline{k}) | 0 \rangle \frac{d^3k''}{(2\pi)^3}$$
(III-33)

where $p_i^! = p_i$ is assumed for $i \neq 1$, 2, and \overline{f} is the pion nucleon scattering amplitude with the kinematics derived in the previous section included,

$$\overline{f}(k,k') = p_1(b_0 + b_1 t \cdot \tau) + \frac{1}{p_1} (c_0 + c_1 t \cdot \tau) k \cdot k'$$

$$- \frac{1}{2} (1 - p_1^{-1}) (c_0 + c_1 t \cdot \tau) q^2 + p_1 (1 - p_1^{-1})^2 c_0 \kappa(q) .$$
(III-34)

Here $p_1 = 1 + \varepsilon$ with $\varepsilon = \frac{\omega_0}{M}$. As the last two terms are already small, their contribution to the second and higher order optical potential is neglected.

The second order s-wave term is generated from the s-wave parts of $\overline{f}(\underline{k}',\underline{k}'')$ and $\overline{f}(\underline{k}'',\underline{k})$. The two terms of equation III-33, from the 1 and |0><0| in brackets, can be evaluated using equations C-27 and C-9 of Appendix C, respectively. The result is

$$2\overline{\omega}U_{ss}^{(2)}(\underline{k},\underline{k}') = (-4\pi)^{2} \frac{A-1}{A} p_{1}^{2} \int (b_{0}^{2} + 2b_{1}^{2})C(\underline{r},\underline{r}')$$

$$\times \rho(r)\rho(r')e^{-i(\underline{k}'-\underline{k}'')\cdot\underline{r}} e^{-i(\underline{k}''-\underline{k})\cdot\underline{r}'}$$

$$\times d^{3}r d^{3}r' \frac{1}{-k''^{2} + k_{0}^{2} + i\varepsilon} \frac{d^{3}k''}{(2\pi)^{3}}$$
(III-35)

where

$$C(\underline{r},\underline{r}') = -\frac{1}{4} \left[\frac{3j_1(k_F|\underline{r} - \underline{r}'|)}{k_F|\underline{r} - \underline{r}'|} \right]^2.$$

Note that the first term on the right-hand side of equation C-27 exactly cancels the |0><0| term. The integration over terms in k" gives

$$\int e^{ik''\cdot(r-r')} \frac{1}{-k''^2+k_0^2+i\epsilon} \frac{d^3k''}{(2\pi)^3} = -\frac{1}{4\pi} \frac{e^{ik_0|x|}}{|x|}, \quad (III-36)$$

where x = r - r'. Equation III-35 becomes

$$2\overline{\omega} \int_{SS}^{(2)} (k, k') = 4\pi p_1^2 \frac{A - 1}{A} (b_0^2 + 2b_1^2) \int_{\rho(r)} \rho(r)$$

$$\times e^{-i(k'-k)\cdot r} [(-) \int_{C(x)\rho(r')} e^{-ik\cdot x} \frac{e^{ik_0|x|}}{|x|} d^3x d^3r$$

$$= 4\pi p_1^2 \frac{A - 1}{A} (b_0^2 + 2b_1^2) \int_{\rho(r)} \rho(r) e^{-i(k'-k)\cdot r} d^3r$$
(III-37)

The integral I, sometimes denoted $<\frac{1}{r}>_{corr}$, can be performed assuming: (1) an on-shell approximation, $k = k_0$; (2) a specific form for the correlation function; and (3) $\rho(r')$ approximately constant over the region in which C(x) is large. With the Fermi gas model value for C(x), equation C-28, and $\rho(r') \cong \frac{2k_F^3}{3\pi^2}$, the integral I can be done analytically for $k_0 = 0$ or numerically for any given k_0 . For $k_0 = 0$ the result is

$$I_0 = \frac{3k_F}{2\pi} . \tag{III-38}$$

With I approximated by a constant for a given k_0 , equation III-37 is a function of \underline{q} only and can be Fourier transformed, giving

$$2\overline{\omega}U_{ss}^{(2)}(r) = 4\pi p_1^2 \frac{A-1}{A} (b_0^2 + 2b_1^2)I_{\rho}(r) . \qquad (III-39)$$

Ericson and Ericson (10) made somewhat different assumptions in their derivation of the s-wave effect, leading to a term in $\rho^2(r)$.

The form given here is taken from Krell and Ericson (45), and requires slightly less radical assumptions.

The value of I, obtained by numerical integration, is shown in Figure 5 as a function of pion lab kinetic energy (solid line). In order to obtain a value of I for low energy scattering Thies (18) $i k_0^{X} i k_0^{\circ} r$ expanded e and e to first order in k_0 , resulting in

$$I_{\mathsf{T}} = \frac{3\mathsf{k}_{\mathsf{F}}}{2\pi} + \mathsf{i}\mathsf{k}_{\mathsf{O}} \tag{III-40}$$

As can be seen in the figure, this is not a good approximation above about 10 MeV, as the real part of I falls quickly from its zero energy value $\frac{3k_F}{2\pi}$, and the imaginary part does not follow k_0 (dashed line). Both real and imaginary parts of I go to zero at high energies, the imaginary part falling off more slowly than the real part.

Because the second order s-wave term is proportional to $\rho(r)$, it can be combined with the first order s-wave term, giving

$$2\overline{\omega}U_{\text{opt}}^{(s)}(r) = -4\pi p_1[\overline{b}_0\rho(r) + \varepsilon_{\pi}b_1(\rho_p(r) - \rho_n(r))] \qquad (III-41)$$

where

$$\overline{b}_0 = b_0 - p_1 \frac{A-1}{A} (b_0^2 + 2b_1^2) I$$
 (III-42)

Figure 6 shows b_0 and \overline{b}_0 as a function of pion kinetic energy. As expected, the difference is greatest at low energies and also of greatest importance, as b_0 is small there.

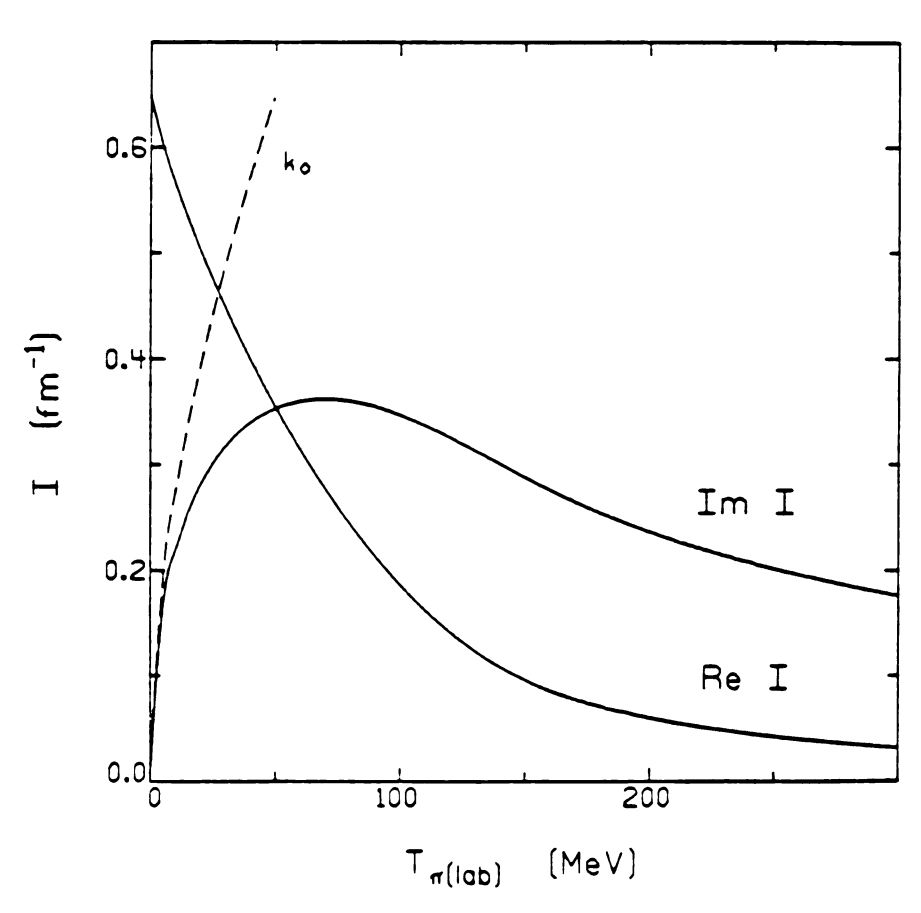


Figure 5. The integral I as a function of pion lab kinetic energy, and the approximation $Im(I) = k_0$.

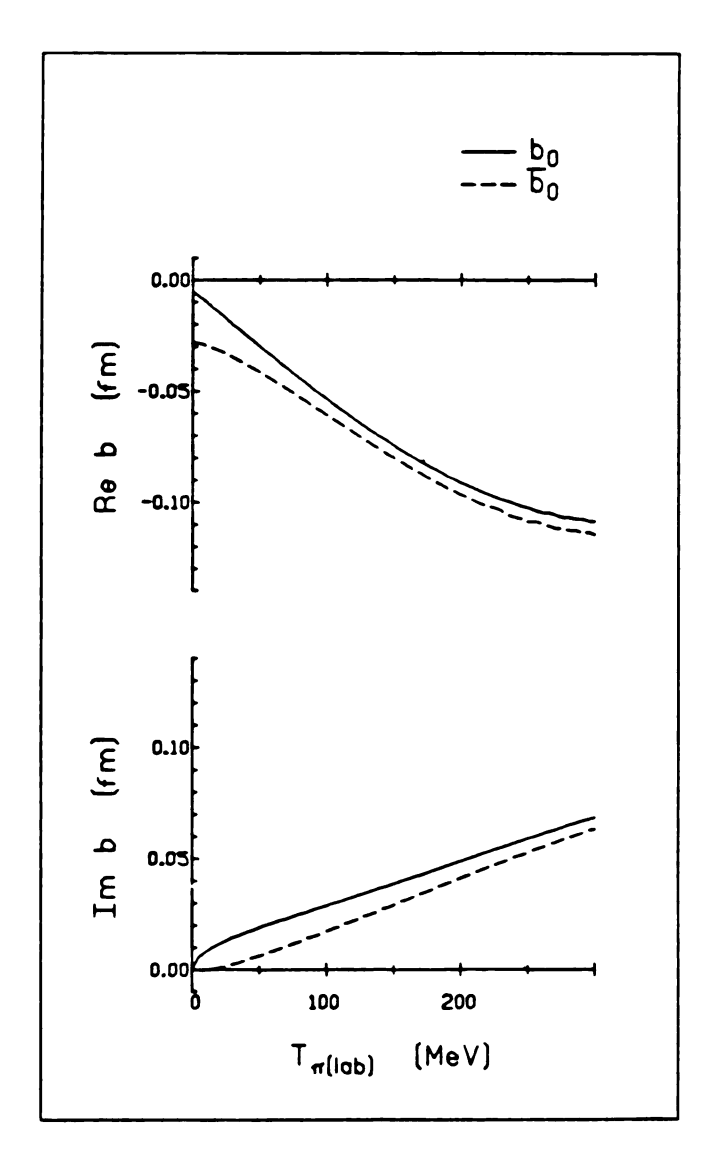


Figure 6. The first order s-wave optical potential parameter b_0 , and the same parameter but with the second order correction included, \overline{b}_0 , as a function of pion lab kinetic energy.

In Figure 7 differential cross sections calculated with the optical potential including the second order s-wave term (solid curve) are compared with those calculated with the first order optical potential equation III-29 (dashed curve). Also shown at 50 MeV is the effect of treating I in equation III-42 in the zero energy approximation, $I = \frac{3k_F}{2\pi}$ (dotted curve). At 50 MeV the second order s-wave term makes an appreciable difference, especially at backward angles. It has no effect at all, however, in the resonance region.

The second term of equation III-33 to be considered is the s-p interference term. This arises from

$$\overline{f}(\underline{k}',\underline{k}'')\overline{f}(\underline{k}'',\underline{k}) = (b_0 + b_1\underline{t}\cdot\underline{\tau})(c_0 + c_1\underline{t}\cdot\underline{\tau})(\underline{k}'\cdot\underline{k}'' + \underline{k}''\cdot\underline{k})$$
(III-43)

and is zero by symmetry.

The second order term due to the p-wave parts of $\overline{f}(\c k',\c k'')$ and $\overline{f}(\c k'',\c k)$ in equation III-33 is

$$2\overline{\omega} U_{pp}^{(2)}(\underline{k},\underline{k}') = (-4\pi)^{2} A(A - 1)p_{1}^{-2} \int_{0}^{\infty} \frac{(\underline{k}' \cdot \underline{k}'')(\underline{k}'' \cdot \underline{k})}{-\underline{k}''^{2} + \underline{k}_{0}^{2} + i\varepsilon}$$

$$\times \delta(\underline{p}'_{1} + \underline{k}' - \underline{p}_{1} - \underline{k}'')[1 - |0><0|] \delta(\underline{p}'_{2} + \underline{k}'' - \underline{p}_{2} - \underline{k})$$

$$\times (c_{0} + c_{1}\underline{t} \cdot \underline{\tau}_{1})(c_{0} + c_{1}\underline{t} \cdot \underline{\tau}_{2})|0> \frac{d^{3}\underline{k}''}{(2\pi)^{3}}$$
(III-44)

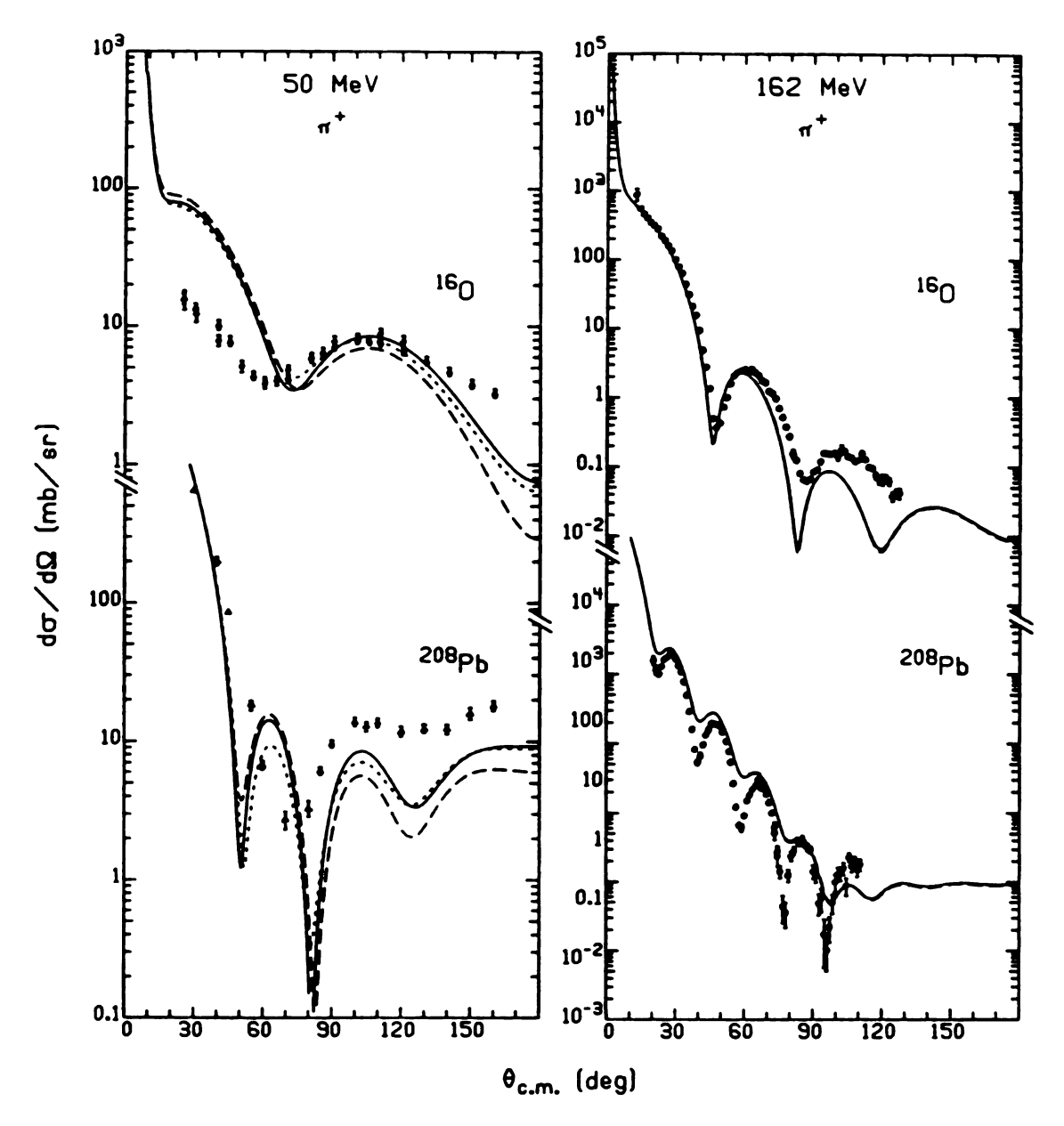


Figure 7. The effect of the second order s-wave term (solid curve) compared to calculations with the first order term only (dashed curve) and with the second order term in zero energy approximation (dotted curve).

The operator $(k' \cdot k'')(k'' \cdot k)$ can be written as the sum of a second rank tensor and a scalar in k'',

$$(k' \cdot k'')(k'' \cdot k) = \sum_{i,j} k'_i k_j [k''_i k''_j - \frac{1}{3} \delta_{i,j} k''^2] + \frac{1}{3} k''^2 k \cdot k'$$
 (III-45)

The tensor part is negligible at low energies and will be ignored at all energies considered here. As in the s-wave term, the integrals over nucleon momenta give the Fourier transforms of functions of r and r'. The remaining terms in k'' can be integrated over as before.

$$\int k^{2} \frac{1}{-k^{2} + k_{0}^{2} + i\varepsilon} e^{ik^{2} \cdot (r-r')} \frac{d^{3}k^{2}}{(2\pi)^{3}} = -\nabla_{x}^{2} \left[-\frac{1}{4\pi} \frac{e^{ik_{0}x}}{x} \right]$$
(III-46)

where x = r - r' and x = |x|. This gives two terms,

$$\frac{1}{4\pi} \nabla_{x}^{2} \frac{e^{ik_{0}x}}{x} = -\delta(x) - \frac{k_{0}^{2}}{4\pi} \frac{e^{ik_{0}x}}{x}.$$
 (III-47)

In the zero energy limit only the first term contributes, giving $\underline{r} = \underline{r}'$. As was noted in Appendix C, the first term in brackets in equation III-44 gives zero contribution for $\underline{r} = \underline{r}'$, assuming hard core repulsion between nucleons. Equation C-9 gives for the second term

$$2\overline{\cup} U_{pp}^{(2)}(k,k') = (4\pi)^{2} \frac{A-1}{A} p_{1}^{-2} \frac{1}{3} \int [c_{0}\rho(r) + c_{0}\rho(r)]^{2} e^{i(k'-k)\cdot r} k\cdot k'd^{3}r$$
(III-48)

in momentum space or

$$2\overline{\omega}U_{pp}^{(2)}(r) = -(4\pi)^2 \frac{1}{3} \frac{A-1}{A} \nabla \cdot [c_{0p}(r) + t_{3}c_{1}(\rho_{p}(r) - \rho_{n}(r))]^2 \nabla$$
(III-49)

in coordinate space.

The p-wave terms can be calculated to all orders in the zero energy limit, assuming tensor terms in the intermediate momenta do not contribute. The delta functions which appear, $\delta(r-r')\delta(r'-r'')$ and so on, insure that only the P_0 pieces of the $(1-P_0)$ operators are nonzero. Thus the Nth order p-wave term is proportional to $\rho^N(r)$. To all orders the p-wave terms are

$$2\overline{\omega} U_{pp}(r) = \nabla \cdot 4\pi p_1^{-1} c_0 \rho(r) \sum_{m=0}^{\infty} \left[-\frac{4\pi}{3} \frac{A-1}{A} c_0 p_1^{-1} \rho(r) \right]^m \nabla = \nabla \cdot \frac{4\pi p_1^{-1} c_0 \rho(r)}{1 - \left[-\frac{4\pi}{3} \lambda \frac{A-1}{A} p_1^{-1} c_0 \rho(r) \right]} \nabla , \qquad (III-50)$$

where the isovector terms have been suppressed for simplicity. This is the Ericson-Eriscon or LLEE effect, with λ = 1.

The Ericson-Ericson effect can be calculated more carefully, giving a term of the same form but with λ different from one. The

best value for λ has been a matter of dispute. Recent calculations by Brown, Jennings, and Rostokin (41), including π , ρ , and ω meson intermediate states and taking into account the finite range of the pion-nucleon interaction, yield a value for λ greater than one. They note that although the finite range of the interaction causes a reduction in the Ericson-Ericson effect, as noted by Eisenberg, Hüfner, and Moniz (46), other terms strengthen it, the net effect being a value of λ which is about 1.6 or higher (47). As their calculations were done in the low energy limit, their conclusions apply to the low energy region only. Oset and Weise (48) have also made an estimate of λ for low energies, based on calculations in the isobar-hole model. They give a value for λ in the range $\lambda = 1.2 - 1.6$. For this work the value $\lambda = 1.6$ is adopted as reasonable.

In the case of nonzero pion kinetic energy each term in the sum, equation III-50, should be modified by the effect of the second term in equation III-47. However, the second term is much more difficult to manage than the first, therefore its effect is calculated here to second order only, giving a rough idea of its importance. The second order term is quite similar to the s-wave term, and can be evaluated in a similar manner, giving

$$-4\pi \frac{A-1}{A} p_1^{-2} \frac{1}{3} k_0^2 k_0 k' k' (c_0^2 + 2c_1^2) I \int_{\rho(r)e^{\frac{iq \cdot r}{2}}} d^3r , \qquad (III-51)$$

where I is defined in equation III-37. The p-wave optical potential in coordinate space is, with the inclusion of this term,

$$U_{pp}(r) = 4\pi \nabla \cdot \left\{ \frac{p_1^{-1}[c_0\rho(r) + t_3c_1(\rho_p(r) - \rho_n(r))]}{1 + \frac{4\pi}{3} \frac{A-1}{A} \lambda p_1^{-1} [c_0\rho(r) + t_3c_1(\rho_p(r) - \rho_n(r))]} \right\}$$

$$+\frac{A-1}{A}p_1^{-1}c'\rho(r)\bigg\} \overset{\nabla}{\sim}$$
 (III-52)

where

$$c' = p_1^{-1} \frac{1}{3} k_0^2 (c_0^2 + 2c_1^2) I$$
 (III-53)

Note that the isovector part of the c' term has been neglected.

Figure 8 gives the energy dependence of c', as compared with that of c_0 . As c' goes as k_0^2 it is small at low energies, and dies away at high energies due to the falling off of both I and the p-wave scattering parameters. It is, however, a large effect in the resonance region.

In Figure 9 the effect of the Ericson-Ericson correction is illustrated. The differential cross sections calculated with only the first order p-wave term (dashed curve) are compared with those calculated with the full Ericson-Ericson effect with λ = 1.6 (solid curve), with λ = 1.0 (dotted curve), and with the Ericson-Ericson effect to second order only, λ = 1.0 (dash-dotted curve). At 50 MeV the differences are quite large; at 162 MeV there is a difference at backward angles between calculations with and without the

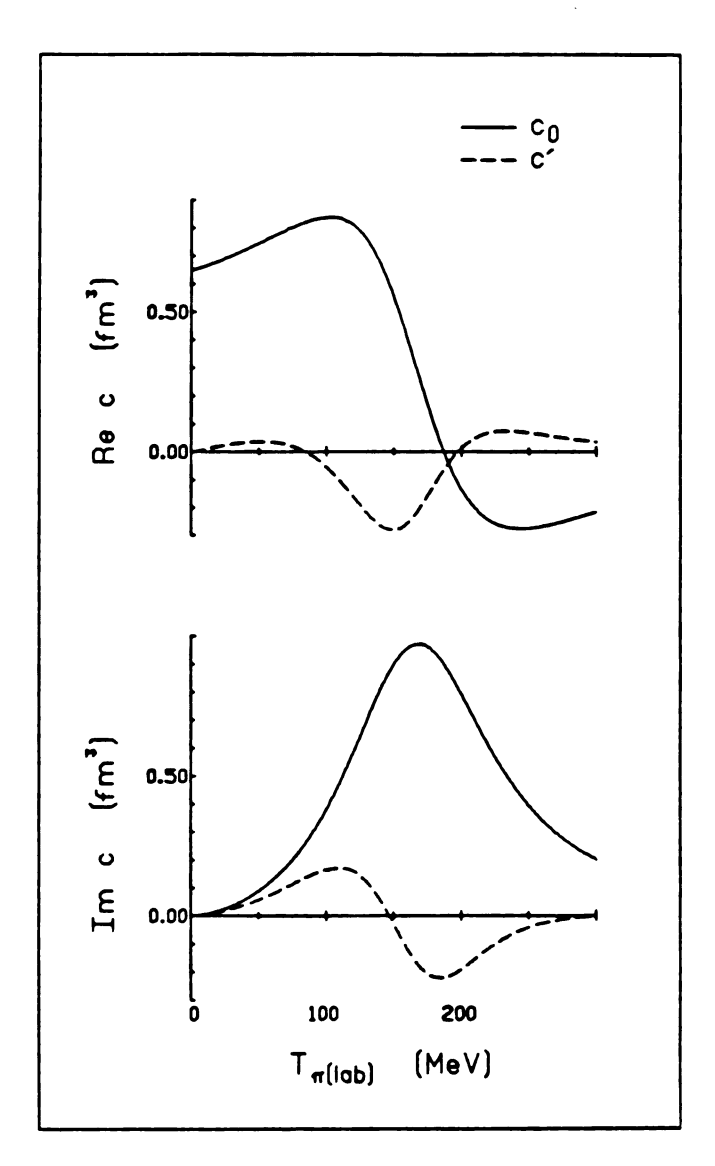


Figure 8. The parameter c' compared to the first order p-wave parameter \mathbf{c}_0 as a function of pion lab kinetic energy.

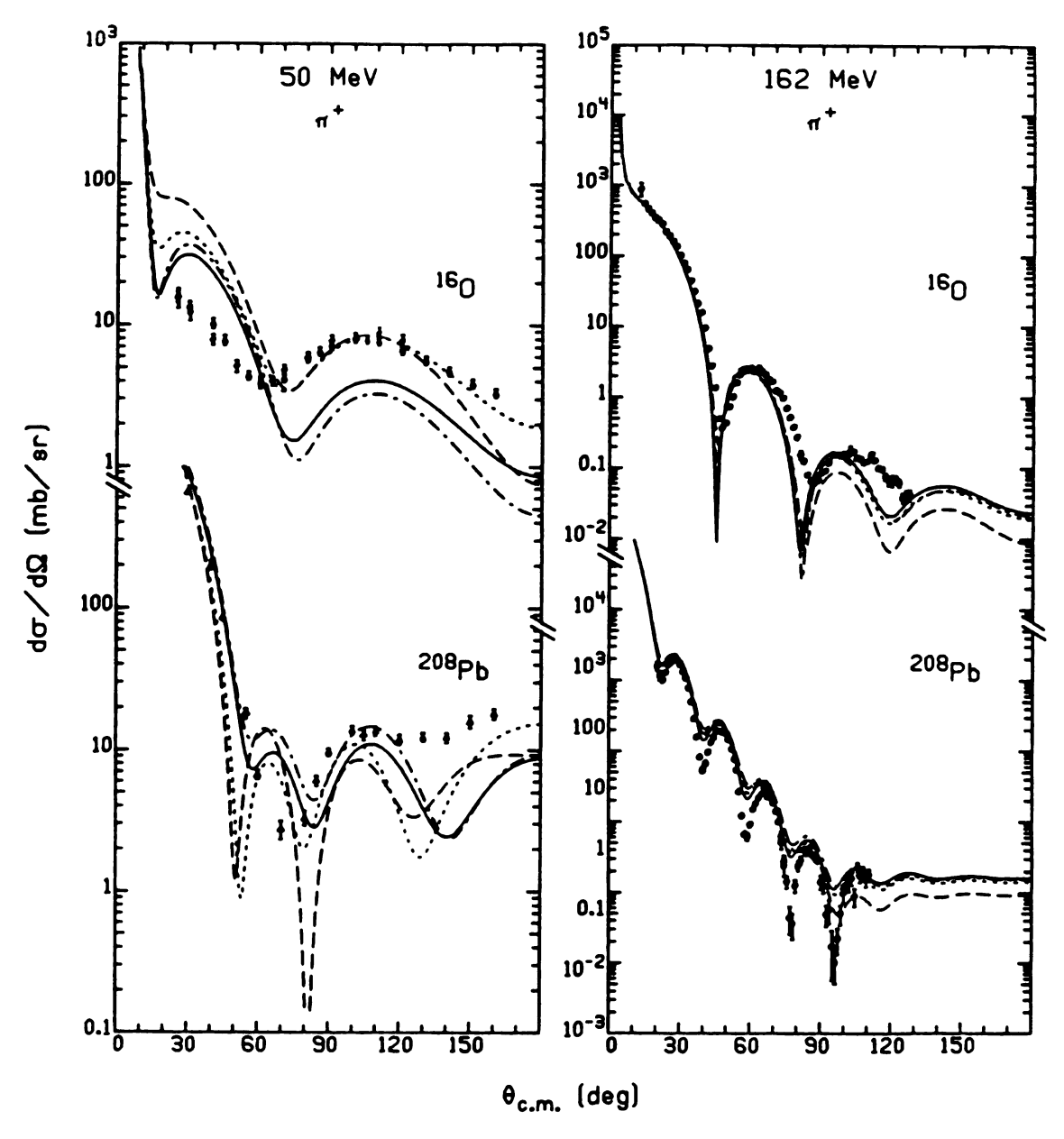


Figure 9. The effect of the Ericson-Ericson correction to the p-wave, λ = 1.6 (solid curve) and λ = 1.0 (dotted curve), compared to calculations with no correction (dashed curve) and with the correction included to second order only, λ = 1 (dash-dotted curve).

Ericson-Ericson effect, but almost none between the full effect and the second order approximation to it.

Figure 10 shows calculations with (solid curve) and without (dashed curve) the c' term. Because of the crudeness of the calculation it is likely that the effect is greatly overestimated, especially at higher energies. Other terms such as the tensor terms may also begin to contribute in the resonance region. Therefore this term is dropped in future calculations.

One other comment should be made about the Ericson-Ericson effect. The pion-nucleus T-matrix given in equation II-30 can be expressed in terms of $\hat{\tau}_i$, using the same reasoning that leads to II-38. The result is (29)

$$T = \sum_{i} \hat{\tau}_{i} + \sum_{j \neq i} \sum_{j \neq i} \hat{\tau}_{i} \hat{G}^{0} \hat{\tau}_{j} + \sum_{i} \sum_{j \neq i} \sum_{k \neq j} \hat{\tau}_{i} \hat{G}^{0} \hat{\tau}_{j} \hat{G}^{0} \hat{\tau}_{k} + \dots$$
(III-54)

This series, the Watson multiple scattering series for T, is just the Born series with an effective potential $\hat{\tau}_i$. Using the same arguments which lead to the Ericson-Ericson effect, it is seen that the second term of equation III-54 is zero. Thus the first Born approximation should be a reasonable approximation to the full calculation. This argument breaks down, of course, for $\lambda \neq 1.0$.

3. True Pion Absorption Terms

The conventional multiple scattering series includes only intermediate states consisting of one pion plus the nucleus, since

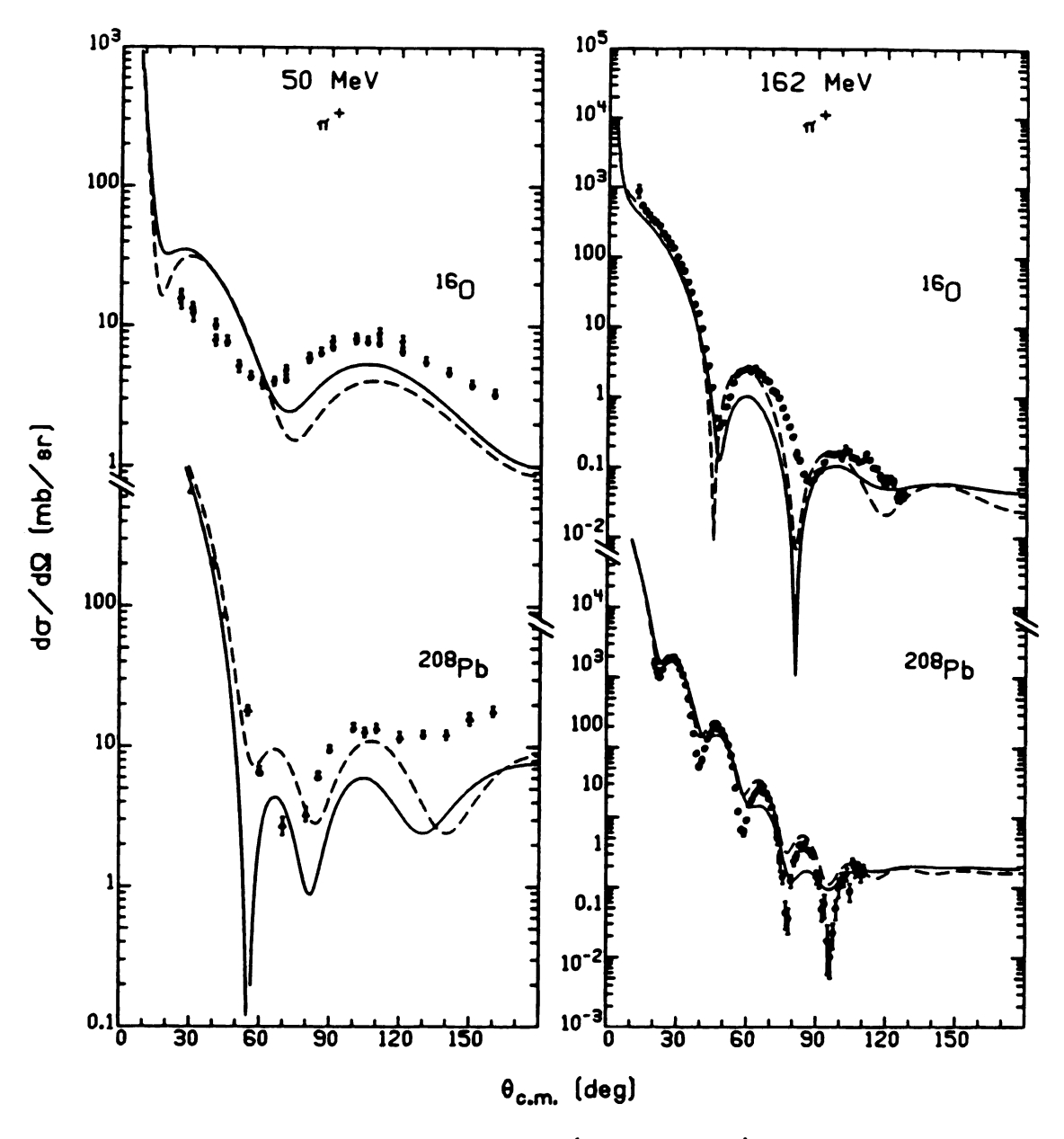


Figure 10. The effect of the c' term (solid curve) compared to calculations without this term (dashed curve).

the τ_i in the multiple scattering series correspond to pion nucleon scattering. Because the pion is a meson, however, it can be absorbed on one or more nucleons, resulting in intermediate states with no pion. This process gives a non-negligible contribution to both the real and imaginary parts of the optical potential, and is especially important at low energies. The parametrization of this process as terms in the optical potential is discussed in this section.

Analogous to the scattering T-matrix τ , define an absorption operator τ and emission operator τ^{\dagger} for the pion, describing respectively the processes $N\pi \to N$ and $N \to N\pi$. Although there is some contribution from pion absorption on one nucleon at very low energies, the dominant absorption mechanism is two nucleon absorption, in which the pion scatters from one nucleon and is absorbed by the second, with the two nucleons sharing the kinetic energy due to the disappearance of the pion mass. The lowest order optical potential term due to such a process can be written

$$<0 |A(A - 1)\hat{\tau}\hat{G}^{0}(1 - P_{0})A\tau^{\dagger}G_{N}(1 - P_{0})A\tau\hat{G}^{0}(1 - P_{0})A\hat{\tau}|0>,$$
(III-55)

where G_N is the propagator for the nucleus. Although this is, in a sense, a fourth order term, it has a large imaginary part, describing flux lost from the elastic channel due to true absorption of the pion. At low energies the other imaginary terms in the

optical potential, due to quasielastic processes, are nearly zero, and the absorption terms make the dominant contribution.

In their discussion of pionic atoms Ericson and Ericson (10) introduce absorption by defining a pion-two nucleon amplitude describing pion absorption and reemission,

$$f_{(2)} = B_0 + C_0 \underset{\sim}{k_{2cm}} \cdot \underset{\sim}{k_{2cm}}$$
 (III-56)

where the subscript 2cm refers to the pion-two nucleon center of mass frame in which $f_{(2)}$ is defined. The B_0 and C_0 can be determined in principle from the various amplitudes of the angular momentum and isospin states of the pion-two nucleon system. A fair amount of data does exist for the reaction $\pi + d \rightarrow N + N$, but it is difficult to eliminate effects of deuteron structure from the amplitudes.

The amplitude $f_{(2)}$ can be related to expression III-55 by defining

$$\hat{\tau}^{(2)} \equiv \hat{\tau} \hat{G}^{0} (1 - P_{0}) A \tau^{\dagger} G_{N} (1 - P_{0}) A \tau \hat{G}^{0} (1 - P_{0}) A \hat{\tau}$$
 (III-57)

and

$$\tau^{(2)} = \frac{1}{2\overline{\omega}_{(2)}} \hat{\tau}^{(2)}$$
 (III-58)

where $\overline{\omega}_{(2)}$ is the reduced energy of the pion-two nucleon system in that system's center of mass. Then the impulse approximation gives

$$\hat{\tau}^{(2)} = -4\pi f_{(2)}$$
 (III-59)

Equation III-57 may include more than s- and p-wave terms; however, the first two partial waves are assumed to dominate.

As the amplitude $f_{(2)}$ is defined in the pion-two nucleon center of mass, a kinematic transformation to the pion-nucleus center of mass is required for $\tau^{(2)}$. The results derived in Section 1 for τ can be immediately applied to $\tau^{(2)}$ with the substitution M + 2M in the kinematic factors. Thus the lowest order absorption terms in the optical potential are

$$2\overline{\omega} U_{\text{opt}}^{\text{(abs)}} (\underline{k}, \underline{k}') = \langle 0 | A(A - 1)\tau^{(2)} | 0 \rangle$$

$$= \langle 0 | (2\pi)^3 \delta(\underline{k}' + \underline{p}_1' + \underline{p}_2' - \underline{k} - \underline{p}_1 - \underline{p}_2)(-4\pi)$$

$$\times A(A - 1)[\underline{p}_2 B_0 + \underline{p}_2^{-1} C_0 \underline{k} \cdot \underline{k}' - \frac{1}{2} (1 - \underline{p}_2^{-1}) C_0 \underline{q}^2] | 0 \rangle$$
(III-60)

where the term analogous to $\kappa(r)$ has been neglected. Note that the details of the two nucleon absorption process are buried in the parameters B_0 and C_0 . By expression C-31 of Appendix C the Fourier transform of equation III-60 is

$$2\overline{\omega}U_{\text{opt}}^{(\text{abs})}(r) = -4\pi[p_{2}B_{0}\rho_{2}(r,r) - p_{2}^{-1}C_{0}\nabla \cdot \rho_{2}(r,r)\nabla + \frac{1}{2}(1 - p_{2}^{-1})C_{0}\nabla^{2}\rho_{2}(r,r)$$
(III-61)

The two-body density $\rho_2(r,r)$ is replaced with $\rho^2(r)$, assuming all correlation effects are included in B_0 and C_0 . This rather awkward situation is due to the simplified form of equation III-60. A more careful derivation is given by Rockmore, Kanter, and Goode (49). They write the absorption term of the optical potential schematically as

$$\begin{array}{l} 2 \bar{\omega} U_{\rm opt}^{(abs)}(x',x) \sim A^2 \int \psi^{\star}(\underline{r}_1',\underline{r}_2',\underline{r}_3...\underline{r}_A) U^{\dagger}(\underline{r}_1',\underline{r}_2';\underline{x}') \\ & \times G_N(\underline{r}_1',\underline{r}_2',\underline{r}_1,\underline{r}_2) U(\underline{r}_1,\underline{r}_2;\underline{x}) \psi(\underline{r}_1,\underline{r}_2,\underline{r}_3...\underline{r}_A) d^3r_1' d^3r_2' \Pi d^3r_1 \end{array}$$

where U and U † are the two nucleon absorption and emission operators and \underline{x} and \underline{x} ' are the pion coordinates. The two nucleon propagator G_N is diagonal in momentum space,

$$G_{N}(\underline{p}_{1}^{\prime},\underline{p}_{2}^{\prime},\underline{p}_{1}^{\prime},\underline{p}_{2}) = \delta(\underline{p}_{1} - \underline{p}_{1}^{\prime})\delta(\underline{p}_{2} - \underline{p}_{2}^{\prime}) \frac{1}{\omega - \frac{p_{1}^{2}}{2M} - \frac{p_{2}^{2}}{2M} - i\varepsilon}$$
(III-63)

neglecting interactions between the two nucleons. Let

Then the Fourier transform of equation III-63 is

$$G_{N}(\underline{r}_{1}',\underline{r}_{2}',\underline{r}_{1},\underline{r}_{2}) = \int e^{-i(\frac{1}{2}\underline{p}-\underline{p})\cdot(\underline{r}_{1}'-\underline{r}_{1})} \times e^{-i(\frac{1}{2}\underline{p}+\underline{p})\cdot(\underline{r}_{2}'-\underline{r}_{2})} \frac{1}{\omega - \frac{\underline{p}^{2}}{4M} - \frac{\underline{p}^{2}}{M} - i\varepsilon} \frac{d^{3}\underline{p}}{(2\pi)^{3}} \frac{d^{3}\underline{p}}{(2\pi)^{3}}$$
(III-65)

The dinucleon momentum P is, by momentum conservation, roughly the same size as k, the incoming pion momentum. The relative momentum of the two nucleons, p, is large, however, because of the kinetic energy gained when the pion is absorbed. Therefore the $\frac{p^2}{4M}$ term in G_N is dropped. This gives

$$G_{N}(\tilde{R}',\tilde{r}',\tilde{R},\tilde{r}) = \delta(\tilde{R} - \tilde{R}') \int e^{i\tilde{p}\cdot(\tilde{r} - \tilde{r}')} \frac{1}{\omega - \frac{p^{2}}{M} - i\varepsilon} \frac{d^{3}p}{(2\pi)^{3}}$$

$$= \delta(R - R')G_{p_0}(r - r')$$
(III-66)

where $p_0 = \sqrt{\omega M}$ and

$$G_p(x) \sim \frac{e^{ipx}}{x}$$
 (III-67)

Putting this in equation III-62 and making the coordinate transformations III-64 gives

$$2\overline{\omega} U_{\text{opt}}^{(\text{abs})}(\underline{x}',\underline{x}) \sim A^{2} \int \psi^{*}(\underline{R} - \frac{\underline{r}'}{2}, \underline{R} + \frac{\underline{r}'}{2}, \underline{r}_{3} \dots \underline{r}_{A})$$

$$\times U^{\dagger}(\underline{R},\underline{r}',\underline{x}')\delta(\underline{R} - \underline{R}')G_{p_{0}}(\underline{r} - \underline{r}')U(\underline{R},\underline{r},\underline{x})$$

$$\times \psi(\underline{R} - \frac{\underline{r}}{2}, \underline{R} + \frac{\underline{r}}{2}, \underline{r}_{3} \dots \underline{r}_{A})d^{3}Rd^{3}R'd^{3}r'd^{3}r' \underline{i}_{\geq 2} d^{3}r_{i} . \tag{III-68}$$

The wavefunction product is expanded about R, giving

$$\int \psi^{*}(R - \frac{r'}{2}, R + \frac{r'}{2}, r_{3} \dots r_{A}) \psi(R - \frac{r}{2}, R + \frac{r}{2}, r_{3} \dots r_{A})$$

$$\times \prod_{i \geq 2} d^{3}r_{i} \approx \rho(R)\rho(R)e^{-\frac{1}{2}r^{2}/a^{2}} e^{-\frac{1}{2}r^{2}/a^{2}} f(r)f(r')$$
(III-69)

where the functions f insure the proper correlations between the two nucleons, f(0) = 0 and $f(r) \rightarrow 1$ for r large. With zero range interactions equation III-68 becomes a local potential and the U[†] and U depend only on r' and r. Thus the absorption term of the optical potential goes as ρ^2 with the effect of correlations included in the integrals over r and r' which give rise to the absorption parameters. The lowest order absorptive terms in the optical potential are then

$$2\overline{\omega}U_{\text{opt}}^{(\text{abs})}(r) = -4\pi[p_2B_0\rho^2(r) - p_2^{-1}C_0\nabla \cdot \rho^2(r)\nabla + \frac{1}{2}(1 - p_2^{-1})C_0\nabla^2\rho^2(r)]$$
(III-70)

The only higher order multiple scattering terms due to absorption to be calculated here are those which contribute to the Ericson-Ericson effect. The other terms involve long range correlation functions of three or more particles, which are not well known. It is to be hoped that they make only small contributions to the optical potential and can be ignored. The absorptive terms can be included in a simple way in the Ericson-Ericson effect by replacing τ in the derivation by τ + $\tau^{(2)}$, with $\tau^{(2)}$ given by equation III-59. As $\tau^{(2)}$ is a two nucleon operator, the delta functions of position, $\delta(\overset{.}{r}-\overset{.}{r}'),\ \delta(\overset{.}{r}'-\overset{.}{r}''),$ and so on, become delta functions of the coordinates of one particle and the center of mass of a pair of particles, or of the centers of mass of two pairs. The two body density $\rho_2(r,r')$ is replaced by three and four particle densities. It must then be argued that the nucleons in the pair are close enough so that the three particle density is zero when the coordinate of one particle corresponds to the center of mass of a pair, and similarly with the four particle density and two pairs. With these assumptions the Ericson-Ericson term is

$$2\overline{\omega} U_{\text{opt}}^{(\text{EE})}(r) = -4\pi \nabla \cdot \frac{p_1^{-1} c_0 \rho(r) + p_2^{-1} c_0 \rho^2(r)}{1 + \frac{4\pi}{3} \lambda \frac{A-1}{A} \left[p_1^{-1} c_0 \rho(r) + p_2^{-1} c_0 \rho^2(r) \right]} \nabla$$
(III-71)

for an N = Z nucleus.

With the form of the absorption terms determined, it is necessary to choose the parameters B_0 and C_0 . Rather than attempt to construct these directly from π + d \rightarrow N + N amplitudes, the results

of calculations of B_0 and C_0 for nuclear matter by Riska, Bertsch, Chai, and Ko (50) will be adopted. Only a brief summary of their calculations will be given, as they are fully described in the references cited, and are fairly long. Riska and collaborators write the lowest order two particle absorptive term of the optical potential

$$U_{\text{opt}}^{(\text{abs})} = \frac{1}{\Omega} \sum_{f \neq i} T_{if} \left\{ \frac{P}{E_i + \omega - E_f} - i\pi\delta(E_i + \omega - E_f) \right\} T_{fi}$$
(III-72)

where ${\bf P}$ stands for principle value. The T_{fi} are the two nucleon absorption and emission operators, with i and f labelling the nuclear states. Note that this expression is simply related to equation III-57 for $\tau^{(2)}$, with the expression in brackets above equal to G_N .

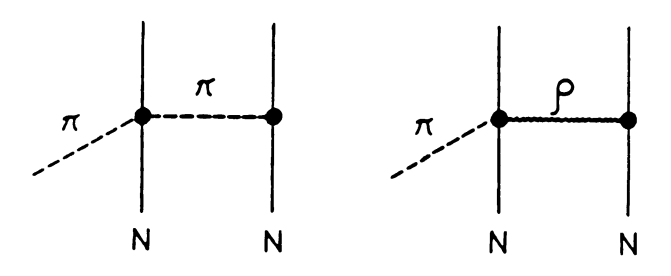
The T_{fi} are obtained from the evaluation of the diagrams shown in Figure 11. For the s-wave, the rescattering vertex is described by a phenomenological Hamiltonian (51),

$$H = 4\pi \frac{\lambda_1}{m} \psi^{\dagger} \underbrace{\phi}_{} \cdot \underbrace{\phi}_{} \psi + 4\pi \frac{\lambda_2}{m^2} \psi^{\dagger} \underbrace{\tau}_{} \cdot \underbrace{\phi}_{}^{\times} \underbrace{\pi}_{} \psi , \qquad (III-73)$$

where ψ^{\dagger} and ψ are nucleon field operators and ϕ and π are the pion field operator and the momentum operator conjugate to it. The coupling constants λ_1 and λ_2 are determined by the π -N phase shifts. The pion absorption vertex is described by

$$H = -\frac{f}{m} \psi^{\dagger} (\vec{\sigma} \cdot \vec{\nabla}) \phi \cdot \tau \psi , \qquad (III-74)$$

s-wave





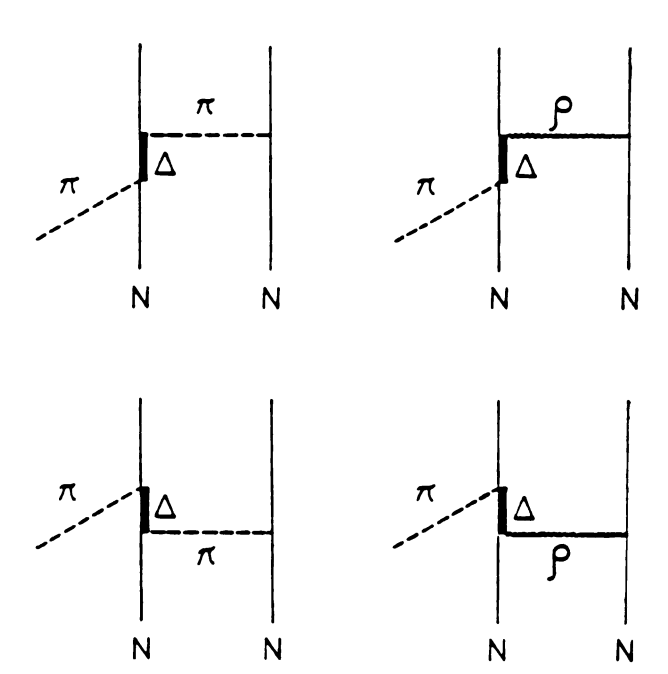


Figure 11. Diagrams of the s and p-wave processes included in the calculation (50) of the absorption parameters.

where
$$\frac{f^2}{4\pi} = 0.081$$
.

The p-wave rescattering is assumed to be dominated by the Δ_{33} resonance, as shown in the p-wave diagrams of Figure 11. Both π and ρ intermediate states are included. The Lagrangians for the various vertices are

$$L_{\pi NN} = \frac{f}{m} \psi^{\dagger} \vec{\sigma} \cdot \vec{\nabla} (\phi \cdot \tau) \psi$$

$$L_{\rho NN} = \frac{g_{\rho}}{2M} (1 + K) \psi^{\dagger} (\vec{\sigma} \times \vec{\nabla}) \vec{\rho} \cdot \tau \psi$$

$$L_{\pi N\Delta} = \frac{f_{\Delta}}{m} \psi^{\dagger} \cdot \vec{\nabla} \phi \psi + h.c.$$

$$L_{\rho N\Delta} = \frac{g_{\rho \Delta}}{2M} \psi^{\dagger} \cdot (\vec{\nabla} \times \vec{\rho}) \psi + h.c.$$
(III-75)

where ψ is the nucleon operator, ψ the delta operator, which is a vector-spinor in spin and isospin spaces, ϕ the pion operator, and ρ the rho operator, which is a vector in spin and isospin spaces. The symbols "+" and "~" to denote vectors are both used in order to distinguish vectors in different spaces. The values of the coupling constants adopted are $\frac{f_{\Delta}^2}{4\pi} = 0.32$, $\frac{g_{\rho}^2}{4\pi} = 0.55$, K = 6.6, and $g_{\rho\Delta} = \frac{6\sqrt[4]{2}}{5} g_{\rho}(1 + \text{K})$.

The vertex factors are combined with the propagator for the intermediate particle to give the two nucleon absorption operator T. The initial and final nuclear states for which T is evaluated are two nucleon states in nuclear matter, i.e. plane wave states,

which are symmetric or antisymmetric in the two nucleon coordinates, chosen so that the total wavefunction including space, spin, and isospin parts is antisymmetric. The isospin and spin sums over the two particle initial and final states are performed first, assuming equal numbers of protons and neutrons. Multipole expansions are made of the initial and final wavefunctions and T, and the nucleon coordinates are expressed in terms of the center of mass R and relative coordinate r, with the integral over R giving conservation of momentum. The sums over initial and final spatial states are converted to integrals over momenta, and the final integrals are performed numerically.

The s- and p-wave optical potential parameters thus obtained are shown as a function of energy in Figure 12. The imaginary part of B_0 increases with energy; the real part is approximately zero at zero energy and becomes more negative with increasing energy. The imaginary p-wave parameter shows a peak near resonance, as does the real part.

It should be noted that the real parts of the absorptive terms of the optical potential are, unlike the imaginary parts, quite sensitive to Pauli blocking effects, and somewhat sensitive to the radius assumed for the hard core repulsion, and the form factors assumed for the pion and rho meson. The inclusion of Pauli blocking increases the values of the real parts; thus the values given here can be considered lower bounds on these numbers.

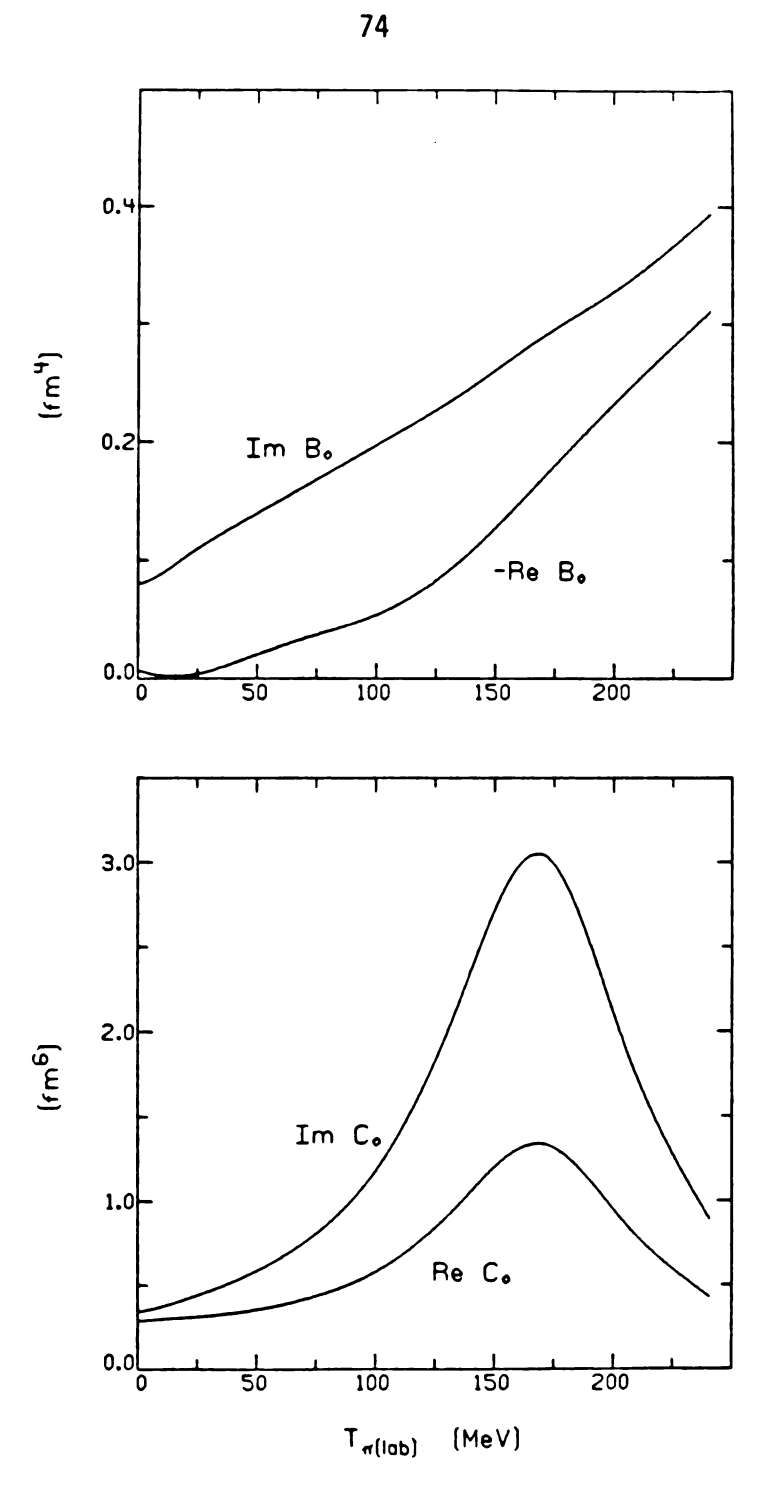


Figure 12. The absorptive parameters B_0 and C_0 as a function of pion lab kinetic energy.

There are several problems with calculations of this type. Because it is a nuclear matter calculation, the form of the absorption terms for a finite nucleus must be derived separately; hence the inclusion of the argument of Rockmore et al. A more serious problem is the possibility of double counting in the p-wave, as part of the amplitude equation III-57 looks like a third order multiple scattering term with far off shell components, and is therefore already included in the Ericson-Ericson effect derived in the previous section. This problem is perhaps best resolved by a different approach, in which absorption and scattering terms are considered together at the outset.

Other calculations of these parameters have been performed. The s-wave absorption parameters have been calculated at threshold by Hachenberg and Pirner (52), who obtain the value $B_0 = (0.375 + i\ 0.144) fm^4$. This has a somewhat larger imaginary part and much larger real part than the Riska value $B_0 = (0.0067 + i\ 0.080) fm^4$. G.A. Miller (53) has calculated the p-wave parameter; his values are $C_0 = (-0.05 + i\ 0.57) fm^6$ at 50 MeV and $C_0 = (-0.03 + i\ 0.72) fm^6$ at 150 MeV. Oset, Weise, and Brockmann (54) have also calculated C_0 , obtaining $(0.96 + i\ 0.64) fm^6$ at threshold, $(1.20 + i\ 0.88) fm^6$ at 50 MeV. These numbers can be compared with those calculated by Riska et al., $C_0 = (0.287 + i\ 0.343) fm^6$ at threshold, $(0.373 + i\ 0.622) fm^6$ at 50 MeV, and $(1.20 + i\ 2.55) fm^6$ at 150 MeV.

Figure 13 shows the effect of the absorptive terms on the elastic scattering cross sections. Shown are calculations without

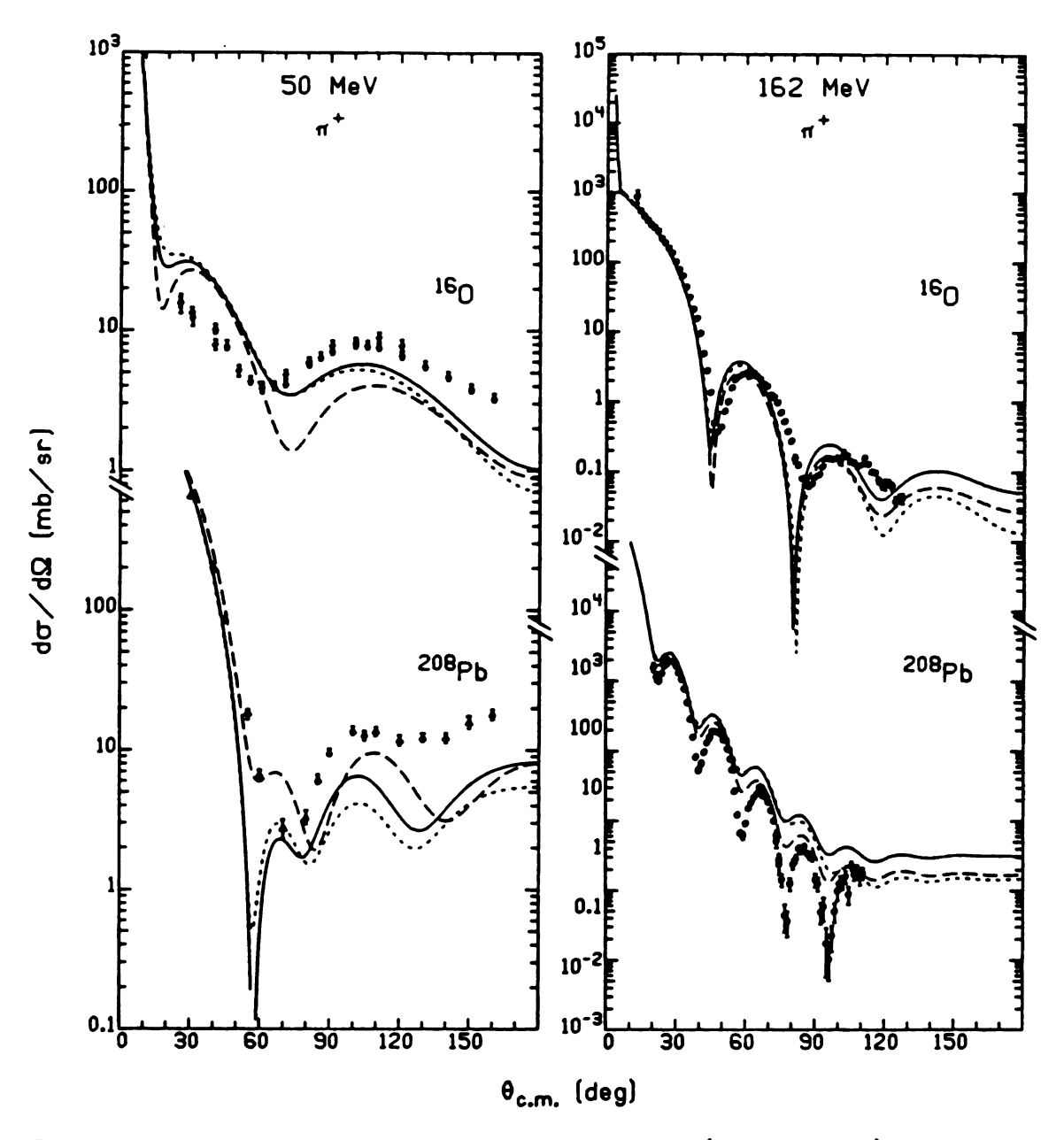


Figure 13. The effect of the absorption terms (solid curve) compared to calculations without these terms (dashed curve) and with the absorption terms included to first order only (dotted curve).

absorption (dashed curve), with absorption as discussed (solid curve), and with absorption included to first order only, i.e. with the C_0 term not included in the Ericson-Ericson effect but added separately (dotted curve). Clearly absorptive terms of the size calculated by Riska and collaborators are not negligible even in the resonance region. Although the absorption terms have both real and imaginary parts, most of the effect on the scattering cross sections is due to the imaginary parts both at low energies and in the resonance region. Near resonance the effect of the real parts is not seen at all except at very backward angles.

The reaction and total cross sections are not greatly changed by the inclusion of absorptive terms. The reaction cross section for 16 0 at 50 MeV increases by 30%; the total by 14%. For 208 Pb at 50 MeV the increase in the reaction cross section is only 7%; the total cross sections are nearly equal. The differences are much less pronounced at 162 MeV, with almost no difference at all for 208 Pb.

4. Pauli and Coulomb Corrections

Two corrections to the optical potential remain to be made. The first is due to the Pauli exclusion principle, limiting the intermediate states accessible to the struck nucleon. This correction has already been made for the isoscalar s-wave part by explicitly calculating the second order term which includes the Pauli correlations. The calculation of the corresponding p-wave term could only be made in second order, but the Ericson-Ericson effect includes

terms of all orders. Therefore this method is abandoned and the effect of the Pauli principle is approximated by reducing the imaginary parts of the parameters \mathbf{c}_0 and \mathbf{c}_1 by a factor Q which corresponds to the fraction of phase space available to the nucleon. This is also done for \mathbf{b}_1 , as the second order isovector term was not calculated.

The Pauli factor Q is taken from the Goldberger (55) classical calculation as given for pions by Landau and McMillan (56). The particles in the nucleus can be thought of as occupying a sphere in momentum space of radius $k_F = 1.36~{\rm fm}^{-1}$. When a pion of given momentum strikes a nucleon the nucleon may or may not gain enough momentum to displace it into the allowed momentum region outside the Fermi sphere. Q is the probability that for a given pion momentum the nucleon will scatter into the allowed region, averaged over nucleon initial momentum and scattering angle. Figure 14 shows Q as a function of pion kinetic energy. As expected, Q goes to zero at zero energy, as no states are accessible, and approaches one at high energies.

The absorption parameters also have imaginary parts; however, as the nucleons gain a large amount of momentum when the pion is absorbed, they are likely to be in unoccupied states. Therefore, no correction is made.

Figure 15 shows the effect of the Pauli corrections just discussed (solid curve) compared to calculations with no Pauli factor, i.e. Q = 1 (dashed curve). At 50 MeV Q = 0.31; at 162 MeV Q = 0.75.

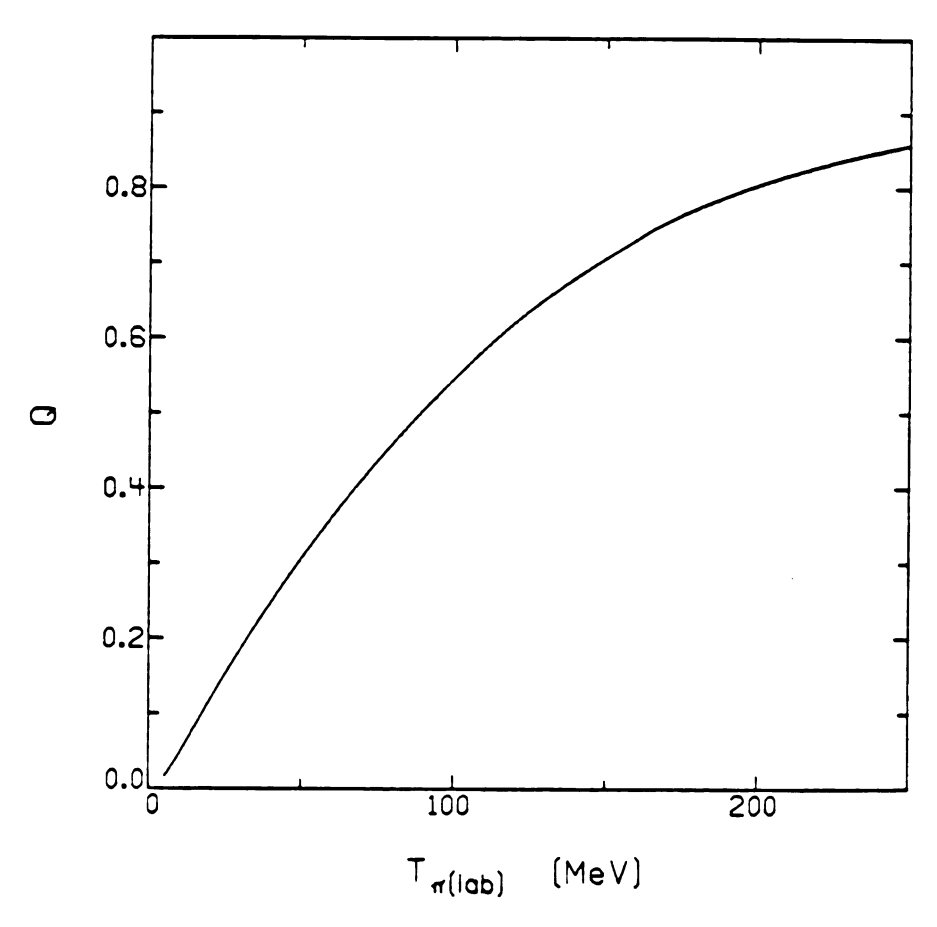


Figure 14. The Pauli factor Q as a function of pion lab kinetic energy.

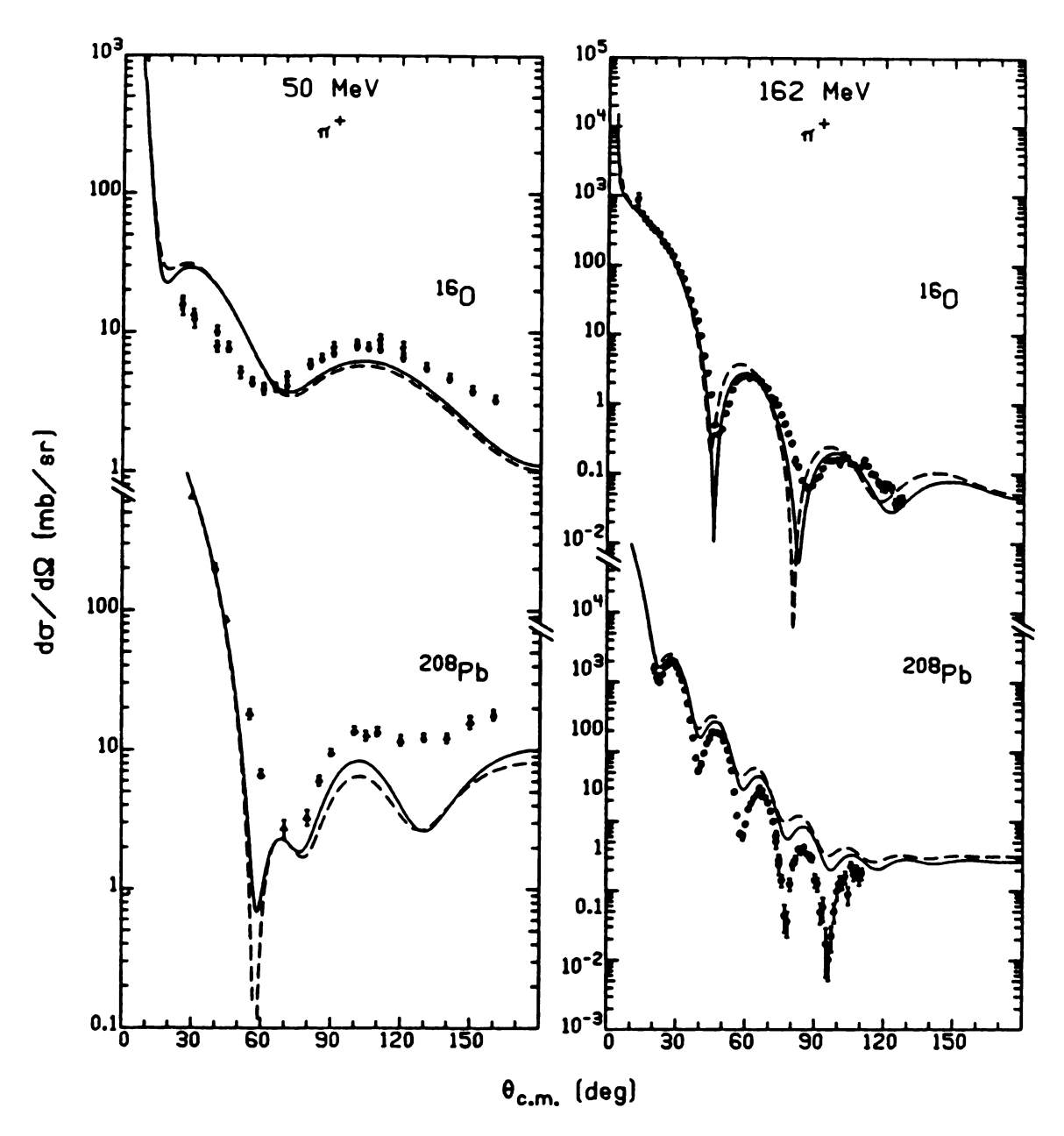


Figure 15. Comparison of calculations with (solid curve) and without (dashed curve) Pauli corrections.

Although the Pauli effect is larger at 50 MeV, the changes resulting from its inclusion are more pronounced at higher energies, where the scattering is more sensitive to the magnitude of the imaginary p-wave terms. As is evident in both Figures 13 and 15, the effect of increasing the imaginary part of the optical potential in the resonance region is to raise the differential cross section curve and make the minima shallower.

The second correction to be discussed is due to the Coulomb interaction. This correction is necessary because the electromagnetic part of the interaction was not treated consistently in the derivation of the optical potential; the Coulomb potential was ignored until the end of the calculation and then put back in. The needed correction can be considered in the following way: When a negative pion approaches the nucleus it is accelerated by the Coulomb field; a positive pion is decelerated. Thus positive and negative pions strike the nucleus with different effective energies. To account for this the scattering parameters are calculated at an energy different from the incoming pion energy by $\mathbf{E}_{\mathbf{C}}$, the magnitude of the Coulomb field at the nuclear surface, assuming the interaction is surface peaked. This Coulomb shift is an important effect for large nuclei in the resonance region. It is not so important for light nuclei and at low energies, where the parameters vary only slowly with energy. Values of $\mathbf{E}_{\mathbf{C}}$ for various nuclei are given in Table 2.

Table 2. The Coulomb energy shift $\mathbf{E}_{\mathbb{C}}$, evaluated at the nuclear surface, for various nuclei.

Nucleus	E _C (MeV)
4 _{He}	1.6
7 _{Li}	2.1
9 _{Be}	2.5
¹² C	3.4
160	4.2
²⁴ Mg	5.4
27 _{A1}	5.7
²⁸ Si	6.0
⁴⁰ Ca	7.6
⁵⁶ Fe	8.9
⁵⁸ Ni	9.5
⁹⁰ Zr	11.7
¹²⁰ Sn	13.3
208 _{Pb}	18.1

To illustrate the effect of the Coulomb shift, the elastic scattering of π^+ and π^- from 16 O and 208 Pb at 162 MeV is shown in Figure 16 with (solid curve) and without (dashed curve) the Coulomb shift in the energy of the parameters. The main effect of this is to deepen the minima for π^- and make them more shallow for π^+ . This is important, as the data for π^+ and π^- in the resonance region are quite similar, but the calculations give pronounced differences when the Coulomb shift is not included.

5. The Optical Potential

The various pieces can now be put together to give the full optical potential,

$$\begin{split} & 2 \overline{\omega} U_{\text{opt}}(r) = -4\pi \ p_1[\overline{b}_0 \rho(r) + \varepsilon_{\pi} b_1(\rho_p(r) - \rho_n(r))] + p_2 B_0 \rho^2(r) \\ & - \overline{\nabla} \cdot \left\{ \frac{p_1^{-1}[c_0 \rho(r) + \varepsilon_{\pi} c_1(\rho_p(r) - \rho_n(r))] + p_2^{-1} c_0 \rho^2(r)}{1 + \frac{4\pi}{3} \lambda \left\{ p_1^{-1}[c_0 \rho(r) + \varepsilon_{\pi} c_1(\rho_p(r) - \rho_n(r))] + p_2^{-1} c_0 \rho^2(r) \right\}} \right\} \overline{\nabla} \\ & + \frac{1}{2} (1 - p_1^{-1}) \overline{\nabla}^2[c_0 \rho(r) + \varepsilon_{\pi} c_1(\rho_p(r) - \rho_n(r))] \\ & + p_1 (1 - p_1^{-1})^2 c_0 \kappa(r) + \frac{1}{2} (1 - p_2^{-1}) \overline{\nabla}^2[c_0 \rho^2(r)] \end{split}$$

where all $\frac{1}{A}$ terms have been dropped. The parameters b_0 , c_0 , b_1 , and c_1 will be denoted single nucleon parameters, to distinguish them from the absorption parameters B_0 and C_0 . The parameters are

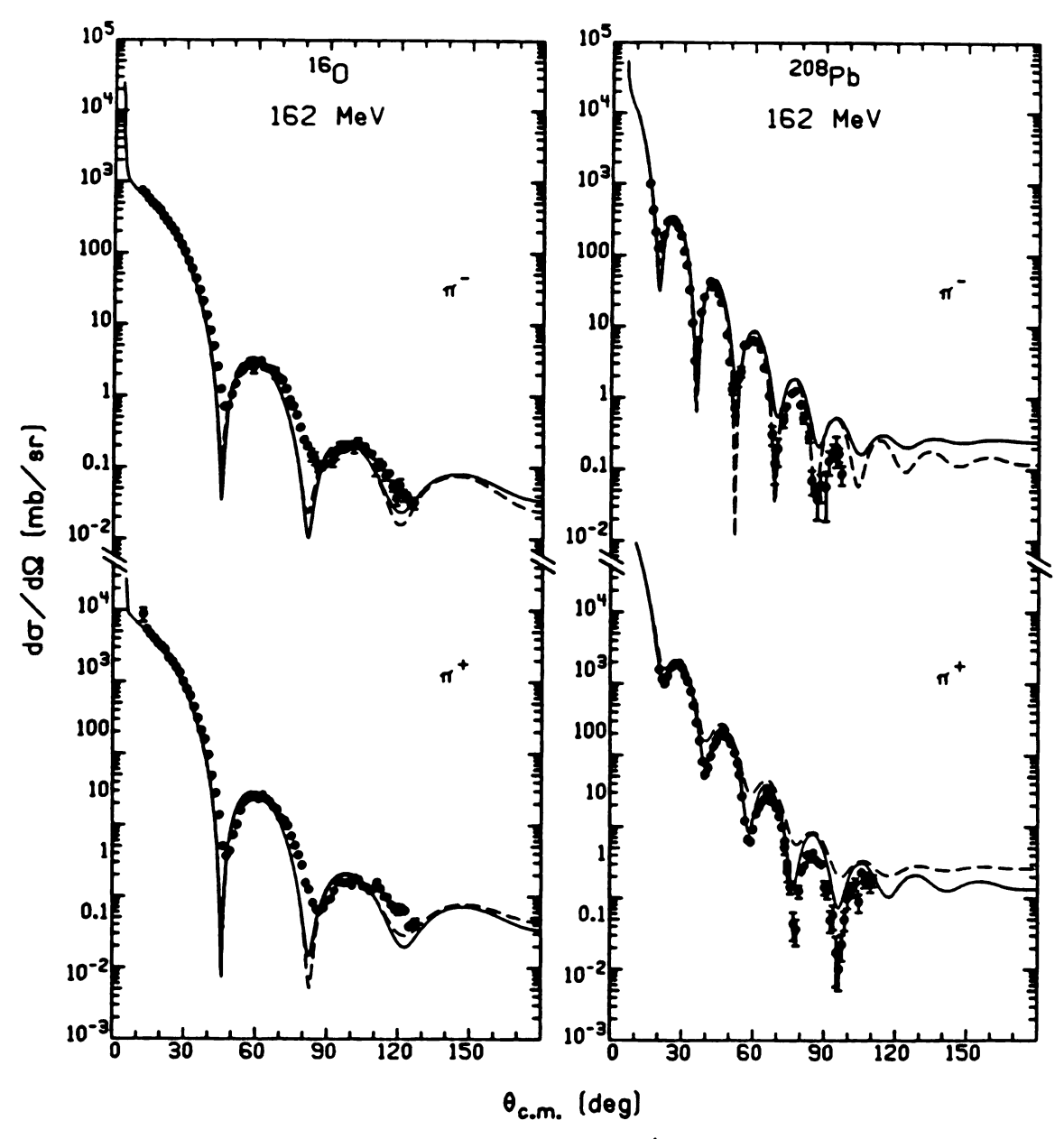


Figure 16. Comparison of calculations of π^+ and π^- scattering on $^{16}0$ and ^{208}Pb at 162 MeV with (solid curve) and without (dashed curve) the Coulomb shift. The references for the π^- data are the same as for the corresponding π^+ data.

to be calculated at the energy ω - $\epsilon_\pi E_C$. The imaginary parts of b_1 , c_0 , and c_1 are multiplied by the Pauli factor Q.

For all calculations the difference in radii between the proton and neutron distributions is ignored; thus $\rho_p(r) - \rho_n(r)$ can be replaced by $\frac{Z-N}{A}$ $\rho(r)$. The parameters of the charge distribution are taken from the available tables (57,58). For the light nuclei the matter distributions are obtained from the charge distributions by adjusting the size parameter such that

$$R_m^2 = R_c^2 - 0.64 \text{ fm}^2$$
, (III-77)

where R is the radius of the equivalent uniform distribution, $R^2 = \frac{5}{3} < r^2 >$. The density forms and parameters for various nuclei are given in Table 3.

This completes the construction of the optical potential.

The next three chapters will deal with the calculation of various experimental quantities using the potential equation III-76.

Table 3. The forms and parameters of the matter and charge density distributions for various nuclei.

$\rho^{\alpha}(1 + \alpha)$	$\frac{r^2}{a^2}$)e $-r^2/a^2$	$\rho_{c}^{\alpha}(1 + \alpha)$	$\rho_{c}^{\alpha}(1 + \alpha \frac{r^{2}}{a_{c}^{2}})e^{-r^{2}/a_{c}^{2}}$	
	a(fm)	a _c (fm)	α	
7 _{Li}	1.67	1.77	.327	
¹² c	1.57	1.66	1.33	
160	1.75	1.83	1.54	
ρ∝ρ	c ^c [1 + e ^{(r-R)/2}	z]-1		
	R(fm)	z(fm)		
27 _{A1}	3.07	.519		
40 _{Ca}	3.51	.563		
⁵⁶ Fe	3.97	.594		
63 _{Cu}	4.21	.586		
⁹⁰ Zr	4.83	.496		
¹²⁰ Sn	5.32	.576		
208 _{Pb}	6.46	.549		

CHAPTER IV

PIONIC ATOM LEVELS

Measured pionic atom level shifts and widths provide an important test of the optical potential at essentially zero pion kinetic energy, as the data furnish information about the overall strengths of the s and p-wave parts of the real and imaginary potential. As several approximations were made in the low energy limit, the potential form should be most reliable at zero energy. The parameters derived from πN phase shifts are not well known at low energies, however; the values used in this analysis are taken from the Rowe, Salamon, and Landau (RSL) fit (25), extrapolated to zero energy, and are known only within rather large error bars.

Pionic atom calculations are not new; however, a new analysis is worthwhile and necessary because the data has improved greatly in quality in the last few years, because the form of the optical potential used in the present analysis is slightly different from that used in earlier analyses, and because detailed calculations of λ and the absorption parameters are available for the first time. It will be found that the optical potential derived in the previous chapter, with parameters taken from the sources indicated there, does not reproduce the pionic atom data. However, the form can be used with fitted parameters to give an excellent description of the data.

The first section of this chapter describes the general features of pionic atom levels. The details of the calculations of level shifts and widths are discussed briefly in Section 2. The results of calculations with the optical potential as derived, and the same optical potential but with fitted parameters, are discussed in Section 3.

1. General Features

A pionic atom is an atom in which a negative pion is bound in the Coulomb potential of the nucleus in the place of an electron. Because of its large mass, the pion orbitals are much closer to the nucleus; the pion Bohr radius is $\frac{m_e}{m_\pi} \approx \frac{1}{275}$ times the electron Bohr radius. Thus, in the lower orbitals the pion is close enough to interact strongly as well as electromagnetically with the nucleus. This causes a shift in and broadening of the energy levels relative to the positions and widths to be expected from the electromagnetic interaction alone.

The energy shifts and widths are obtained from measurements of the pion transition x-rays. As the strong interaction effects are largest for the lowest & states, in which the pion is closest to the nucleus, most of the difference between measured and electromagnetic transition energies and widths is due to the lower state. The general features of the data are evident in Table 4, which gives the calculated electromagnetic energy of the transition, experimental s-wave shifts and widths from Ref. 59, and experimental p-wave shifts and widths from Ref. 60. Some d and f wave levels have been measured

Table 4. Experimental pionic atom energy level shifts and widths in keV from Refs. 59 and 60.

		<u>s-wave</u>	
Nucleus	$(E_p - E_s)_{EM}$	ΔE _s (exp)	Γ _s (exp)
10 _B	68.714	- 2.977 ± 0.085	1.59 ± 0.11
¹² c	99.066	- 5.874 ± 0.092	3.14 ± 0.12
14 _N	134.740	- 9.915 ± 0.144	4.34 ± 0.24
¹⁶ 0	175.413	-15.03 ± 0.24	7.64 ± 0.49
19 _F	220.952	-24.46 ± 0.35	9.4 ± 1.5
²⁰ Ne	270.952	-33.34 ± 0.50	14.5 ± 3.0
23 _{Na}	327.131	-49.93 ± 0.71	10.3 ± 4.0
		p-wave	
Nucleus	$(E_d - E_p)_{EM}$	ΔE _p (exp)	Γ _p (exp)
²⁷ A1	87.270	0.201 ± 0.009	0.120 ± 0.007
²⁸ Si	101.283	0.308 ± 0.010	0.192 ± 0.009
³² s	132.510	0.635 ± 0.016	0.422 ± 0.018
40 _{Ca}	207.674	1.929 ± 0.014	1.590 ± 0.023
⁵⁶ Fe	352.356	4.368 ± 0.088	6.87 ± 0.21
63 _{Cu}	439.016	6.67 ± 0.24	11.4 ± 0.8
⁶⁴ Zn	469.995	6.44 ± 0.33	12.4 ± 1.4

also (61), but will not be discussed here. As might be expected, the level shifts and widths increase with increasing Z. The s-wave shifts are negative, indicating a repulsive s-wave interaction; the p-wave shifts are positive, indicating an attractive p-wave potential.

In the calculation of pionic atom shifts and widths the various parts of the optical potential are correlated with the measured quantities: the values of the real s- and p-wave optical potential parameters determine the s- and p-wave level shifts, and the imaginary parameters determine the corresponding widths, to a good approximation. As there are only four independent quantities to be measured, only four optical potential parameters can be determined corresponding to the overall real and imaginary s- and p-wave strengths. Thus $Re(b_0)$ and $Re(B_0)$ cannot both be determined, nor can $Re(c_0)$ and $Re(C_0)$ from data on one nucleus. Although it is possible in principle that certain combinations of these related parameters reproduce the A dependence of the data better than others, in practice all reasonable combinations give similar results. That is, the combination $\operatorname{Re}(b_0)\rho(r) + \operatorname{Re}(B_0)\rho^2(r)$ acts like $[\operatorname{Re}(b_0) + \operatorname{Re}(B_0)\rho_{av}]\rho(r)$ with ρ_{av} independent of A. The same is true for the p-wave parameters. Although there are correlations between particular parameters or combinations of parameters and particular measured quantities, there is a fair amount of mixing. Some of this is due to the kinematics, which introduce s-wave terms with p-wave coefficients, some to the Ericson-Ericson effect which mixes real and imaginary terms

in the p-wave. Even without these, however, the s-wave optical potential strength affects the p-wave quantities, and to a lesser extent, vice versa.

It was evident from early measurements of pionic atoms that the first order optical potential with parameters determined from phase shifts could not describe the data. The calculated s-wave strength was too small, the p-wave strength was too large, and the widths could not be explained at all, as the imaginary parts of the single nucleon parameters are zero. This was the original motivation for the calculation of the second order s-wave term, the Ericson-Ericson effect, and the s- and p-wave true pion absorption terms.

2. Details of the Calculations

The pionic atom level shifts and widths were calculated using the program MATOM written by R. Seki (62). This is a position space code which sets up and solves the eigenvalue equation for the pion wavefunction, obtaining the complex eigenvalue corresponding to the energy and width of a given state. The wave equation is first reduced to an equation in r only, noting that the optical potential is independent of angle for a spherical nucleus,

$$u_{\ell}^{"} + f(r)u_{\ell}^{'} + [g(r) - \frac{\ell(\ell+1)}{r^2}]u_{\ell} = 0$$
 (IV-1)

where

$$f(r) = \frac{c'(r)}{c(r) - 1}$$
 (IV-2)

and

$$g(r) = (1 - c(r))^{-1} \{ \frac{c'(r)}{r} + \omega^2 - m^2 - 2\overline{\omega}V_C + V_C^2 - b(r) \}$$
 (IV-3)

with b(r) and c(r) the s- and p-wave terms of the optical potential,

$$2\overline{\omega}U_{\text{opt}}(r) = b(r) + \nabla \cdot c(r)\nabla . \qquad (IV-4)$$

The first derivative term in equation IV-1 is eliminated by a change of variables,

$$y(r) = (1 - c(r))^{\frac{1}{2}}u(r)$$
 (IV-5)

and the equation becomes

$$y'' + \left\{\frac{1}{4}\left(\frac{c'}{1-c}\right)^2 + \frac{1}{2}\frac{c''}{1-c} - f\right\}y = 0$$
 (IV-6)

where

$$f = \omega^2 - m^2 - 2\overline{\omega}V_C + V_C^2 - b(r) - \frac{\ell(\ell+1)}{r^2}$$
 (IV-7)

Equation IV-6 is set up in the nuclear interior and exterior, with a matching radius chosen to be well outside the range of the strong interaction. A guess is made of the eigenenergy ω and the equation is integrated in from infinity and out from zero using Milne's predictor-corrector method (63), with the two wavefunctions compared

at the match point. A new energy guess is made from the size of the mismatch and the process repeated until convergence is reached. The number of nodes is checked against the number proper to the state being calculated at the end of each iteration and a correction to the energy guess is made accordingly. The program includes electromagnetic effects due to the finite charge distribution of the nucleus, vacuum polarization, and electron screening.

The program has been modified to include the full optical potential, equation III-76. One defect has not yet been remedied, however; only one form for the nuclear density is available, the Woods-Saxon form. It was therefore necessary for small nuclei to derive the size parameters from the experimental rms radius and skin thickness.

3. Calculated Shifts and Widths

Calculations of shifts and widths for the nuclei listed in Table 4 have been performed using the optical potential equation III-76 with single nucleon parameters derived from the RSL phase shifts and the absorptive parameters of Riska and collaborators. Two different values of the parameter λ were used, the Ericson-Ericson value (10), λ = 1, and a value in the range suggested by Weise (48) and Brown (47), λ = 1.6. The results are shown in Figure 17, where the lines are simply drawn from one calculated point to the next. The dashed line corresponds to λ = 1, the dotted to λ = 1.6. It is not possible to say with certainty what parameter changes are necessary to bring the curves to the data, but it appears that the

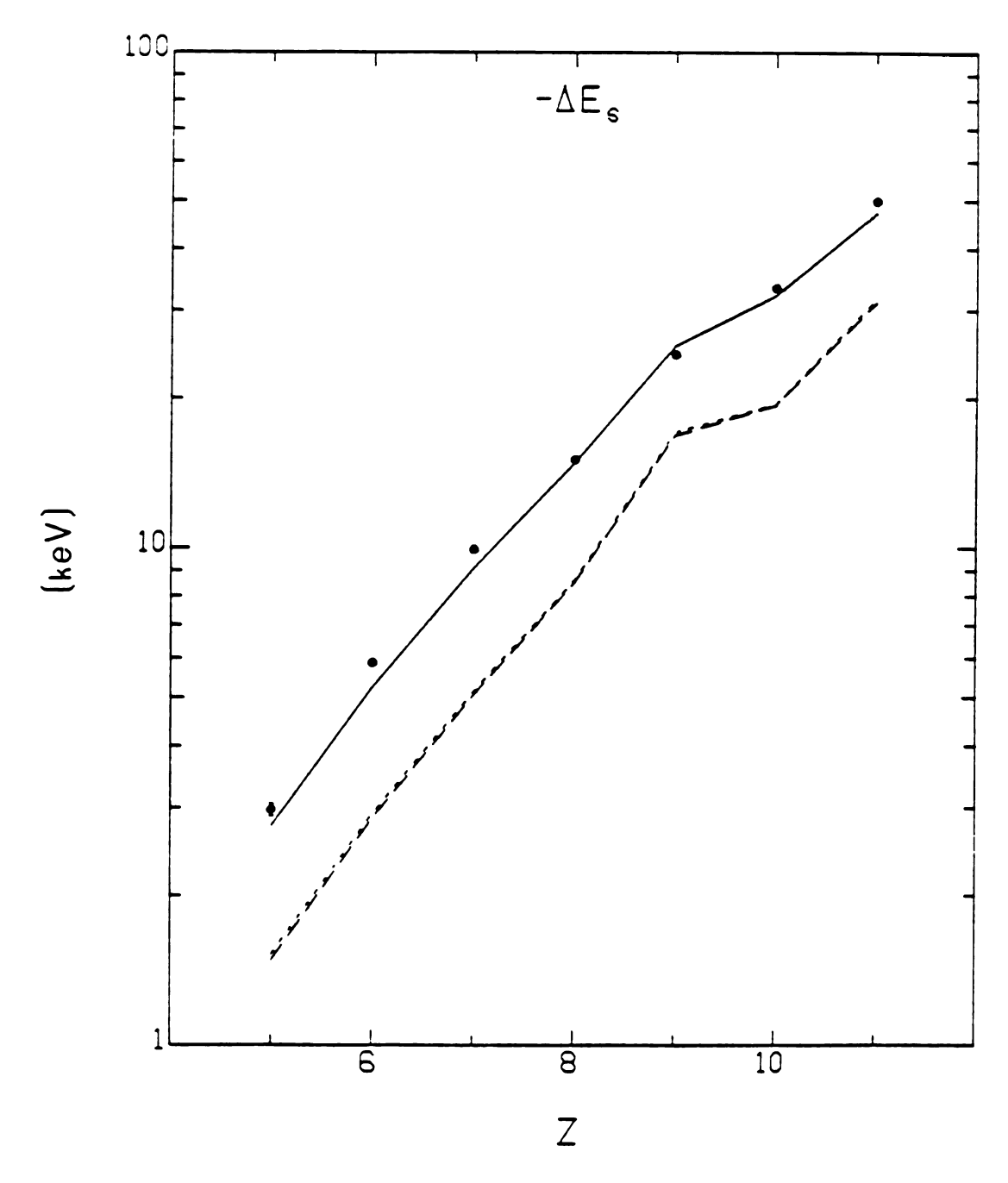


Figure 17a. Calculations of the s-wave shift as a function of Z compared to the experimental data, with the parameters of set 1 of Table 5 with λ = 1 (dashed line), λ = 1.6 (dotted line), and with the parameters of set 2 (solid line). Data are from Ref. 59.

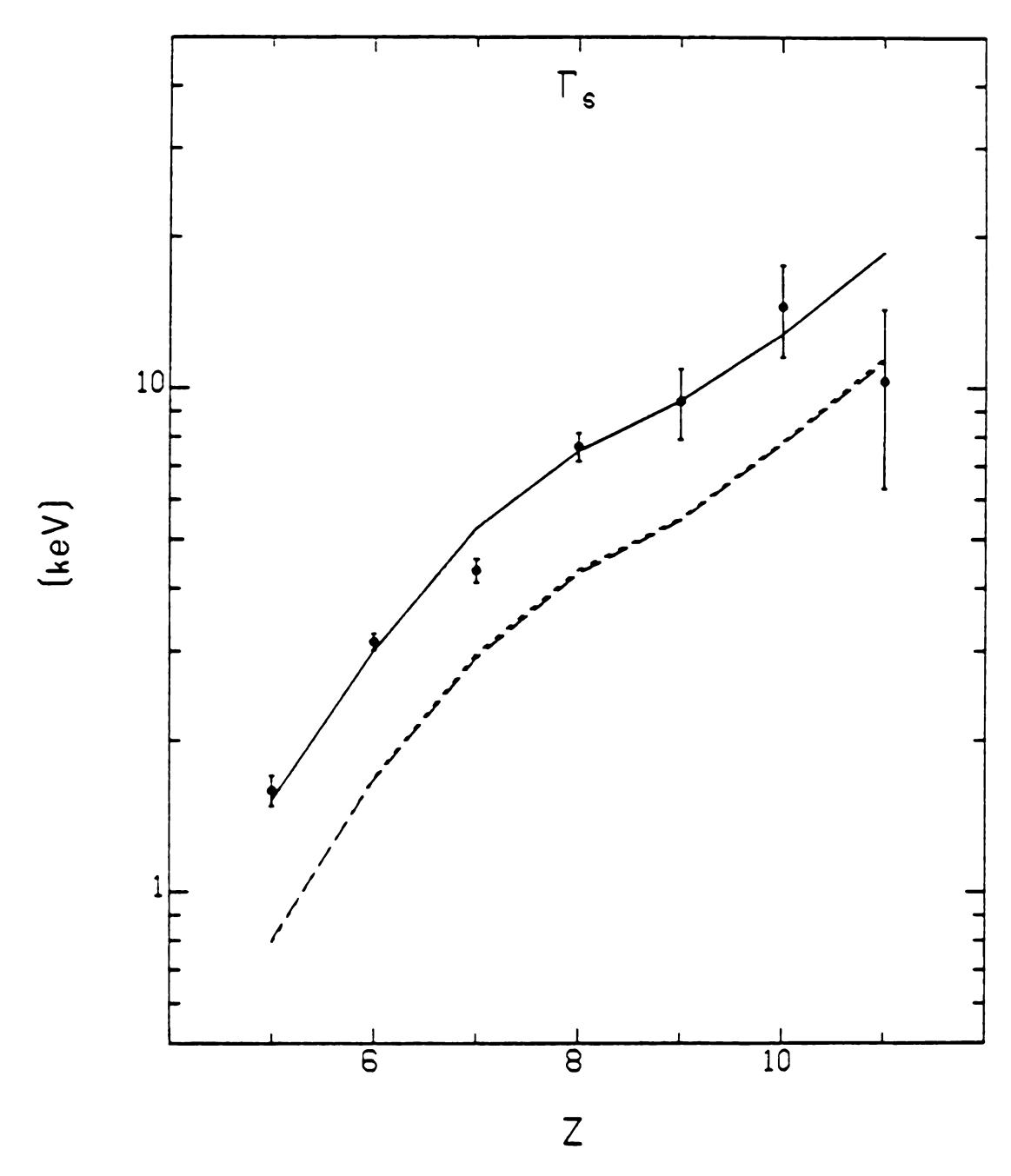


Figure 17b. Calculations of the s-wave width. Data are from Ref. 59.

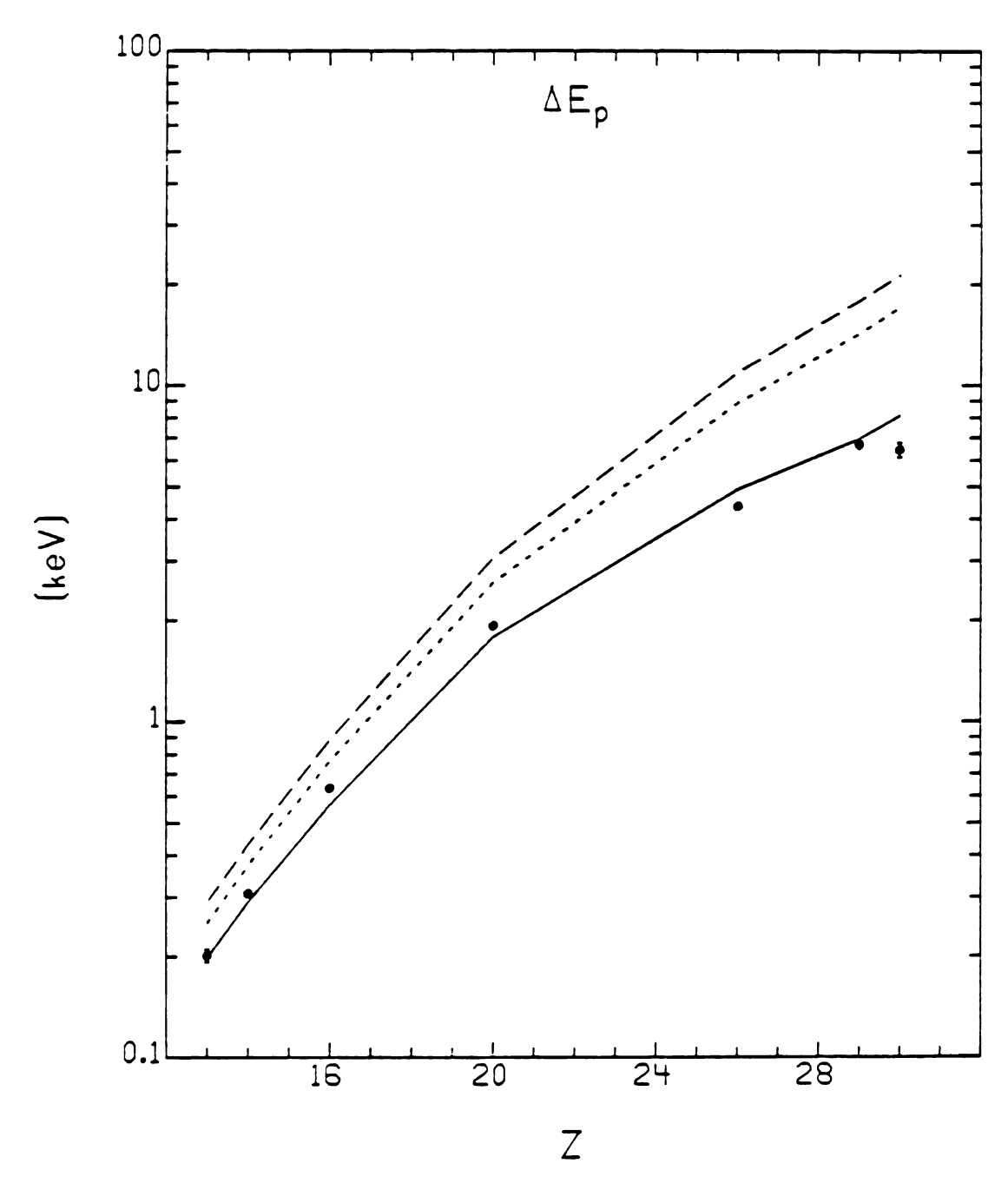


Figure 17c. Calculations of the p-wave shift. Data are from Ref. 60.

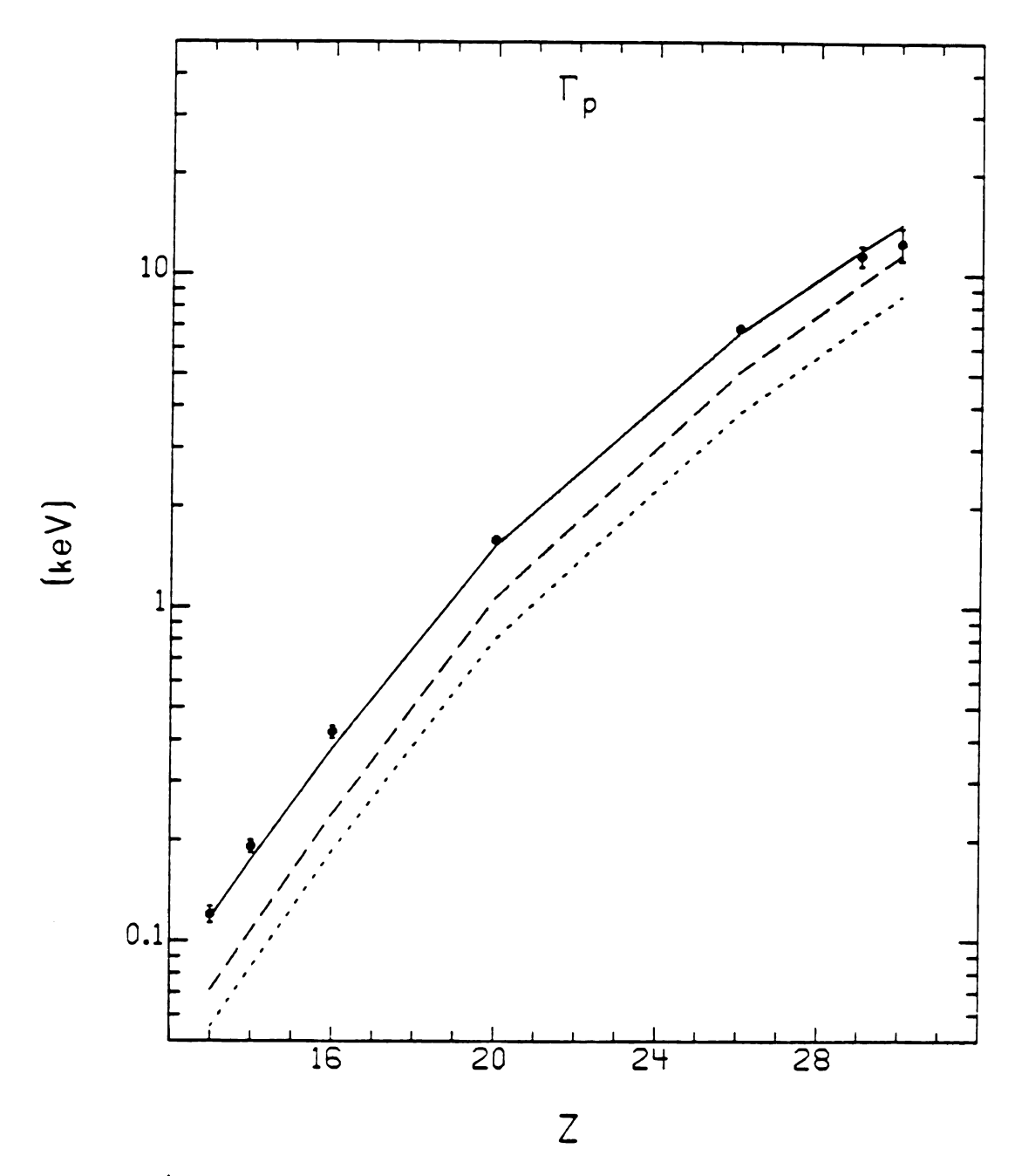


Figure 17d. Calculations of the p-wave width. Data are from Ref. 60.

s-wave is not repulsive enough, while the p-wave is too attractive, especially for the value λ = 1. The s- and p-wave absorption strengths appear to be too weak.

A fit was then made to the data, varying the parameters $Re(b_0)$, $Re(c_0)$, $Im(B_0)$, and $Im(C_0)$. No attempt was made to minimize the χ^2 ; the fit was done only in order to give some idea what parameter changes were necessary to give reasonable results. The parameters thus obtained are given as set 2 in Table 5 along with the parameters of the first calculation, set 1. The results with the fitted parameters are shown as the solid curve in Figure 17. The calculated quantities follow quite well the A dependence of the data, except for the p-wave shift for the larger nuclei. This deviation is not surprising, as the isovector parameters were not fitted. Comparison of the numbers in Table 5 indicates that the parameters $\operatorname{Re}(\mathbf{b}_{\Omega})$, $Im(B_0)$, and $Im(C_0)$ must be increased greatly in magnitude in order to reproduce the data. The parameter $Re(c_0)$ must be increased slightly, although the required value is well within the error bars of the value given by RSL for c_0 at zero energy. Alternatively the RSL value for c_0 can be used if λ is reduced to λ = 1.5, with a corresponding small decrease in $\operatorname{Im}(\mathsf{C}_0)$. Although the discrepancies between the required single nucleon parameters and their phase shift values can be resolved by assuming different values for $\operatorname{Re}(\mathsf{B}_0)$ and $Re(C_0)$, no such remedy exists for the imaginary parameters, except to the extent that $Im(C_{\Omega})$ is sensitive to the value of λ . The one nucleon absorption mechanism, not included in the optical potential,

Table 5. Parameters used in the pionic atom calculations.

		Rea1	Imaginary
Set 1	b ₀ (fm)	-0.029	0.
	b ₁ (fm)	-0.13	0.
	$B_{O}(fm^4)$	0.007	0.08
	$c_0^{(fm^3)}$	0.65	0.
	$c_1^{(fm^3)}$	0.43	0.
	C _O (fm ⁶)	0.29	0.34
	λ	1.0 or 1.6	
Set 2	b ₀ (fm)	-0.050	0.
	b ₁ (fm)	-0.13	0.
	$B_{O}(fm^4)$	0.007	0.19
	$c_0^{(fm^3)}$	0.66	0.
	$c_1^{(fm^3)}$	0.43	0.
	C _O (fm ⁶)	0.29	0.90
	λ	1.6	

is not large enough to make up the difference; it is estimated at not more than 30 percent of the two nucleon strength (64). Thus there is a real discrepancy at zero energy of about a factor of two between the absorption parameters calculated by Riska and collaborators and those required to fit the pionic atom widths. Other calculations of these quantities are somewhat nearer the fitted values: Hachenberg and Pirner (52) obtain $Im(B_0) = 0.144 \text{ fm}^4$; Oset, Weise, and Brockmann (54) calculate $Im(C_0) = 0.64 \text{ fm}^6$. This is clearly a subject which requires further investigation.

The fitting procedure was also carried out for $\lambda=1$ so that comparisons could be made with previous work. Comparison is still difficult because of the $\nabla^2\rho$, $\nabla^2\rho^2$, and $\kappa(r)$ terms in the optical potential used here, which have not been included in other analyses. The effect of these terms is to decrease the s-wave repulsion, thus requiring a more negative $\text{Re}(b_0)$ to compensate. It is clear that the value of the p-wave absorption parameter thus obtained, $\text{Im}(C_0)=0.77~\text{fm}^6$, is smaller than that obtained by, for instance, Krell and Ericson (45) in their fits, $\text{Im}(C_0)=1.12~\text{fm}^6$, and used in the calculations of Ref. 24. Krell and Ericson give an alternate value, which gives better results for certain nuclei in their sample, $\text{Im}(C_0)=0.56~\text{fm}^6$. Fortunately the recent p-wave data is much better than that available to Krell and Ericson, making a more definitive result possible.

From the calculations it can be seen that the objective has not yet been reached; the optical potential with parameters from

theoretical predictions does not reproduce the data. The deficiency in the s-wave repulsion is an unsolved problem, and will appear also in the low energy elastic scattering calculations. The inadequacy of the absorption parameters is a less serious matter, requiring further refinements in the calculations and a more careful treatment of the LLEE effect including absorption and multiple scattering on an equal footing. It is encouraging that the A dependence of the data is reproduced by the optical potential with fitted parameters. Because the theoretical parameters vary slowly with energy in the range zero to 50 MeV, the information gained from the pionic atom analysis is also relevant for the low energy scattering calculations to be discussed in the next chapter.

CHAPTER V

ELASTIC SCATTERING CROSS SECTIONS

In this chapter the pion-nucleus elastic differential cross sections calculated using the optical potential equation III-76 are discussed and comparisons are made to the existing data. The energy region considered in this study, 0-250 MeV, will be divided into two regions: the low energy region, defined roughly as 0-50 MeV, and the resonance region, around 180 MeV. The elastic scattering cross sections from these two energy ranges have quite different characteristics. The low energy scattering shows evidence of interference between the s-wave, p-wave, and Coulomb amplitudes; the real parts of the optical potential are most important. In the resonance region the scattering has a diffractive character, due to the large imaginary part of the p-wave optical potential. The scattering cross sections for energies between these two regions have some characteristics of both.

The data in the low energy region at present consists of cross sections for π^+ on various targets at 30, 40, and 50 MeV. Unfortunately there is as yet very little π^- data, only on ^{12}C and ^{208}Pb at 30 MeV. There is no data for pion energies below 30 MeV. Between 50 and 100 MeV there are measurements of π^+ on ^{16}O and ^{208}Pb at 80 MeV. Above 100 MeV there is an abundance of π^+ and π^- scattering data from various nuclei, clustered about the energies 115, 162,

180, and 240 MeV. A characteristic sample of these data will be compared with the theoretical calculations.

The first section of this chapter describes in a simple model the general features of the low energy elastic scattering cross sections. Section 2 includes a model for diffraction scattering, relevant to scattering in the resonance region. In Section 3 the computer program used for the calculations is briefly described. Finally, the theoretical and experimental differential cross sections are compared in Sections 4 and 5.

1. General Features--Low Energy Scattering

The low energy elastic scattering cross sections are characterized chiefly by the interference between the s- and p-wave amplitudes, the strengths of which are determined by the real parts of the optical potential parameters, and the Coulomb amplitude. This can be seen most easily in Born approximation. As was noted in Section 2 of Chapter III, the second order p-wave term in the Born series is suppressed due to short range correlations. Therefore the Born approximation with a potential which includes only the first order p-wave terms should give a good approximation to the scattering from the full p-wave part of the optical potential including the Ericson-Ericson effect. For an N = Z nucleus the amplitude in Born approximation for scattering from the simple first order optical potential equation II-53 is

$$f_{\pm} = [b_0 + c_0 k^2 \cos \theta] \rho(q) + \frac{2\omega\alpha}{a^2} \rho_c(q)$$
 (V-1)

where the + or - refers to the pion charge and α is the fine structure constant. This can be rewritten

$$f_{\pm} = C[\pm \frac{1}{\sin^2 \frac{\theta}{2}} + 4y^2 \sin^2 \frac{\theta}{2} - 2y^2(1 - x)]$$
 (V-2)

with C = $-\frac{2\omega\alpha}{4k^2}$, x = $-\frac{b_0}{k^2c_0}$, and $y^2 = \frac{c_0k^4}{\omega\alpha}$. Thus, y measures the relative strength of the p-wave and Coulomb potentials and x measures the strength of the s-wave repulsion relative to the p-wave attraction. The nuclear and charge form factors $\rho(q)$ and $\rho_C(q)$ have been ignored in equation V-2, as they decrease only slowly over the range of q^2 relevant for a light nucleus and low pion energy. For 50 MeV pions, the RSL phase shift values for the real parameters are $\text{Re}(\overline{b}_0)$ = -0.042 fm and $\text{Re}(c_0)$ = 0.75 fm³, giving C = -0.0083 fm, x = 0.13, and y = 4.4. The parameters derived from the fit to pionic atoms give the values x = 0.18, y = 4.1 at 50 MeV, assuming the energy dependence of the parameters can be ignored. The behavior of f is considered separately for π^+ and π^- .

For positive pions f has a minimum at $\sin^2\frac{\theta}{2}=\frac{1}{2y}$; thus the position of the minimum is determined only by the p-wave strength. For the RSL value of c_0 this gives $\theta \cong 39^\circ$. The zeros of f are given by

$$\sin^2 \frac{\theta}{2} = \frac{1}{4} \{ (1 - x) \pm [(1 - x)^2 - \frac{4}{y^2}]^{\frac{1}{2}} \}$$
 (V-3)

For y < 2 there are no zeros. For y > 2 two zeros exist for $x < 1 - \frac{2}{y}$, none for $x > 1 - \frac{2}{y}$. This behavior is illustrated in

Figure 18 which shows f_+ (upper left) as a function of x. Here the parameters were arbitrarily chosen to be y = 5 and x = 0.4, 0.6, and 0.8. The square of this amplitude (bottom left) indicates how changes in the s-p interference parameter x produce one minimum, which, with decreasing x, broadens, then becomes two minima separated by a hump.

For negative pions f is monotonically increasing with $\boldsymbol{\theta}$ and has a zero at

$$\sin^2 \frac{\theta}{2} = \frac{1}{4} \{ (1 - x) + [(1 - x)^2 + \frac{4}{y^2}]^{\frac{1}{2}} \}$$
 (V-4)

For the RSL values of the parameters this gives $\theta = 86^{\circ}$. The amplitude f_{-} is also shown as a function of x in Figure 18 (upper right) along with $|f_{-}|^2$ (lower right). Note that the position of the zero of f_{-} becomes the position of the minimum in the differential cross section, and thus depends on both the s- and p-wave strengths.

The full Born amplitude, neglecting the $\kappa(r)$ term, is given by

$$F_{B} = [p_{1}\overline{b}_{0} + p_{1}^{-1}c_{0}\underline{k}\cdot\underline{k}' - \frac{p_{1}-1}{2p_{1}}c_{0}q^{2}]\rho(q)$$

$$+ [p_{2}B_{0} + p_{2}^{-1}C_{0}\underline{k}\cdot\underline{k}' - \frac{p_{2}-1}{2p_{2}}C_{0}q^{2}]\rho^{2}(q)$$

$$- p_{1}^{-1} \frac{2\omega\varepsilon_{\pi}^{\alpha}}{\sigma^{2}} \rho_{c}(q) . \tag{V-5}$$

The Ericson-Ericson effect is not included, as noted above. Figures 19 and 20 show calculations for π^+ and π^- scattering from 12 C.

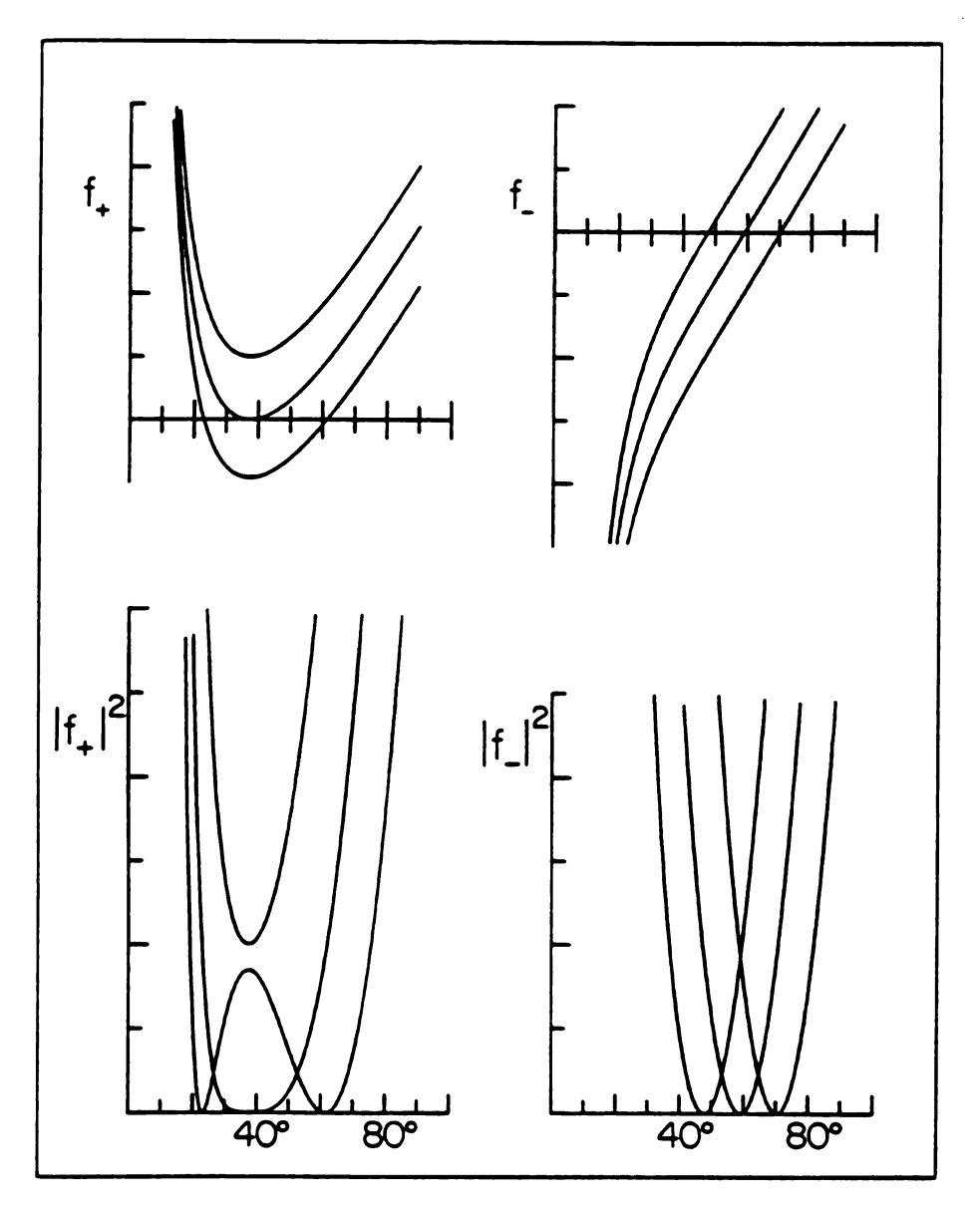


Figure 18. Amplitudes and corresponding cross sections for the first order real optical potential in Born approximation. The vertical scales are arbitrary.

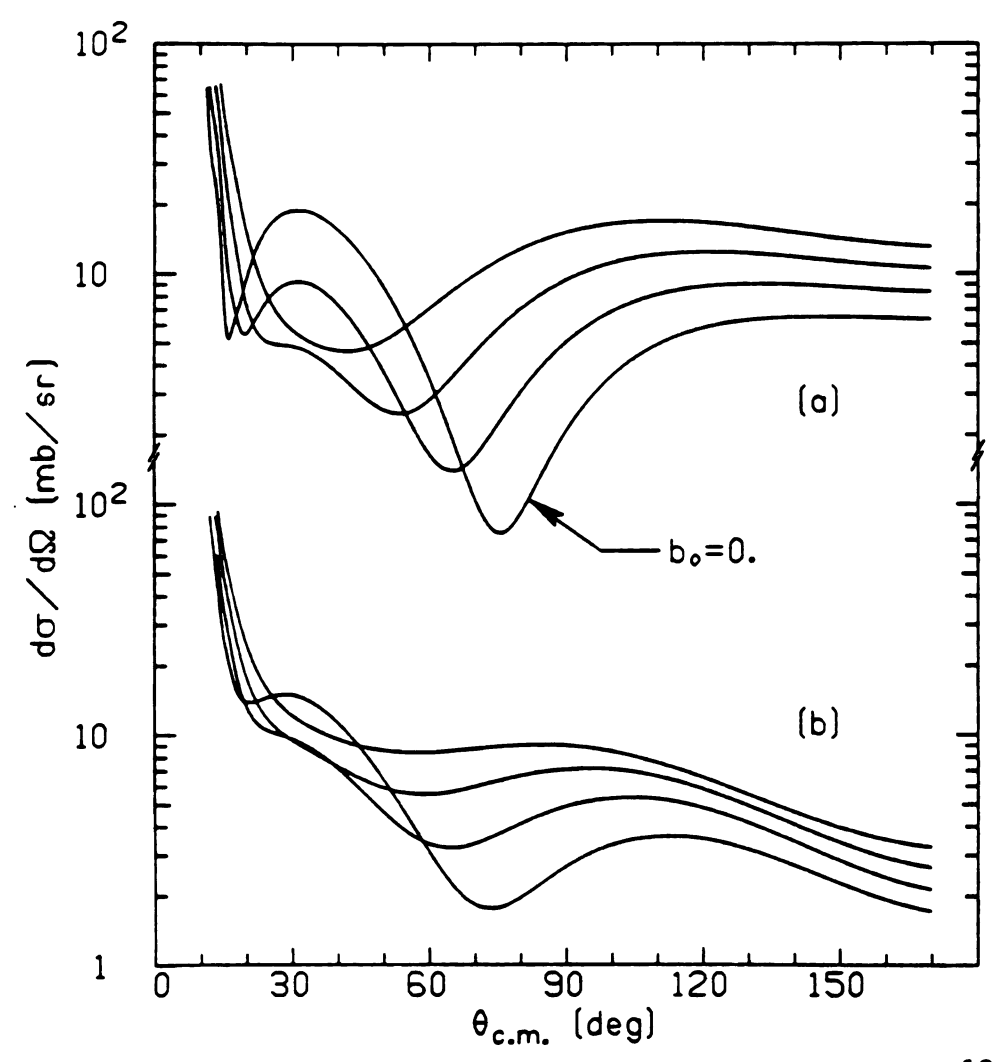


Figure 19. Elastic scattering cross sections for 50 MeV π^+ on ^{12}C with (a) the full Born amplitude and (b) the full optical model calculation, for $\text{Re}(\overline{b}_0)$ = 0., -0.04 fm, -0.08 fm, and -0.12 fm.

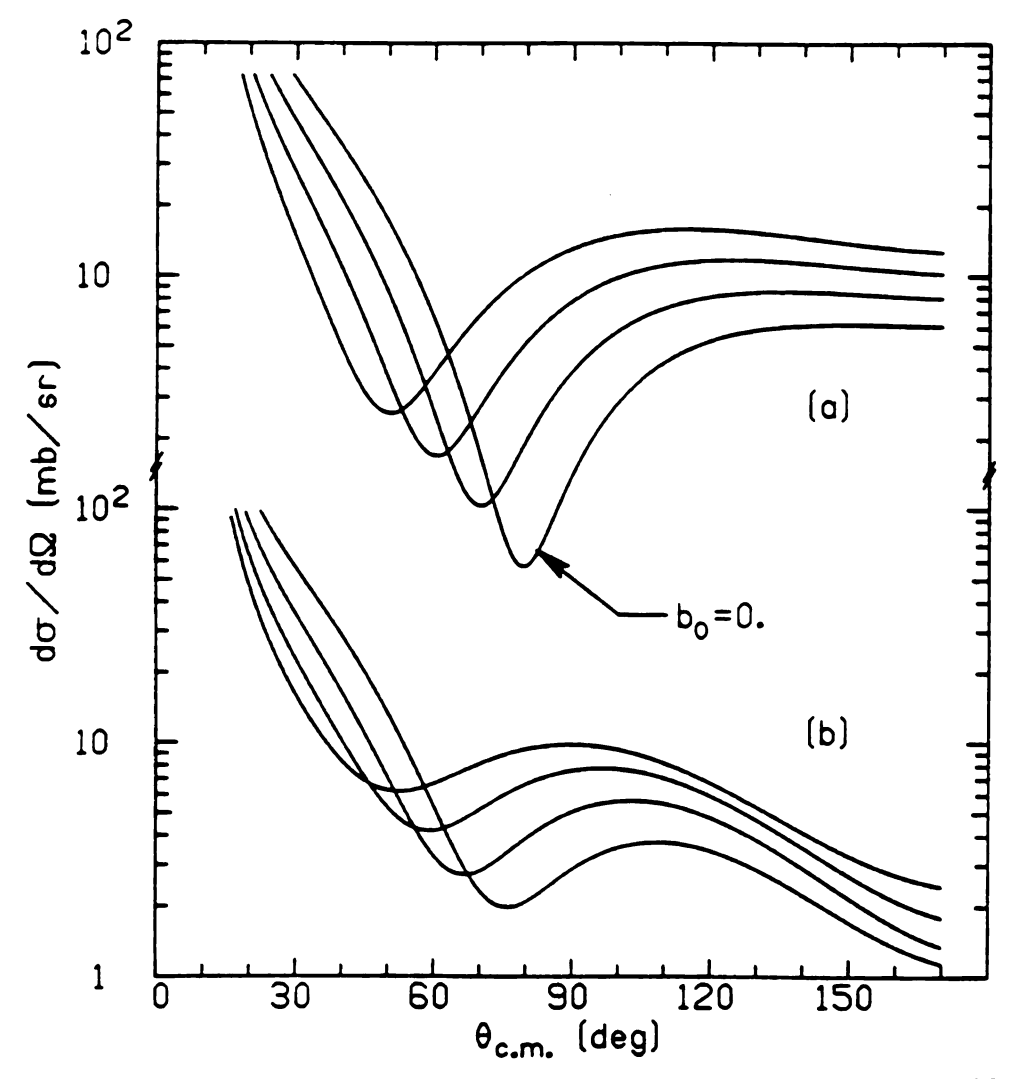


Figure 20. Elastic scattering cross sections for 50 MeV π^- on ^{12}C with curves same as in previous figure.

The curves labeled (a) are Born approximation calculations with reasonable values of the optical potential parameters and $\text{Re}(\overline{b}_0)$ = 0.,-0.04 fm,-0.08 fm, and-0.12 fm. The curves labeled (b) are the full calculations, with the optical potential equation III-76 minus the $\kappa(r)$ term, and the same parameters as were used in calculations (a). It can be seen that the characteristic interference effects persist when the kinematic and absorption terms are added to the Born amplitude, and in the full calculation. Although the imaginary part of the optical potential has some effect, the differential cross sections are most sensitive to the overall real s-wave and p-wave strengths.

2. General Features--Resonance Region Scattering

Because the imaginary part of the p-wave optical potential is large in the resonance region, the nucleus appears nearly "black" to the pion. This gives rise to differential cross sections with a distinctive shape, known as diffractive or shadow scattering.

A semiclassical description can be given for this type of elastic scattering (65). Assume that the nucleus is completely absorbing, so that all pions with impact parameters smaller than R, the radius of the nucleus, are absorbed; those with impact parameter greater than R are transmitted. The scattering amplitude can be written

$$f(\theta) = \sum_{\ell} (2\ell + 1) \frac{\eta_{\ell} - 1}{2ik} P_{\ell}(\cos \theta)$$
 (V-6)

where complete absorption is characterized by $\eta=0$, complete transmission by $\eta=1$. The impact parameter b can be expressed in terms of the angular momentum of the incoming pion, so that $\eta_{\ell}=0$ for $\ell \leq kR$, $\eta_{\ell}=1$ for $\ell > kR$. The differential cross section is just the square of f,

$$\frac{d\sigma}{d\Omega} = \frac{1}{k^2} \left| \sum_{\ell=0}^{kR} (\ell + \frac{1}{2}) P_{\ell}(\cos \theta) \right|^2. \tag{V-7}$$

Assuming kR large and the angular range small, the discrete variable ℓ becomes continuous, $\ell + \frac{1}{2} \rightarrow kb$, and $P_{\ell}(\cos \theta)$ is approximated by $J_0(kb \sin \theta)$, where J_0 is the zeroth order Bessel function. With these replacements equation V-7 becomes

$$\frac{d\sigma}{d\Omega} = \frac{1}{k^2} \left| \int_0^R k^2 b J_0(kb \sin \theta) db \right|^2 = R^2 \left[\frac{J_1(kR \sin \theta)}{\sin \theta} \right]^2$$
 (V-8)

which corresponds to the classical formula for the diffraction scattering from a black sphere.

In Figure 21 this approximate form is compared to optical model calculations for ^{16}O and ^{208}Pb at 163 MeV. The radius used is the effective nuclear radius, $R = R_u + \lambda$, where R_u is the radius of the equivalent uniform distribution and $\lambda = \frac{1}{k}$. The momentum k is calculated for the incoming pion energy minus the Coulomb potential at the surface, $k = \left[\left(\omega - \varepsilon_{\pi} E_C \right)^2 - m^2 \right]^{\frac{1}{2}}$, where E_C is discussed in Section 4 of Chapter III. The simple model does reasonably well

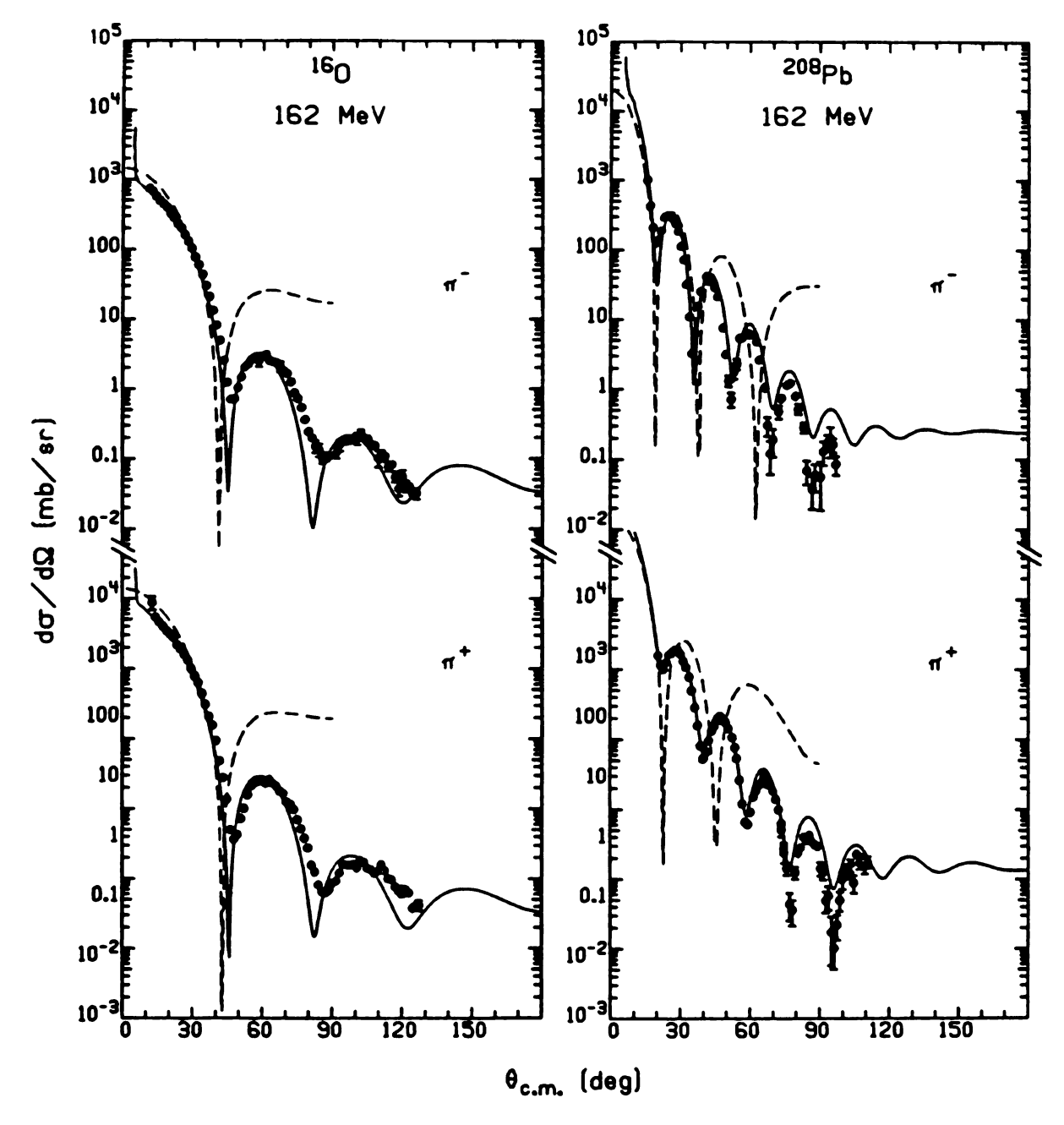


Figure 21. Comparison of black disk model calculation (dashed curve) and full optical potential calculation (solid curve) for π^{+} and π^{-} scattering from 160 and ^{208}Pb at 162 MeV.

in describing the magnitude of the curves and the position of the minima, especially for ^{208}Pb . As it is derived in small angle approximation, the model is not expected to do well near 90°. The inclusion of the Coulomb shift in k reproduces fairly accurately the differences in the position of the minima for π^+ and π^- . It is evident from these calculations that the imaginary part of the optical potential is of principle importance in the resonance region.

3. Details of the Calculations

The differential cross sections were calculated using a modified version of the program PIRK, written by R.A. Eisenstein and G.A. Miller (66). PIRK is a position space code which solves the wave equation II-17 and determines the phase shift between that wavefunction and the exterior Coulomb wavefunction. The wave equation is reduced to a set of equations in r only, noting that the optical potential is independent of angles,

$$u_{\ell}'' + f(r)u_{\ell}' + [g(r) - \frac{\ell(\ell+1)}{r^2}]u_{\ell} = 0$$
 (V-9)

where

$$f(r) = \frac{c'(r)}{c(r) - 1}$$
 (V-10)

and

$$g(r) = (1 - c(r))^{-1} \left\{ \frac{c'(r)}{r} + k_0^2 - 2\overline{\omega}V_C - b(r) \right\}$$
 (V-11)

with b(r) and c(r) the s- and p-wave parts of the optical potential. This is, of course, the same equation as was discussed in Chapter IV, except that the V_C^2 term has been dropped, for reasons to be explained below. Two complex coupled first order equations are formed from the second order equation V-9, by defining v(r) = u'(r). These are solved numerically by a fourth order Runge-Kutta method (63). The differential cross section is obtained from

$$\frac{d\sigma}{d\Omega} = |f_{C}(\theta) + f_{N}(\theta)|^{2}$$
 (V-12)

where the Coulomb amplitude is

$$f_{C}(\theta) = -\frac{\eta_{C}}{2 \sin^{2} \frac{\theta}{2}} \exp \left\{2i\left[\sigma_{0} - \eta_{C}\ln(\sin \frac{\theta}{2})\right]\right\}$$
 (V-13)

with

$$n_{C} = Z \varepsilon_{\pi} \alpha \frac{\omega}{k}$$
 (V-14)

and the nuclear amplitude is

$$f_{N}(\theta) = \frac{1}{ik} \sum_{\ell} (2\ell + 1)e^{2i\sigma_{\ell}} \left[\frac{e^{2i\delta_{\ell}} - 1}{2} \right] P_{\ell}(\cos \theta) \qquad (V-15)$$

where σ_{ℓ} is the Coulomb phase shift and δ_{ℓ} is the phase shift between the Coulomb wavefunction and the solution to equation V-9.

The Coulomb wavefunctions and Coulomb phase shifts are determined for a nonrelativistic particle, i.e. they are solutions to

the Schrödinger equation with a Coulomb potential; no V_C^2 term is included. Because the exterior wavefunction is calculated in this way, it is deemed necessary to drop the $\ensuremath{V_{C}}\xspace^2$ term from the calculation of the interior wavefunction as well. It is found that the inclusion of the ${\rm V}_{\rm C}^2$ term in the equation for the interior causes a small amount of instability of the results with matching radius. In any case, the inclusion or exclusion of the V_c^2 term in equation V-9 makes only a small change in the differential cross sections for ²⁰⁸Pb at low energies, where it is expected to be important, and none at all for the light nuclei. Cooper, Jeppeson, and Johnson (67) look at the effect of the V_{C}^{2} term not only in the interior equation but in the Coulomb wavefunctions and phase shifts as well. For ^{208}Pb at 100 MeV they find discrepancies larger than the experimental errors. It is not clear that the discrepancies are larger than the uncertainties in the theoretical calculations, however. There is a need for further investigation on this point.

The program PIRK has been modified to include all the terms of the optical potential, equation III-76. A routine to calculate total and partial cross sections has also been added, as discussed in Chapter VI.

4. Calculations--Low Energy Region

Several elastic scattering calculations using different parameter sets are discussed in this section. The first of these calculations is that with the theoretical potential derived in Chapter III and used in the pionic atom calculations of Chapter IV. The

theoretical optical potential parameters at 30, 40, and 50 MeV are given as set 1 in Table 6. As before, the single nucleon parameters are taken from the RSL phase shift fit (25), the absorption parameters from the calculation of Riska and collaborators (50), and $\lambda = 1.6$. Note that the imaginary parts of b_1 , c_0 , and c_1 listed in the table are the RSL values multiplied by the Pauli factor Q.

The elastic scattering cross sections calculated with set 1 are shown as the dashed curves in Figures 22. Clearly, the curves do not bear much resemblance to the data. The simple analysis of Section 2 can be used to give an indication of what is amiss in the optical potential. Comparison of the shapes of the $^{12}\mathrm{C}$ and $^{16}\mathrm{O}$ curves with those shown in Figure 19 suggests that the s-wave repulsion in the optical potential is too weak. The same conclusion can be drawn by comparison of the π^- - $^{12}\mathrm{C}$ calculation in Figure 22f and the curves of Figure 20.

The solid curves in Figures 22 are the result of calculations with more negative values of $Re(\overline{b}_0)$, listed as set 2 in Table 6. These were chosen to give reasonable eyeball fits to the ^{12}C and ^{16}O data, and to have the same slope as a function of energy as the original values. The other parameters of the optical potential were left unchanged. Although the fits are not perfect, the energy and A dependence is well reproduced and, on the basis of the two cases available, the π^- data is also well described, including the diffractive appearance of the π^- data for ^{208}Pb at 30 MeV.

Table 6. Parameters used in the low energy elastic scattering calculations.

		30 MeV	40 MeV	50 MeV
Set 1	<u></u>	-0.035 + i0.003	-0.038 + i0.004	-0.042 + i0.006
	$b_1(fm)$	-0.132 - i0.001	-0.131 - i0.001	-0.131 - i0.002
	$B_0(fm^4)$	-0.005 + i0.115	-0.010 + i0.130	-0.020 + i0.140
	$c_0^{(fm^3)}$	0.70 + i0.007	0.72 + i0.015	0.75 + i0.029
	$c_1^{(fm^3)}$	0.44 + i0.004	0.45 + i0.007	0.45 + i0.014
	$C_0^{(fm^6)}$	0.32 + i0.46	0.34 + i0.52	0.37 + i0.62
	λ	1.6	1.6	1.6
Set 2	<u>b</u> 0(fm)	-0.070 + i0.003	-0.073 + i0.004	-0.077 + i0.006
	Other pa	rameters as in Set	1.	
Set 3	<u>Б</u> (fm)	-0.057 + i0.003	-0.060 + i0.004	-0.064 + i0.006
	$b_1(fm)$	-0.132 - i0.001	-0.131 - i0.001	-0.131 - i0.002
	$B_0(fm^4)$	-0.005 + i0.22	-0.010 + i0.24	-0.020 + i0.25
	$c_0^{(fm^3)}$	0.70 + i0.007	0.72 + i0.015	0.75 + i0.029
	$c_1^{(fm^3)}$	0.44 + i0.004	0.45 + i0.007	0.45 + i0.014
	$C_0(fm^6)$	0.32 + i1.02	0.34 + i1.08	0.37 + i1.18
	λ	1.6	1.6	1.6
	Q	0.19	0.24	0.31

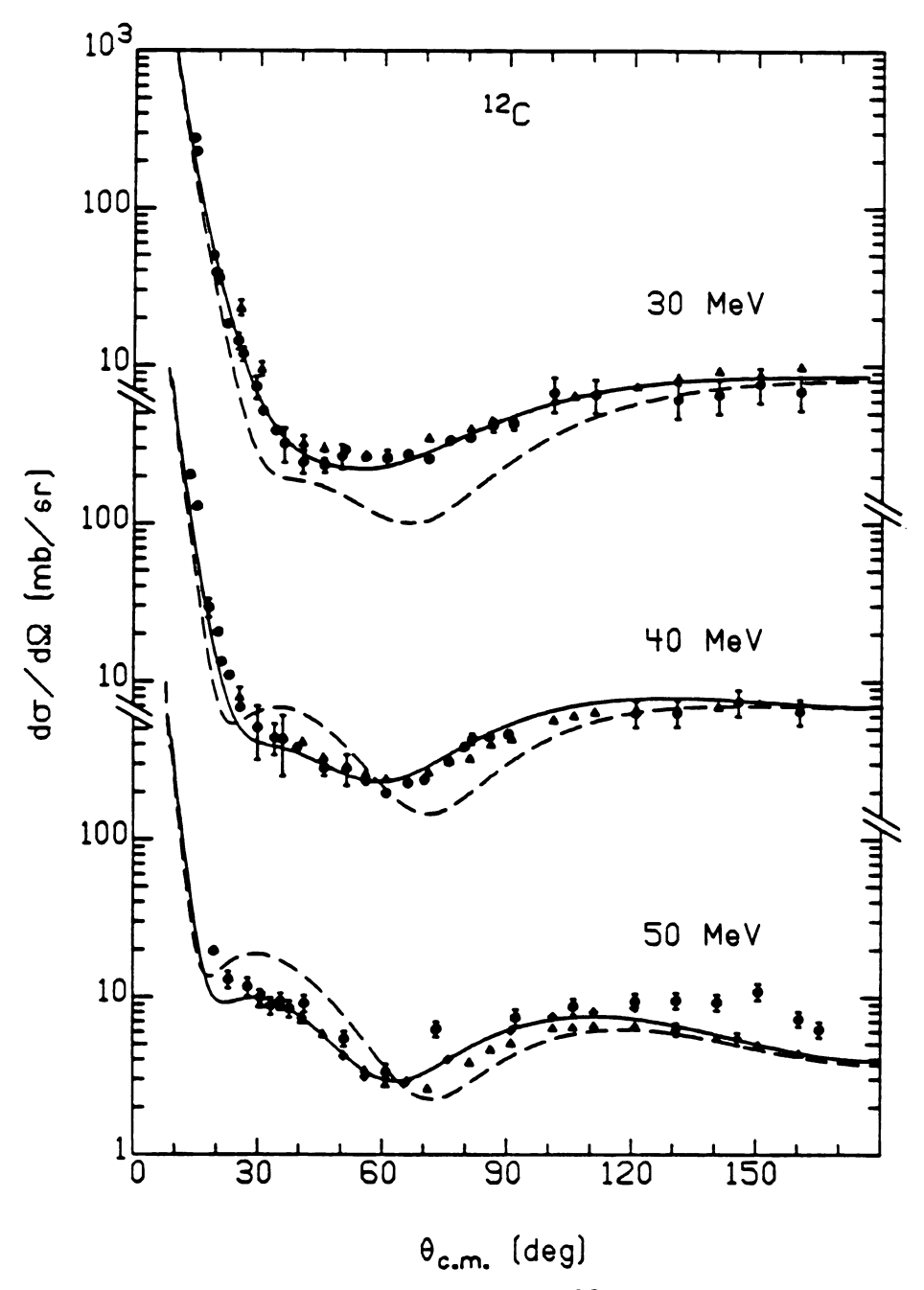


Figure 22a. Elastic scattering of π^+ from ^{12}C at 30, 40, and 50 MeV with the optical potential parameters of set 1 (dashed curves) and set 2 (solid curves). Data are from Refs. 32 (diamonds), 34, 69, 70 (triangles), and 68 (circles).

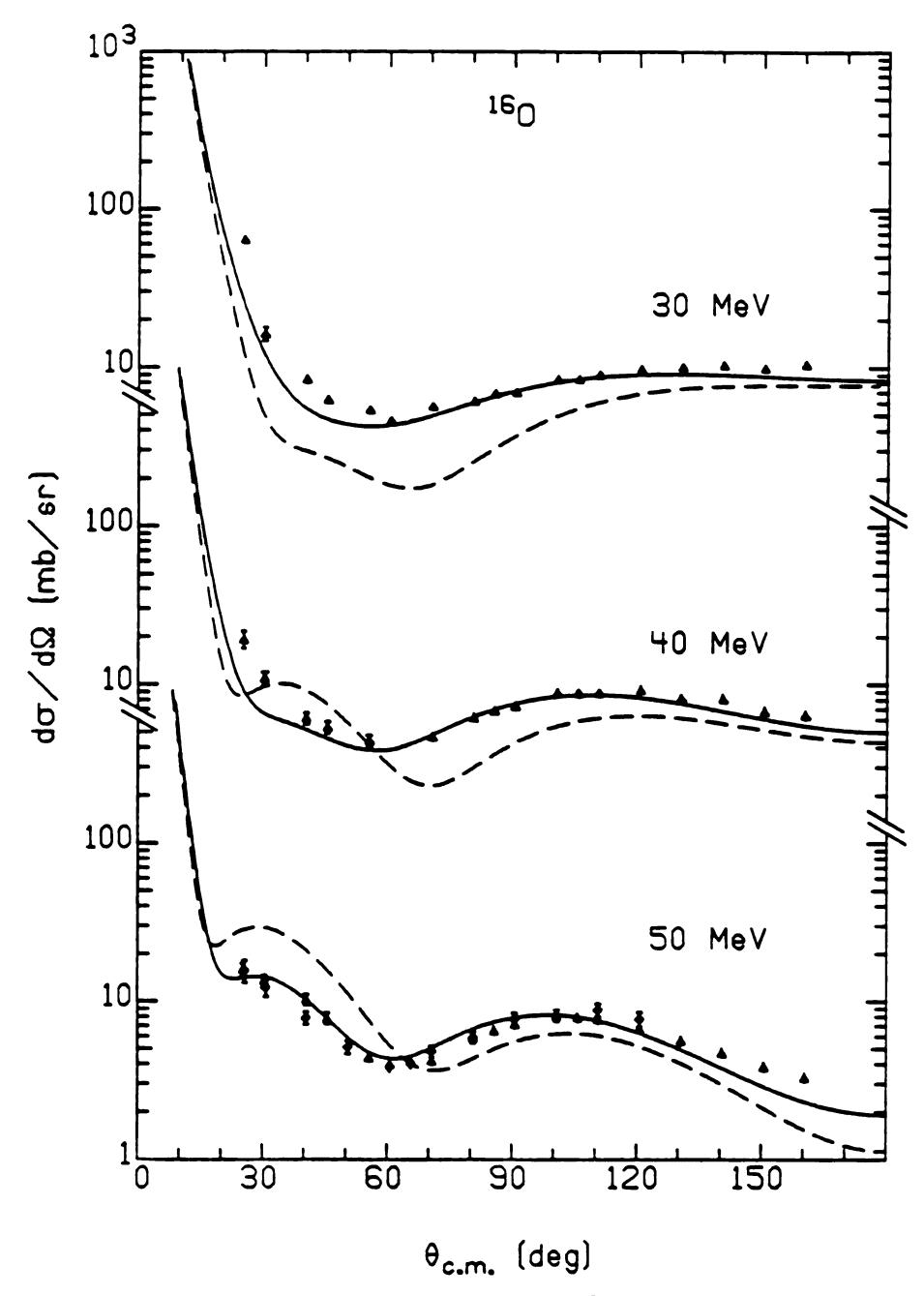


Figure 22b. Elastic scattering of π^+ from $^{16}0.\,$ Data from Refs. 32 (diamonds), and 33, 34, and 69 (triangles).

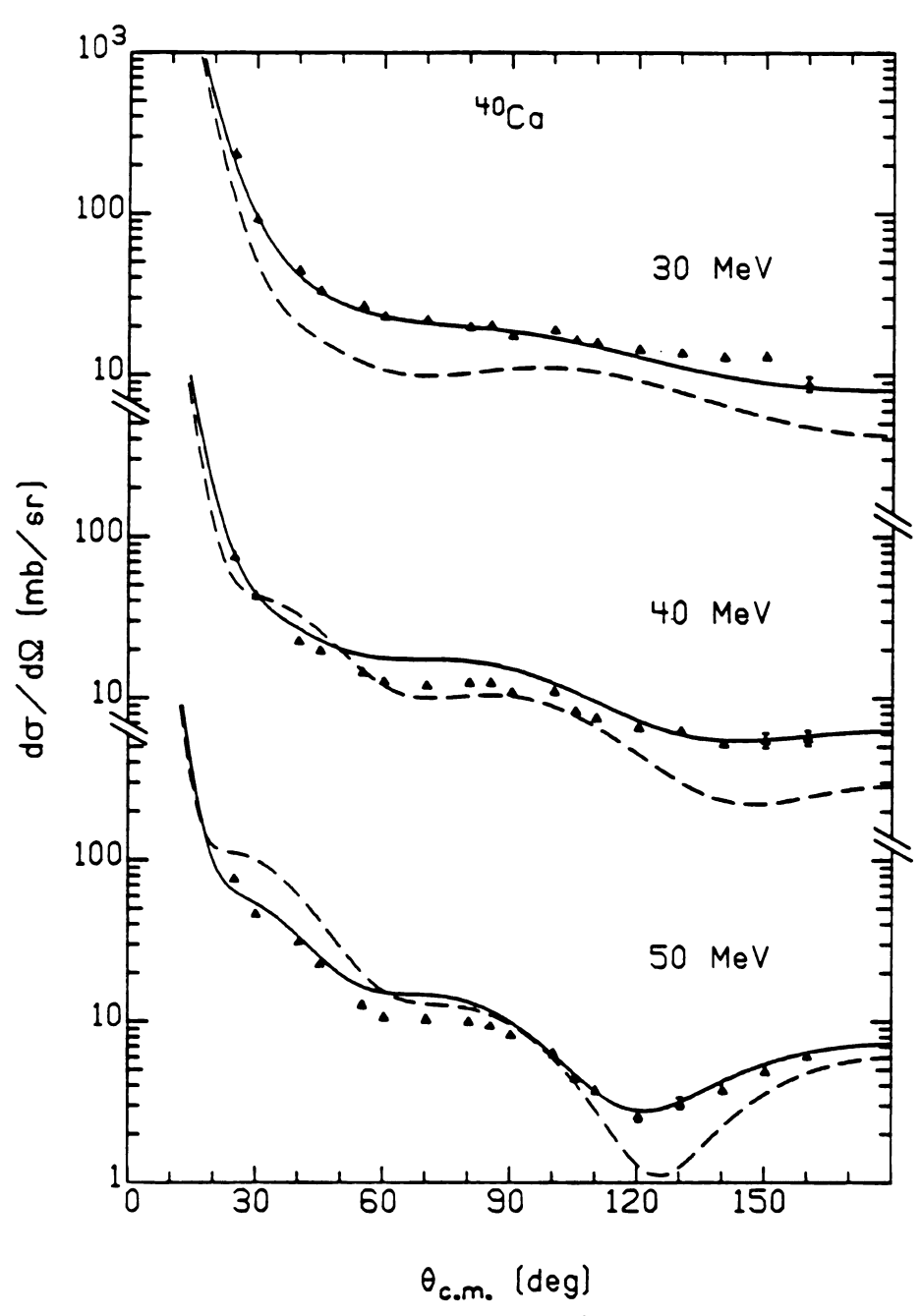


Figure 22c. Elastic scattering of π^+ from $^{40}\text{Ca.}$ Data from Refs. 34, 69.

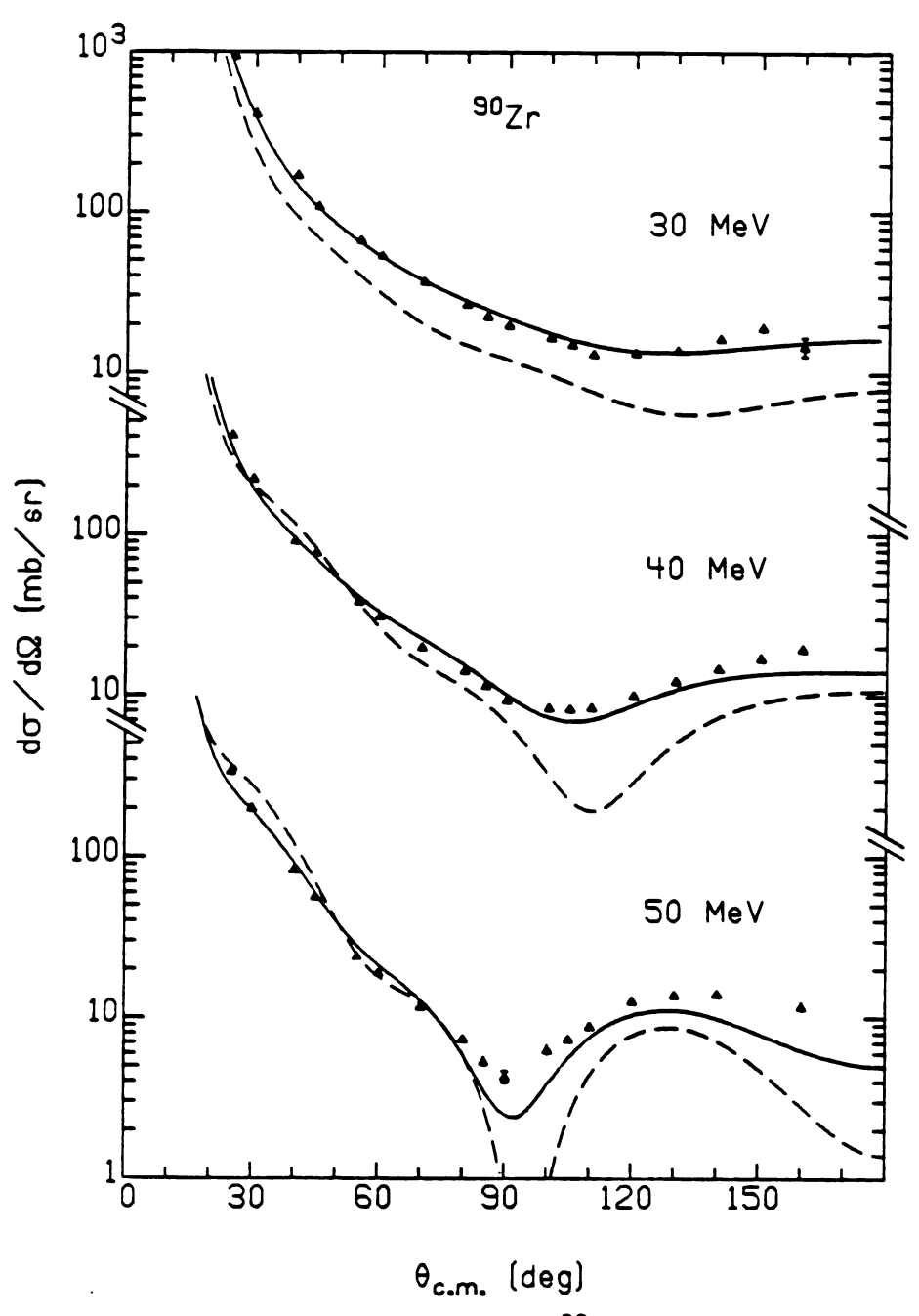


Figure 22d. Elastic scattering of π^+ from $^{90}\text{Zr.}$ Data from Refs. 34, 69.

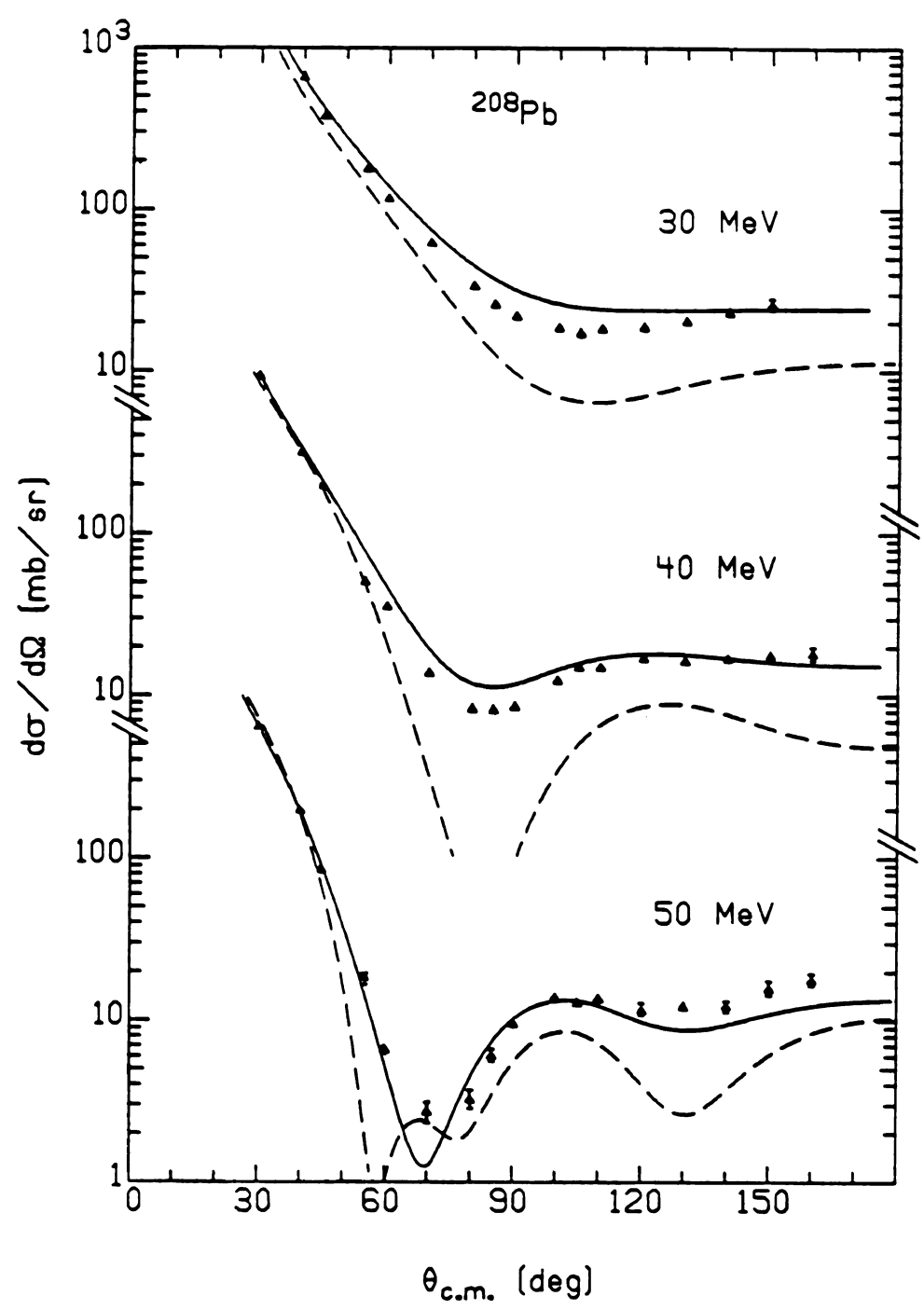


Figure 22e. Elastic scattering of π^+ from ^{208}Pb . Data from Refs. 34, 69.

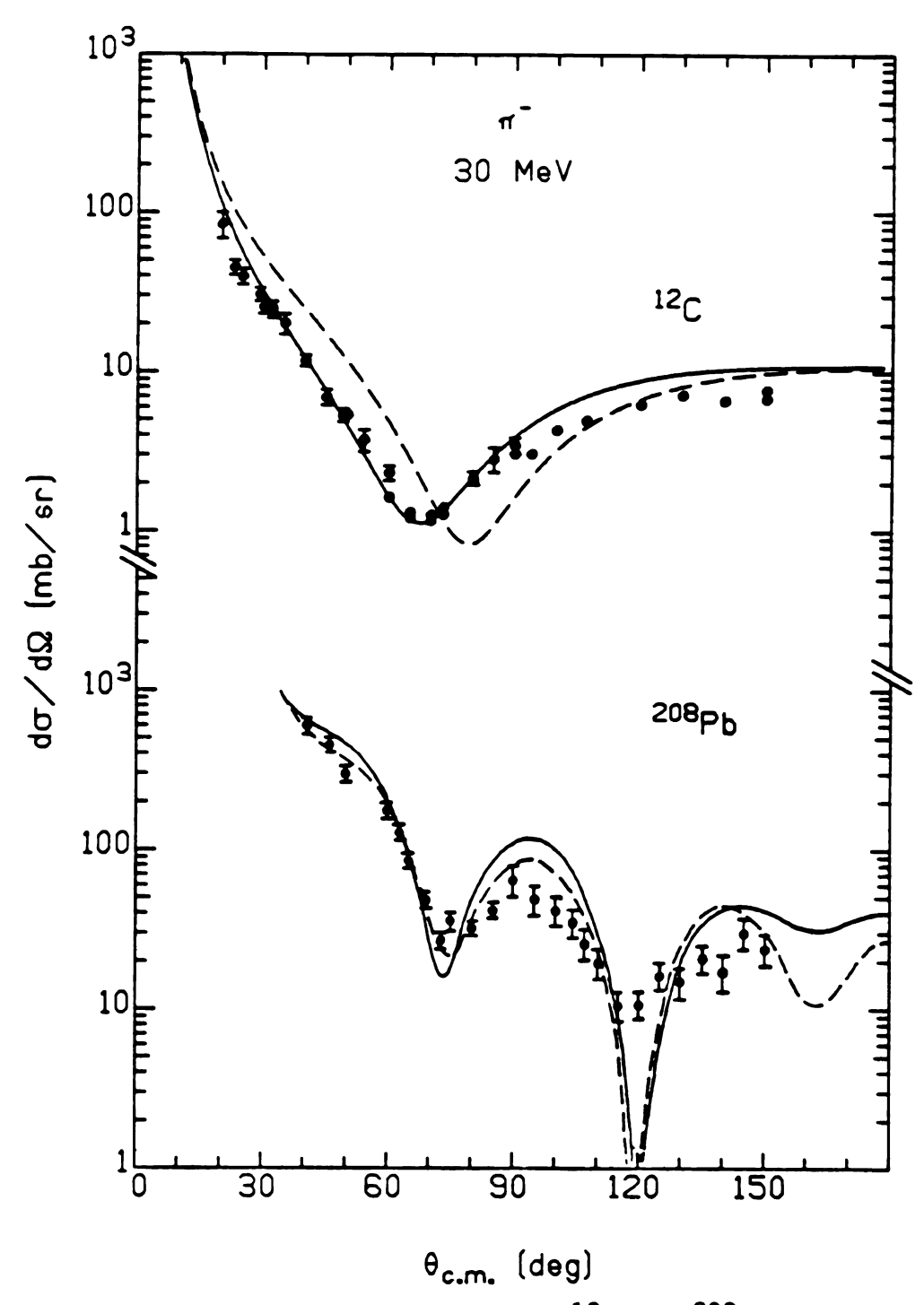


Figure 22f. Elastic scattering of π^- from ^{12}C and ^{208}Pb at 30 MeV. Data from Refs. 71 and 72.

A χ^2 fit to some of the 50 MeV data using the same optical potential as used here but without the $\kappa(r)$ term gives a minimum in χ^2 for $\lambda=1.6$ and $\text{Re}(c_0)=0.75~\text{fm}^3$, with $\text{Re}(\overline{b}_0)=-0.06~\text{fm}$ (73). The value for $\text{Re}(c_0)$ is almost the phase shift value at 50 MeV, $\text{Re}(c_0)=0.74~\text{fm}^3$. The value for $\text{Re}(\overline{b}_0)$ is not as negative as that required in the analysis presented here, due to the absence of the $\kappa(r)$ term. Note that all the induced s-wave terms, the $\nabla^2 \rho$, $\nabla^2 \rho^2$, and $\kappa(r)$ terms, are attractive, requiring more repulsion in the $\overline{b}_0 \rho$ term.

Another approach can be made to the question of choosing optical parameters for the low energy region. The analysis of pionic atom shifts and widths gives the overall strength of the s- and p-wave parts of the optical potential. This information can be extrapolated from zero energy to the required energies assuming some reasonable prescription.

As a first approximation, the optical potential parameters are assumed approximately energy independent in the energy range zero to 50 MeV. This is the approach taken in Ref. 24. The parameters for the calculations are taken from the fits to the pionic data, set 2 of Table 5, with the exception of the imaginary parts of the single nucleon parameters which are taken from set 1 of Table 6. The results of these calculations are shown as the solid curves of Figures 23. These are in fact rather close to the data for the light nuclei and nearly reproduce the s-p interference. They become steadily worse, however, with increasing A.

		; ;

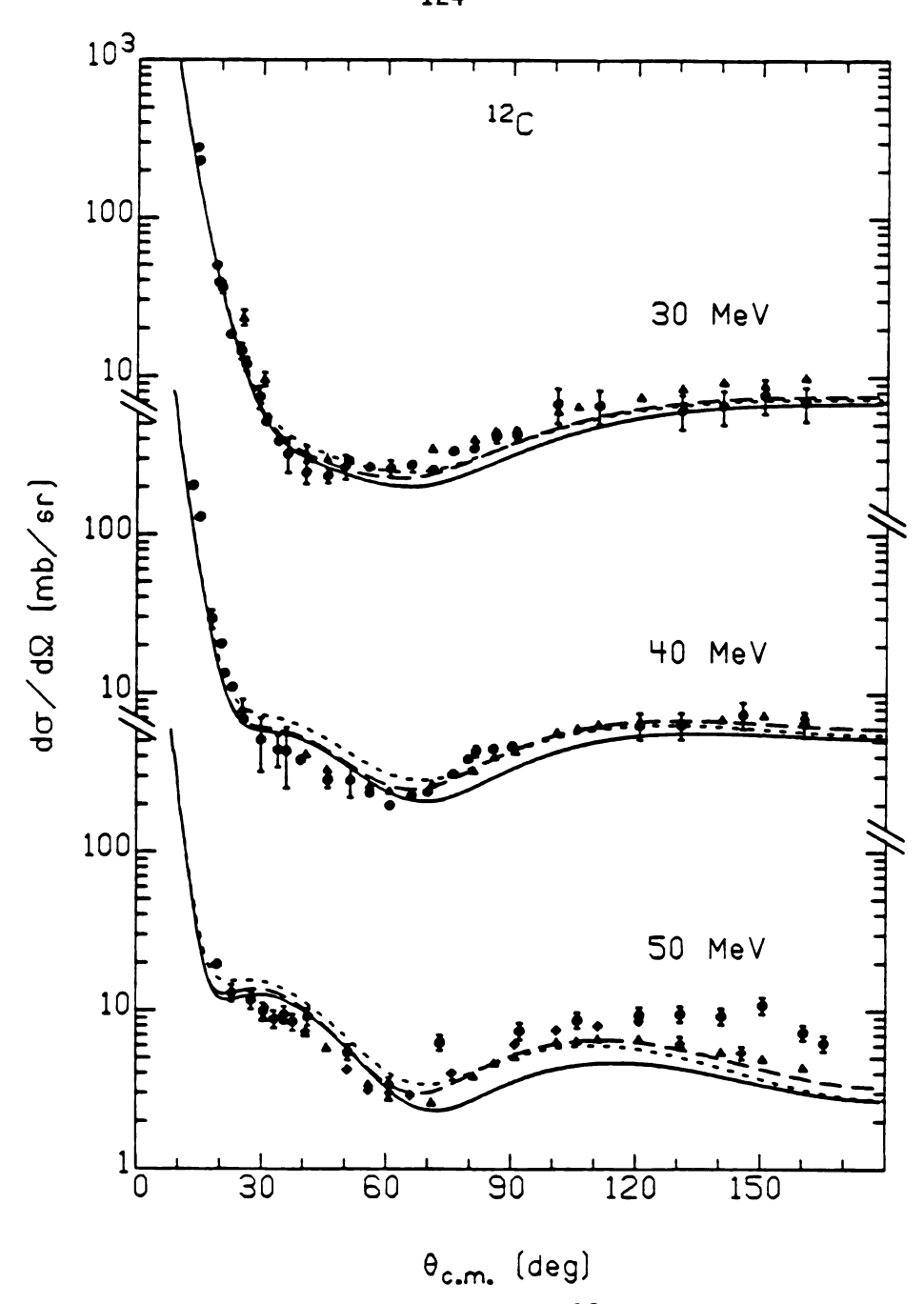


Figure 23a. Elastic scattering of π^+ from ^{12}C at 30, 40, and 50 MeV, with the optical potential parameters from set 2 of Table 5 (solid curves), set 3 of Table 6 (dotted curves), and set 3 but with $\text{Im}(B_0)$ and $\text{Im}(C_0)$ from set 2 of Table 5 (dashed curves).

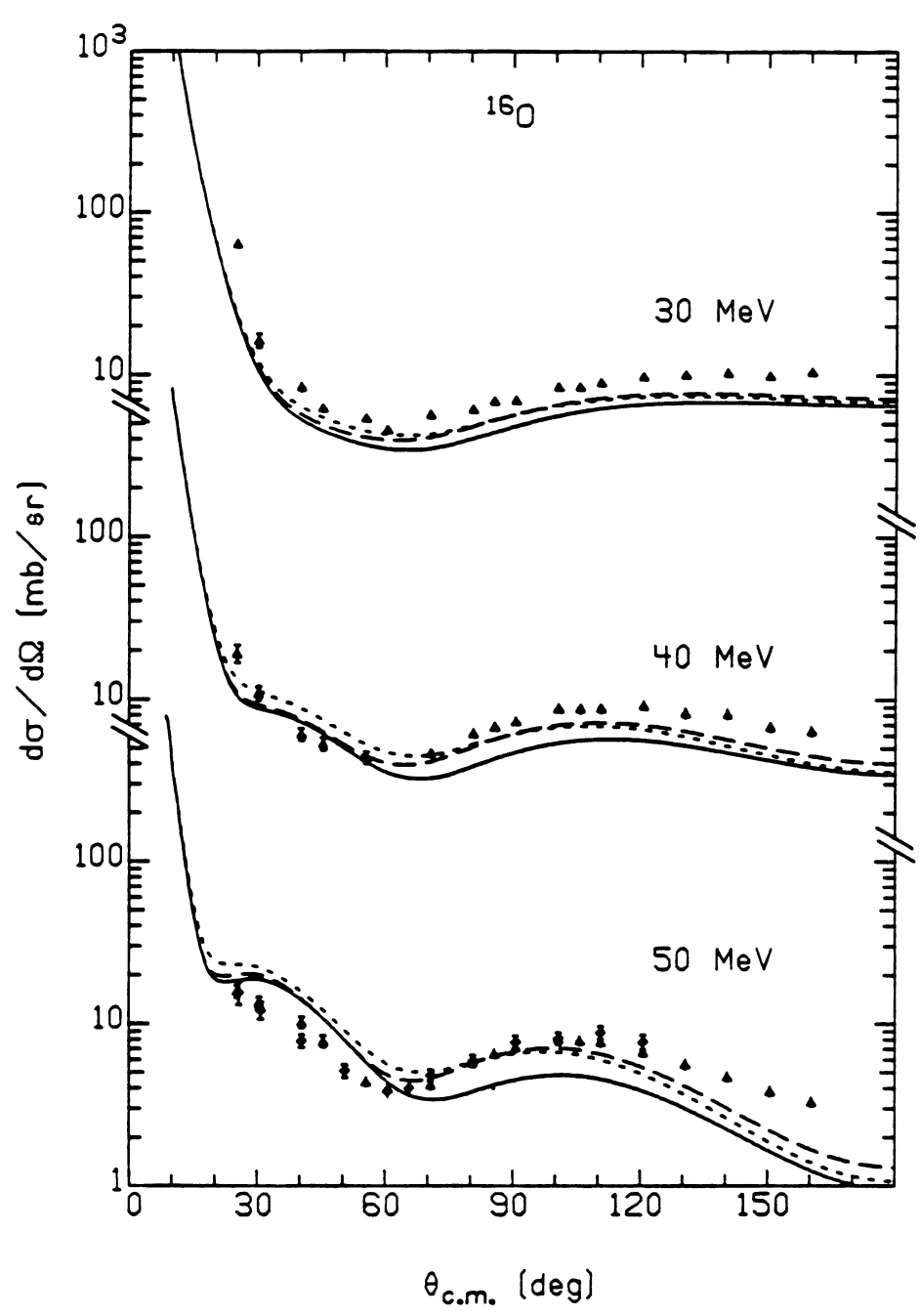


Figure 23b. Elastic scattering of π^{+} from $^{16}\text{O}\text{.}$

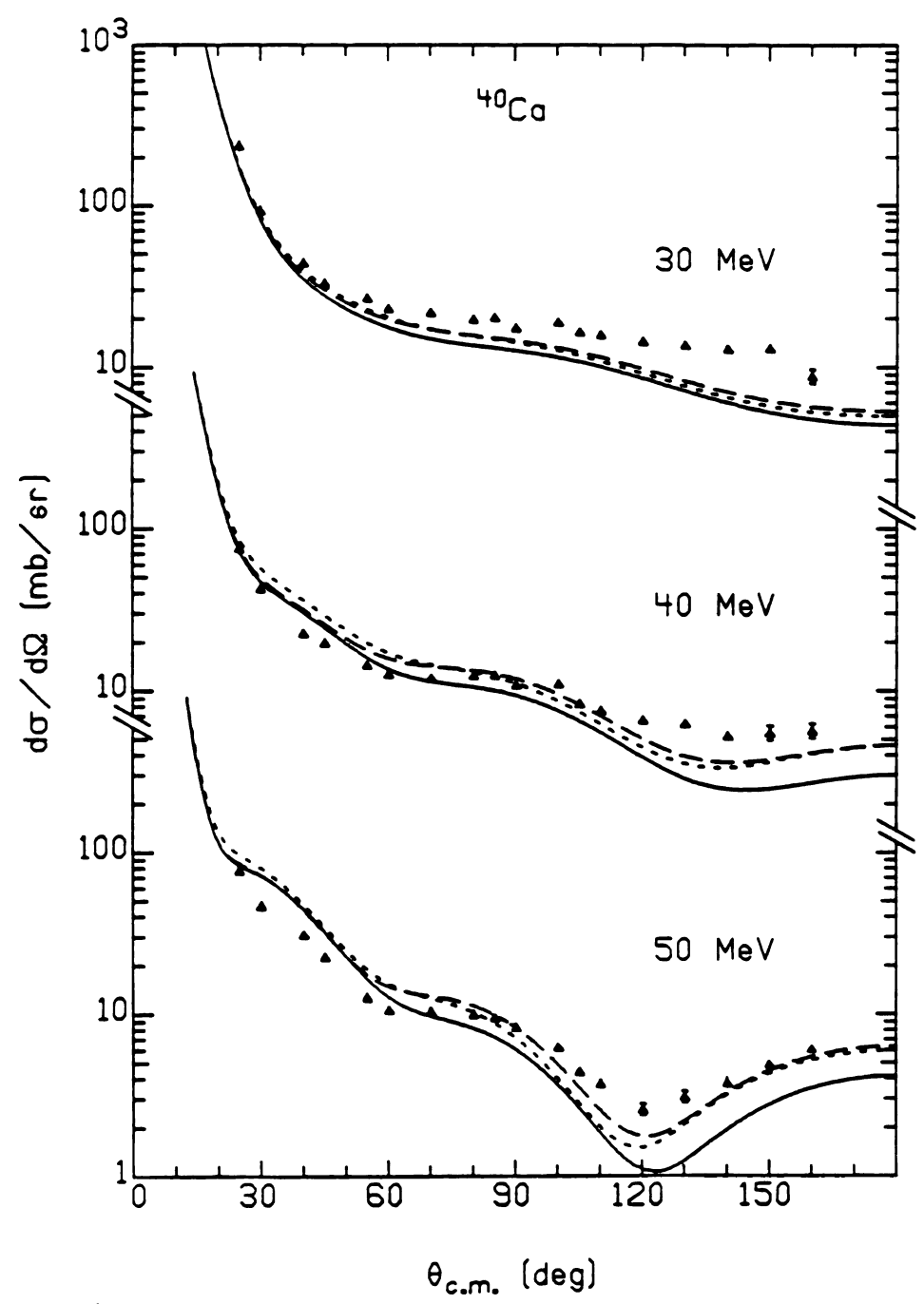


Figure 23c. Elastic scattering of π^+ from $^{40}\text{Ca.}$

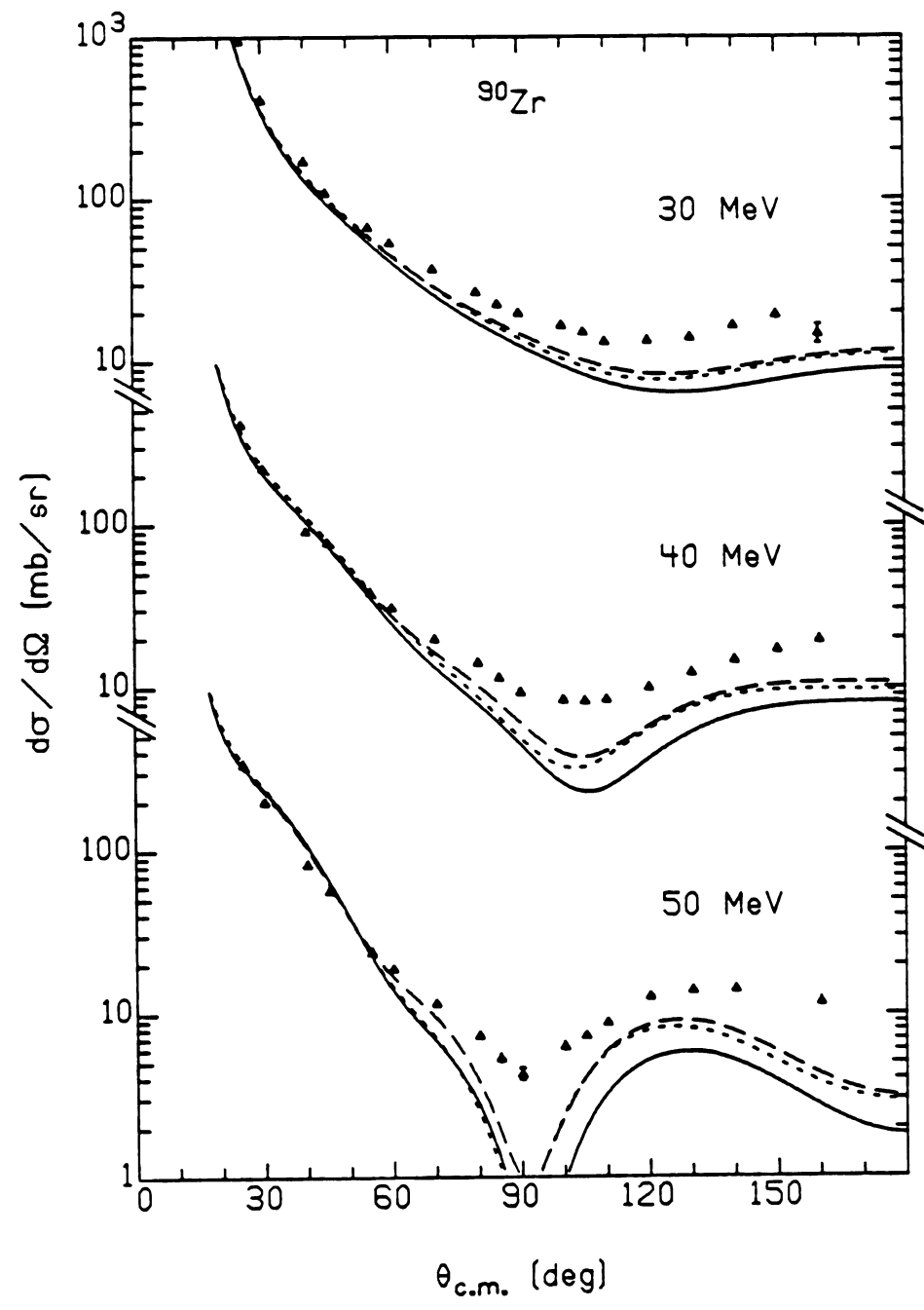


Figure 23d. Elastic scattering of π^{+} from $^{90}\text{Zr.}$

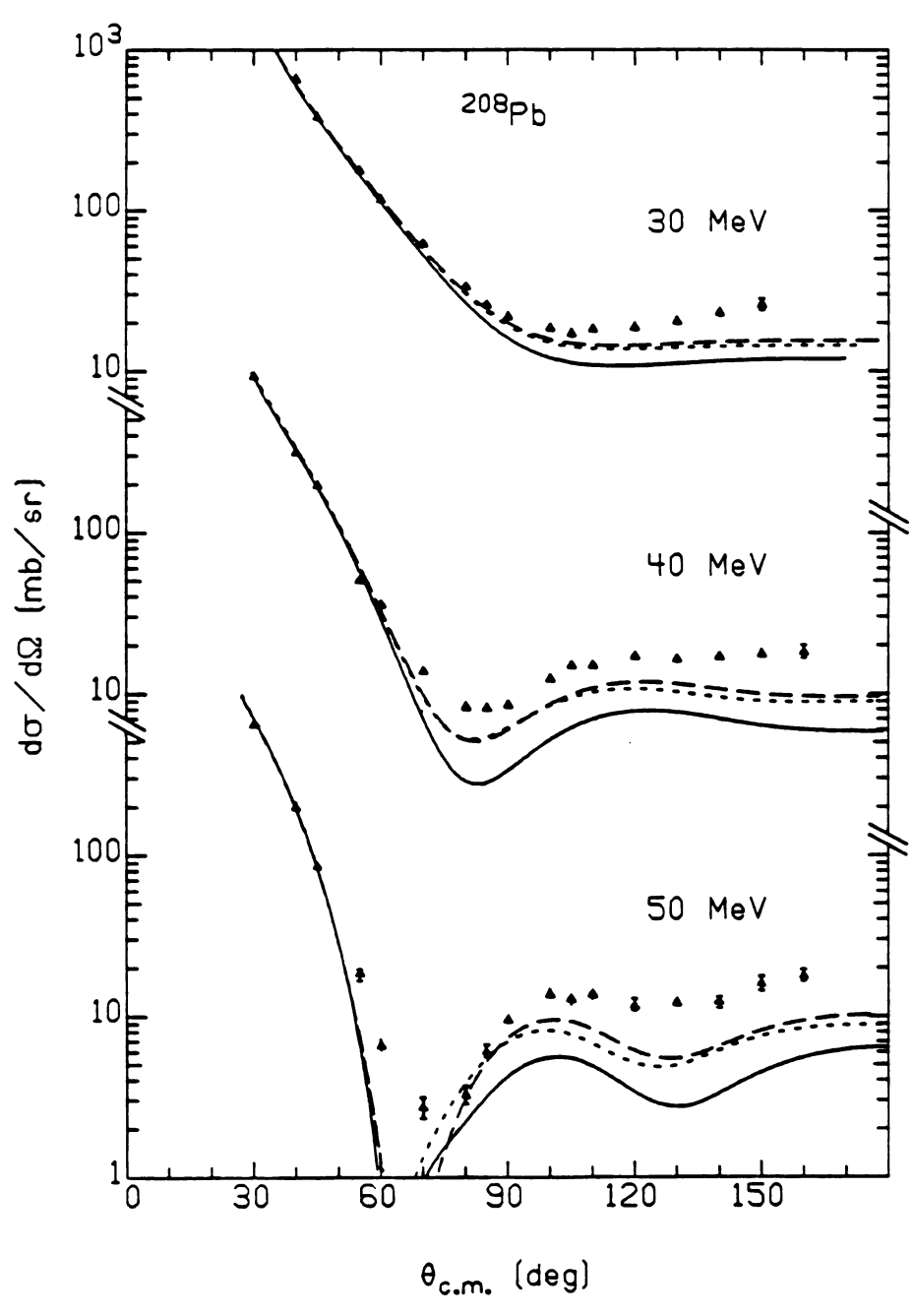


Figure 23e. Elastic scattering of π^+ from ^{208}Pb .

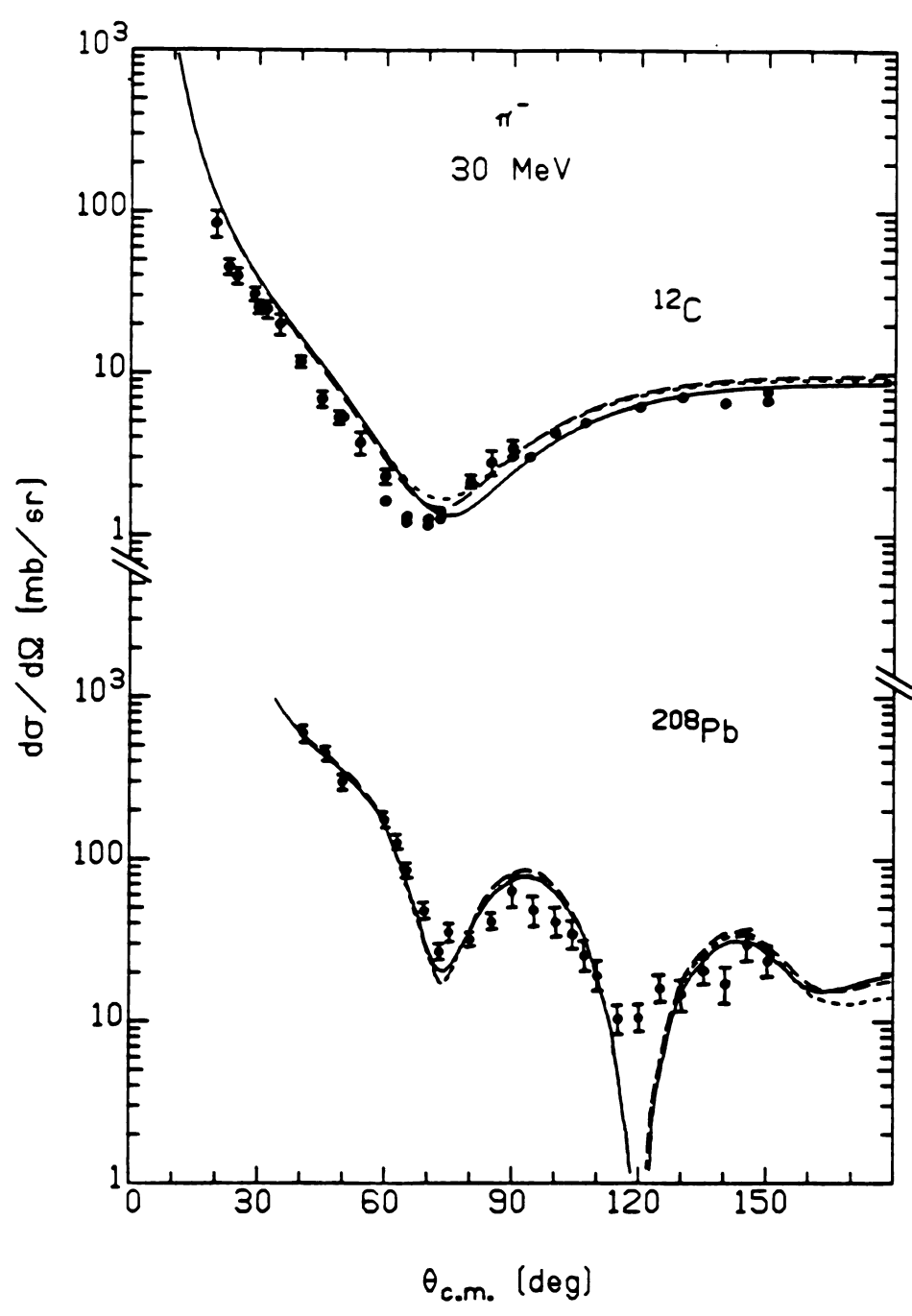


Figure 23f. Elastic scattering of π^- from ^{12}C and ^{208}Pb at 30 MeV.

The optical parameters are not in fact energy independent, even in this energy range. One should, therefore, make some estimate of the energy dependence of these parameters. For the p-wave parameter c_0 this is a straightforward task; as the pionic atom value of $Re(c_0)$ is close to the zero energy RSL phase shift value, these values of \boldsymbol{c}_0 are adopted at all energies. The pionic atom value for $\overline{\mathbf{b}}_{0}$ is not near the value calculated from the RSL phase shifts; therefore, it is extrapolated assuming the same slope as a function of energy as the calculated value, i.e. the difference between the fitted value of $\overline{\mathbf{b}}_0$ and the RSL value at zero energy is added to the RSL value at all energies. The real parts of the absorption parameters were fixed in the pionic atom analysis at the values calculated by Riska et al., therefore the calculated values are used at all energies. In the first set of calculations, the imaginary parts of the absorption parameters were kept at their zero energy fitted values. These are the dashed curves of Figures 23. In the second set of calculations, the dotted curves of Figures 23, the absorption parameters $Im(B_0)$ and $Im(C_0)$ were extrapolated also. This can be done in two ways. The first is simply to assume the slope as a function of energy of $Im(B_0)$ and $Im(C_0)$ is that of the Riska calculations. A more general method is discussed in the next section. The two give nearly identical results for 30-50 MeV. The complete set of extrapolated parameters is given in Table 6 under the heading set 3. A comparison of the dashed and dotted curves indicates that the smaller absorption strength gives quitereasonable

results, especially for the light nuclei, while the calculations with the larger absorption strength are somewhat worse. The calculations are rather insensitive to the imaginary absorptive parameters, and small adjustments of the real s and p-wave strengths can at least partially compensate for differences due to the absorptive strength. Note that both calculations with extrapolated parameters do better than those with the zero energy values. From these calculations one can conclude that although the smaller imaginary absorption parameters calculated by Riska and collaborators seem to give somewhat better fits to the data, the absorption parameters deduced from pionic atom analysis are not inconsistent with the data. In fact, the set of optical potential parameters deduced from pionic atom shifts and widths fits the scattering data rather well, considering the approximate treatment of the energy dependence.

As yet nothing has been said about the relative strengths of the single nucleon and absorption pieces of the real part of the potential. In fact, the scattering is quite insensitive to this; the overall real s and p-wave strengths are the important quantities, just as was the case for the pionic atom shifts. This is illustrated for the s-wave in Figure 24, where the elastic scattering cross sections for π^+ from ^{12}C at 50 MeV are calculated for two different values of Re(B₀) (solid and dashed curves) and several values of Re($\overline{\text{b}}_0$), with the highest curves corresponding to the most negative values of Re($\overline{\text{b}}_0$). The curves are equally spaced except at the most backward angles, indicating the insensitivity of the calculation

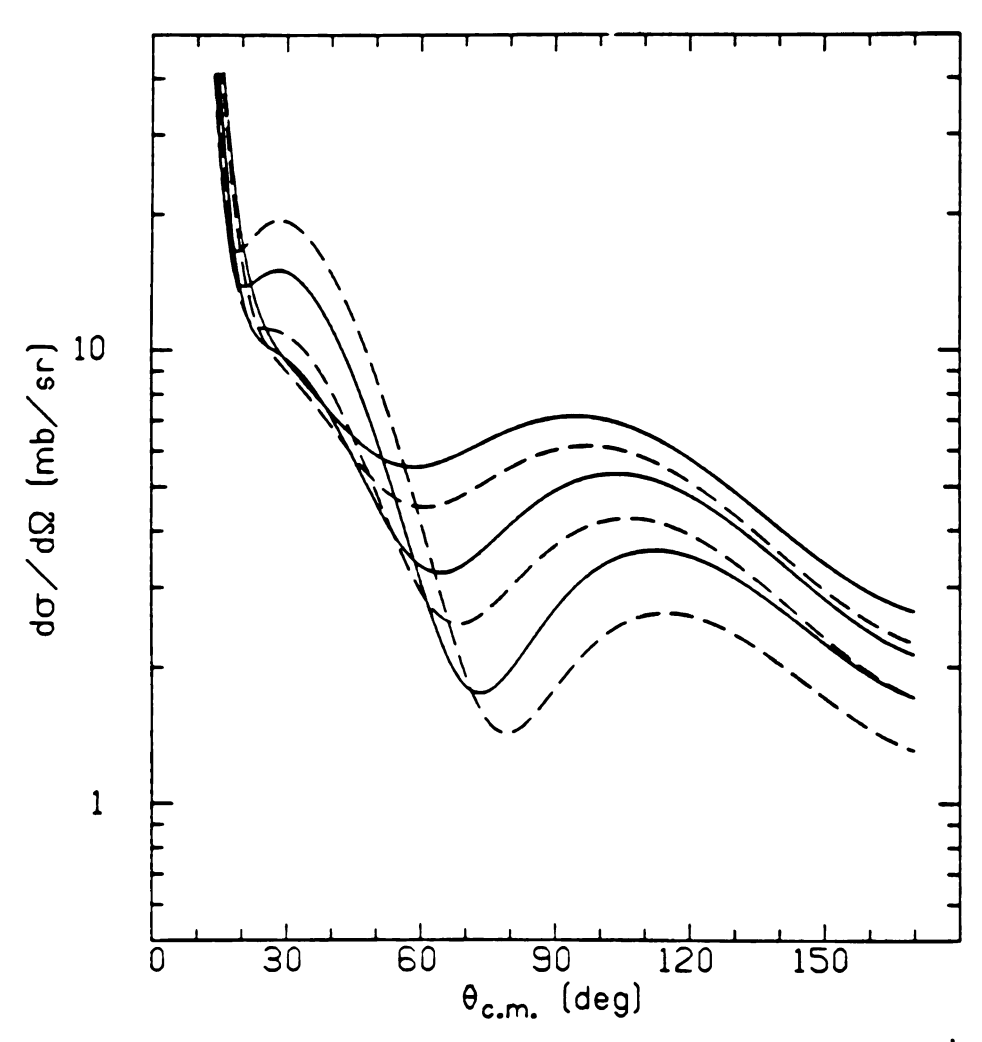


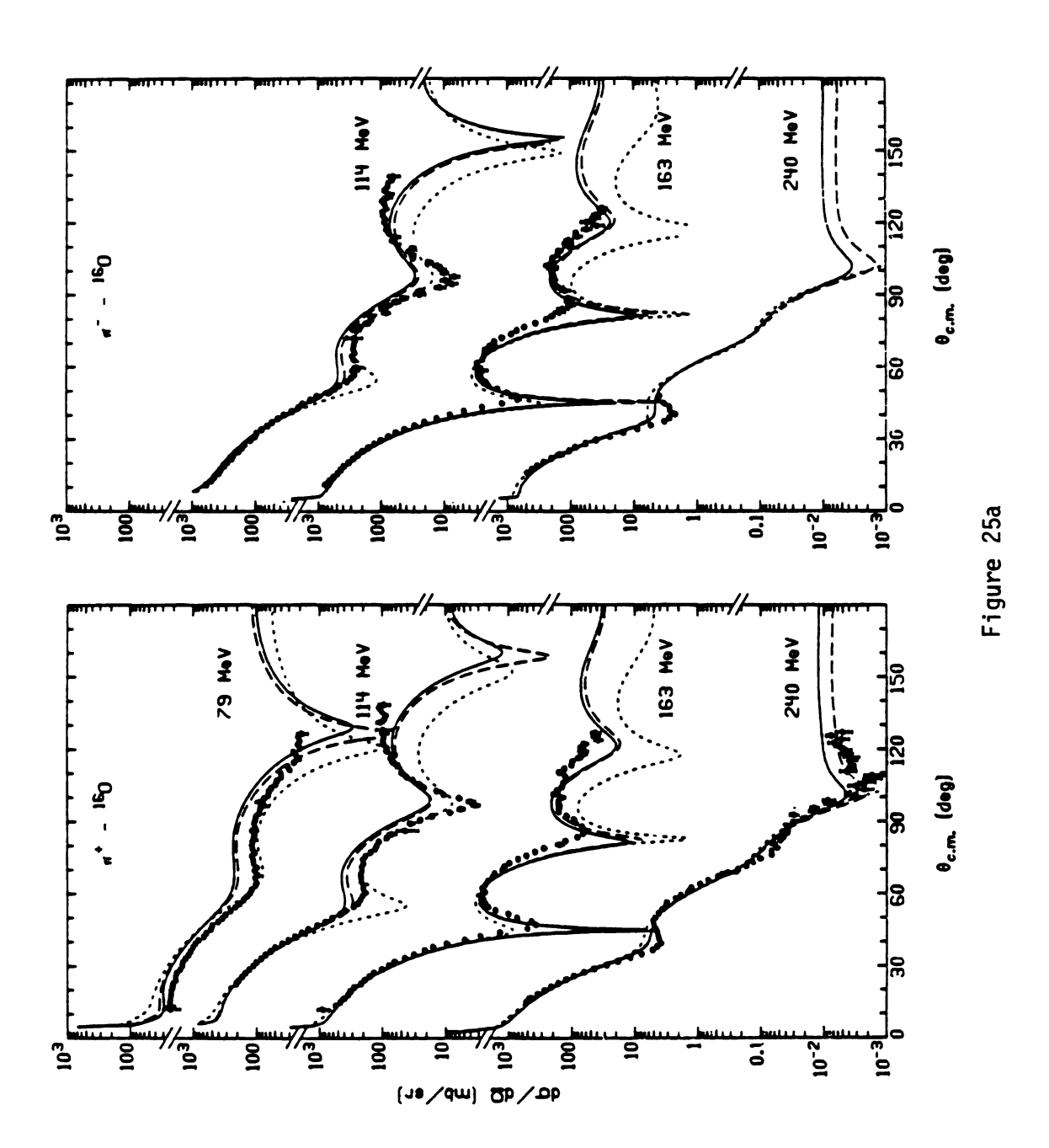
Figure 24. Comparison of elastic scattering calculations for π^+ on ^{12}C with two values of $\text{Re}(\text{B}_0)$ (solid and dashed curves) and a series of values for $\text{Re}(\text{b}_0)$.

to the origin of the s-wave strength. A similar situation exists for the p-wave. Thus, the low energy elastic scattering data yield only a limited amount of information about the parameters of the optical potential, and even less about the form of the potential. The overall real s and p-wave strengths are roughly indicated, and some wide limits are placed on the imaginary strength of the optical potential.

5. Calculations--Resonance Region

In this section several sets of calculations of elastic scattering for energies above 50 MeV are compared with a sample of the data in this energy region. The first set is again that with the theoretical optical potential. It is not clear what value of the LLEE parameter λ should be used at these energies as both the simple model (10), giving $\lambda = 1$, and the calculations of Weise (48) and Brown, Jennings, and Rostoken (41), giving $\lambda \approx 1.6$, are made in the low energy limit. There is as yet no theoretical value for λ above about 50 MeV. It is convenient to choose the value $\lambda = 1.6$, as this was used in the low energy calculations. Calculations using both values, $\lambda = 1.6$ (solid curve), and $\lambda = 1$ (dashed curve), are shown in Figures 25. The differences between these two curves are in each case not large, so that the choice is not a crucial one. Both curves reproduce well the general features of the data, but not the details. The best fits occur when the nucleus is blackest, around 163 MeV, and for the larger nuclei. It is difficult to analyze the optical potential in the intermediate energy range

Elastic scattering of π^+ and π^- from $^{16}0$. Optical potential parameters are taken from the RSL phase shifts and Riska calculations with λ = 1.6 (solid curves) and λ = 1.0 (dashed curves). Also shown are first order Kisslinger potential calculations (dotted curves). Data are from Refs. 35, 74. Figure 25a.



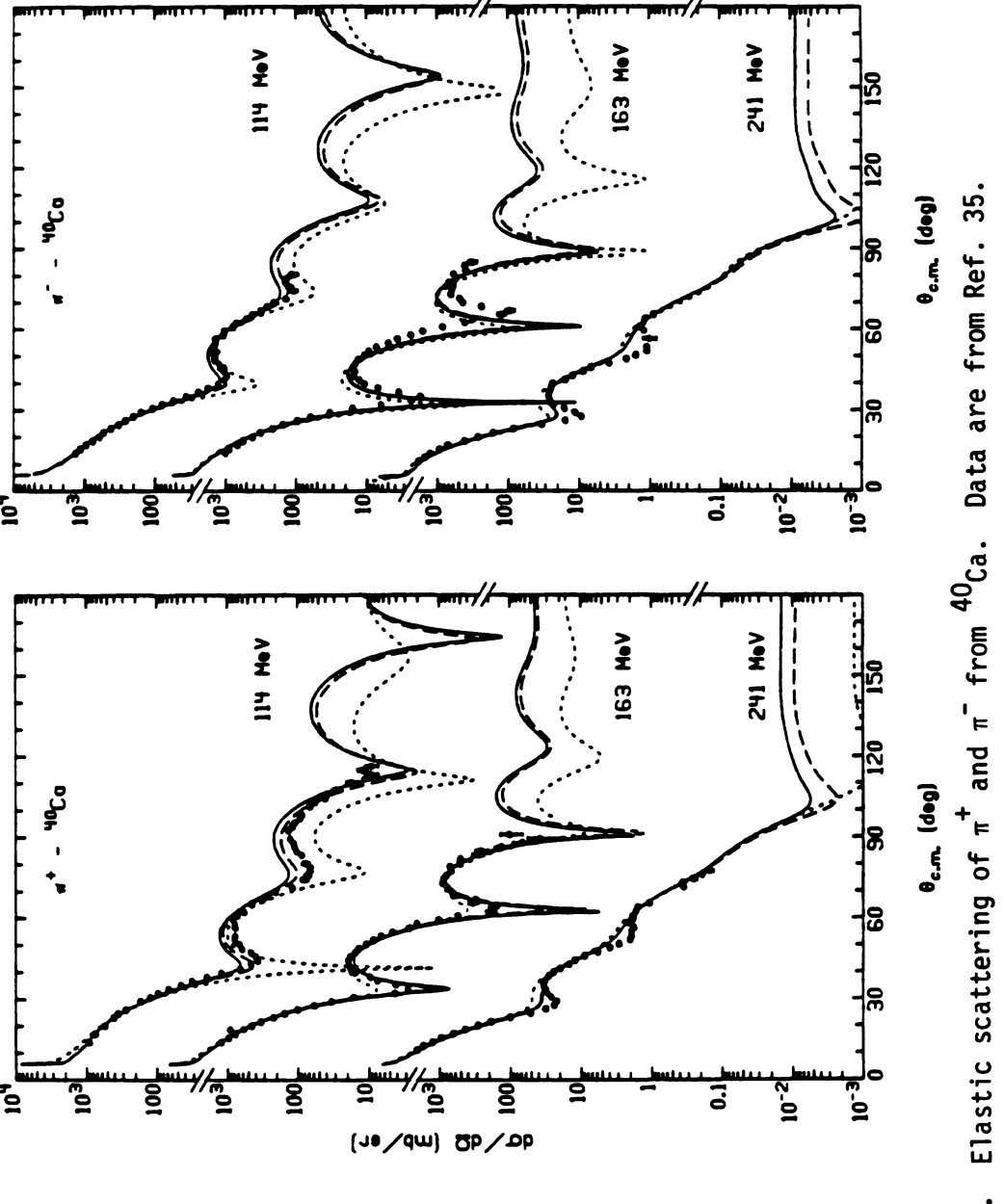


Figure 25b.

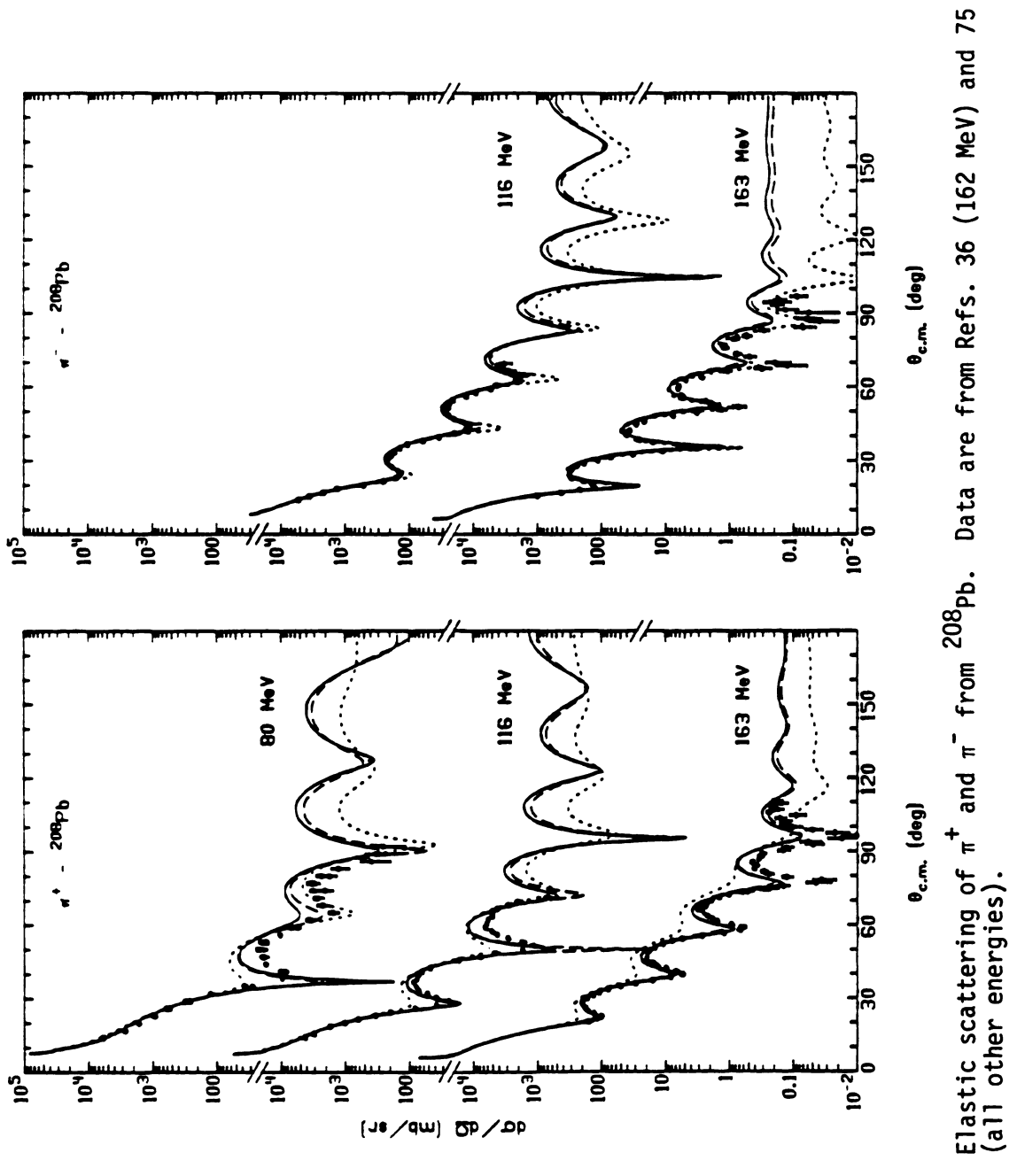


Figure 25c.

80-150 MeV, as the dependence of the scattering on the parameters is not given by a simple model. It is not clear, therefore, what changes in parameters would be required in order to fit the data. Detailed fitting of this data, with a first order optical potential which includes form factors, has been done by Stephenson et al. (76), who vary the radius and skin thickness of ρ and the overall normalization as well as the optical potential and form factor parameters. Thus, it is difficult to correlate their information with the potential used in this investigation.

As the early calculations of resonance region scattering were made with the Kisslinger potential with no modifications, it is interesting to see whether the addition of the higher order corrections, which are extremely important at low energies, improves the fits at these energies. The results of Kisslinger potential calculations, with parameters from π -N phase shifts, are shown as the dotted curves in Figures 25. Although these curves are closer to the data in places, the inclusion of higher order corrections causes an overall improvement in fit for all nuclei at all energies shown here.

The second method discussed in the previous section for choosing the potential parameters, using the zero energy parameters derived from pionic atom analysis, can be applied at these energies also. However, a more sophisticated method of extrapolation is required. As noted before, the real p-wave parameter obtained from pionic atom fits is quite close to the RSL phase shift value, when the value 1.6 is adopted for λ . Although the real s-wave parameter is

not near the phase shift value, the resonance region scattering is not very sensitive to the s-wave strength, and the RSL value for \overline{b}_0 will be adopted. As the real parts of the absorption parameters were fixed at the values given by Riska and collaborators, the only parameters for which an extrapolation procedure is required are $\mathrm{Im}(B_0)$ and $\mathrm{Im}(C_0)$. In order to derive a simple procedure, the assumption is made that in the matrix element of $\tau^{(2)}$, equation III-57, the dominant contribution to the energy dependence is from the scattering operators τ . Thus, the absorption parameters are assumed proportional to the square of the single nucleon parameters. For the s-wave it is necessary to include the isovector contribution, as the isoscalar term b_0 is small. The imaginary parts of the s-wave parameters can be neglected, however, in this simple estimate. The s-wave absorption parameter is therefore taken as (52)

$$Im(B_0) = K_1\{[Re(b_0)]^2 + [Re(b_0) + 2Re(b_1)]^2\}$$
 (V-16)

where K_1 is a constant of proportionality. For the p-wave, the isovector terms are proportional to the isoscalar terms, due to the dominance of the Δ_{33} channel, and need not be considered. The imaginary part of the p-wave single nucleon parameter must be included, however, as it dominates in the resonance region. The p-wave absorption parameter is taken to be

$$Im(C_0) = K_2|c_0|^2$$
 (V-17)

The constants K_1 and K_2 can be determined by evaluating equations V-16 and V-17 at zero energy. With $Im(B_0) = 0.19 \text{ fm}^4$ and $Im(C_0) = 0.90 \text{ fm}^6$ from Table 5, and the zero energy RSL values for b_0 , b_1 , and c_0 , the constants K_1 and K_2 are determined to be $K_1 = 2.6$ fm² and $K_2 = 2.1$. The absorption parameters obtained in this way are shown as a function of pion energy in Figure 26 (dashed curves), compared to the Riska values (solid curves). Both absorption parameters derived from pionic atom fits are higher than the calculated values at low energies, but the simple extrapolation gives a flatter energy dependence so that the calculated values overtake the extrapolated ones in the resonance region. The peak in the extrapolated value of $Im(C_{\Omega})$ is also shifted in energy compared to the calculated values. Although the imaginary parts of the absorption parameters can be estimated in this simple way, the real parts cannot, due to the more complicated form of the real part of the nuclear propagator G_N in equation III-57. (The imaginary part of G_N is just a delta function giving energy conservation.) The calculations of Riska and collaborators must be used to give the energy dependence of the real absorptive terms.

Calculations using this second set of parameters are shown as the dashed curves in Figures 27, and are compared to the previous calculations with λ = 1.6, shown as the solid curves. Again, there are not large differences between the two sets of calculations, although the extrapolated parameters give slightly better fits on the whole.

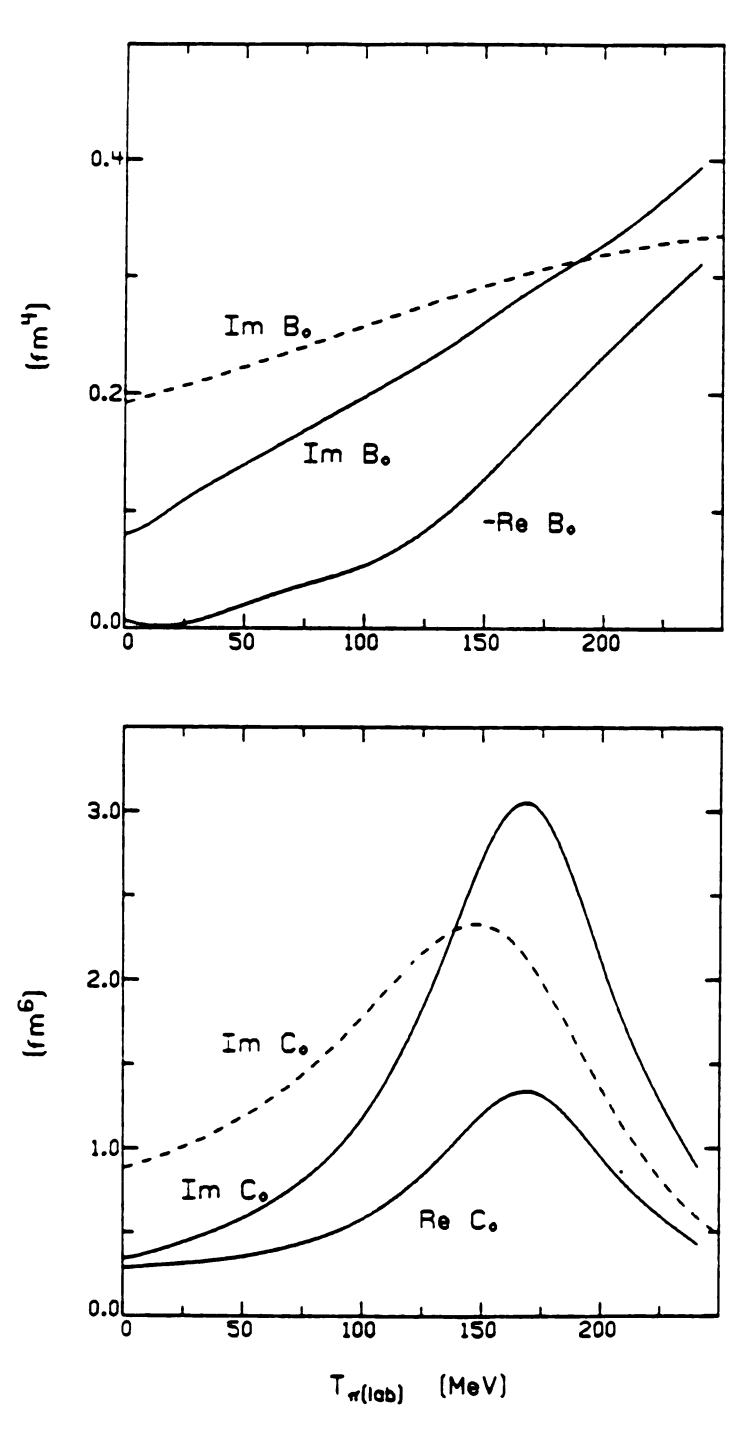
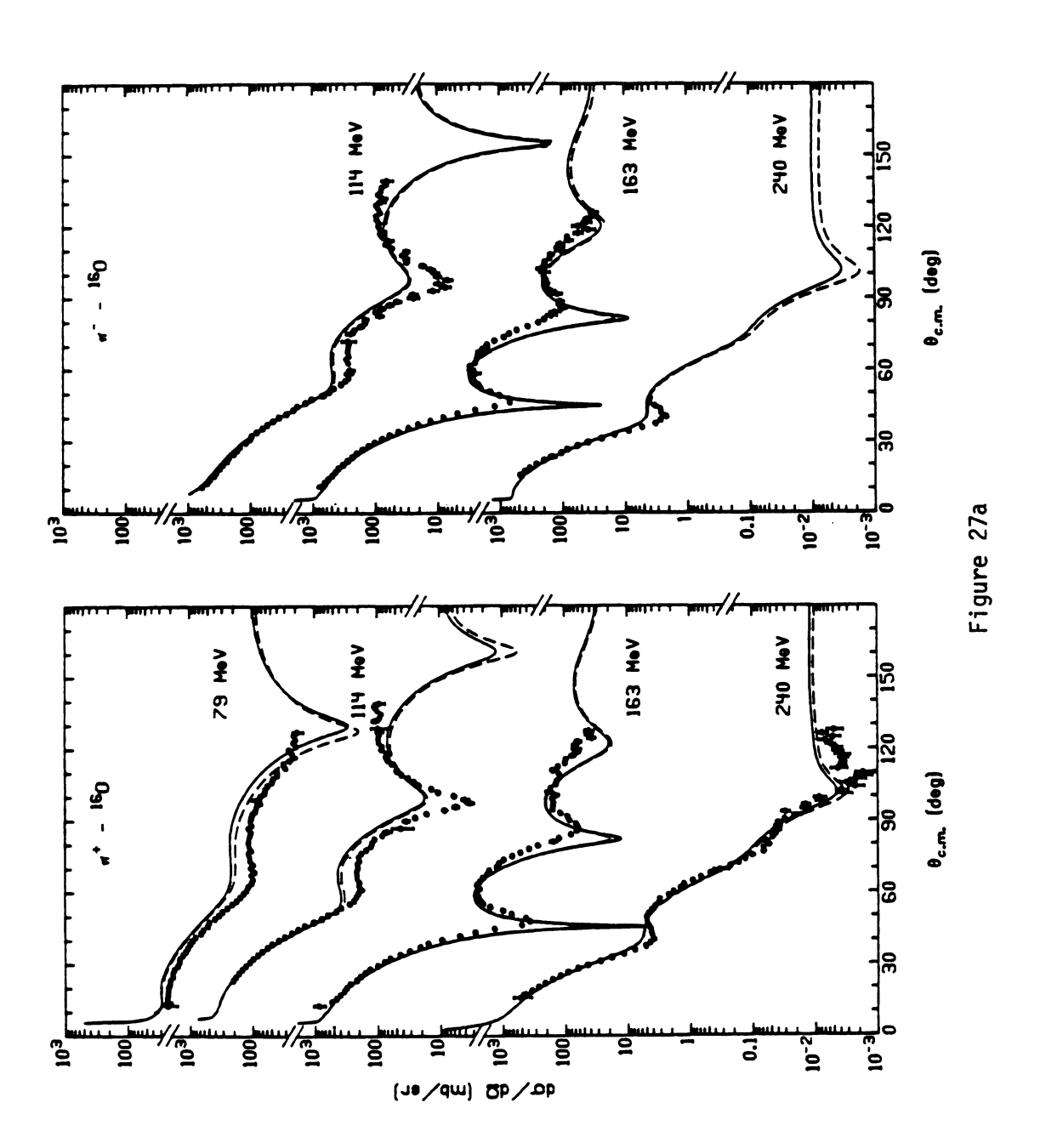


Figure 26. Imaginary absorption parameters extrapolated from pionic atom values (dashed curves) compared to those of Ref. 50 (solid curves).

Elastic scattering of π^+ and π^- from $^{16}0$. Absorption parameters are taken from Ref. 50 (solid curves) and extrapolated from pionic atom values (dashed curves) with other parameters from the RSL phase shifts and λ = 1.6. Figure 27a.



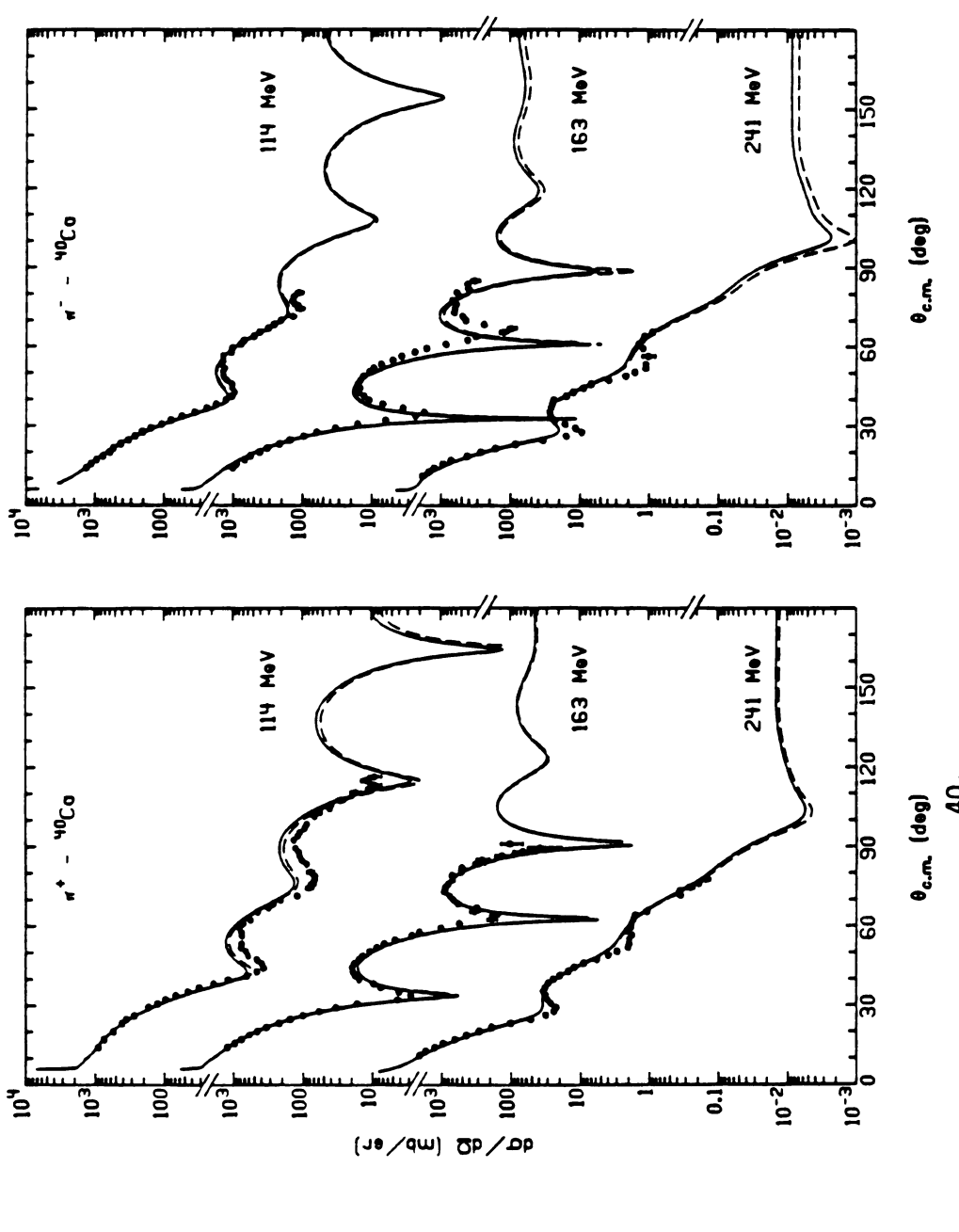


Figure 27b. Elastic scattering from ^{40}Ca .

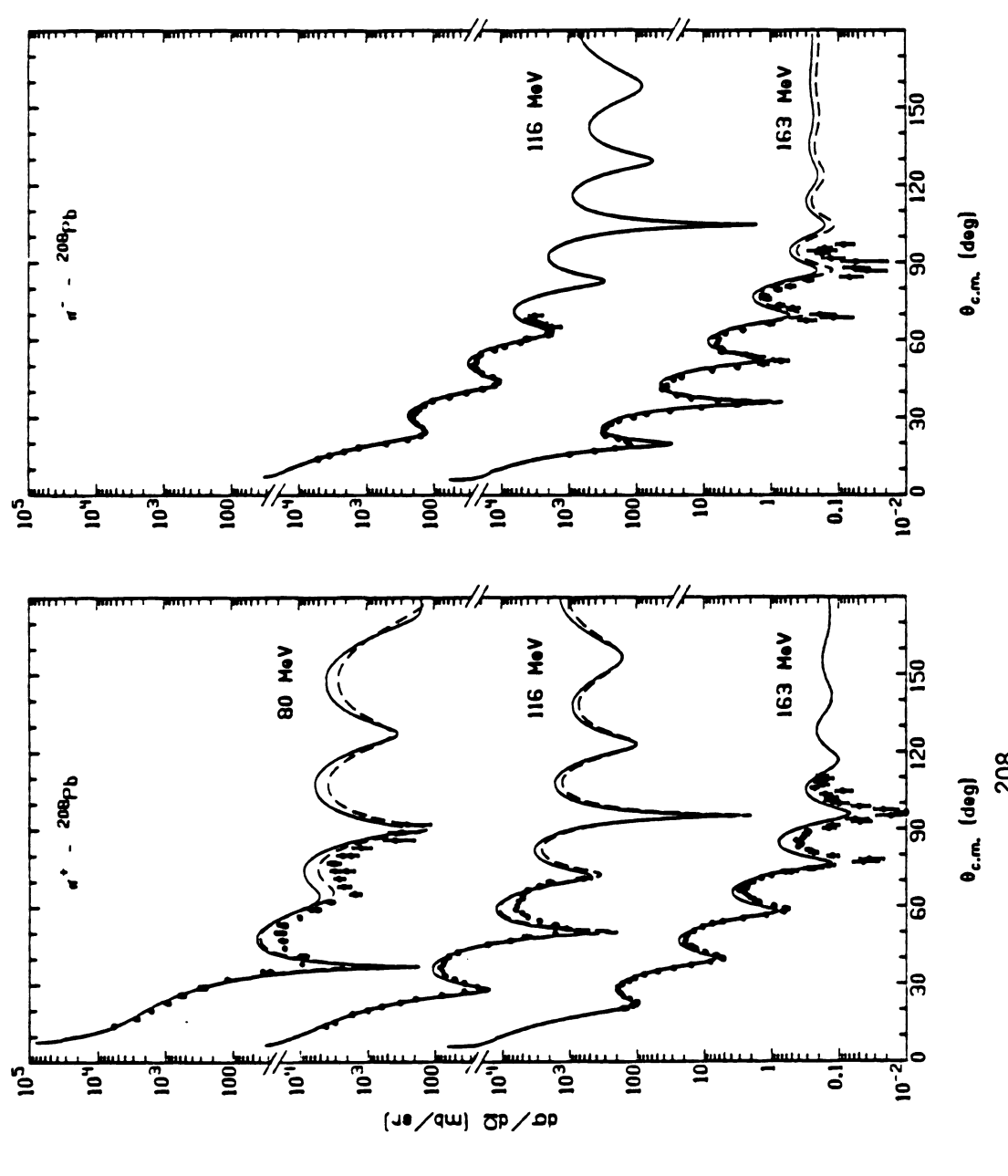


Figure 27c. Elastic scattering from ²⁰⁸Pb.

It is not clear whether the parameters or the optical potential itself should be blamed for the lack of detailed agreement between theory and data. The form of the optical potential is open to question, as several terms were calculated in the low energy limit. The concept of an optical potential in the resonance region has been questioned by Weise (77), who deduces from isobar-hole calculations that the potential is too nonlocal to be treated in this simple way at these energies. Unfortunately, detailed calculations, such as the isobar-hole calculations, are quite complex and must be done on a case by case basis. The optical model is the best simple approach, allowing calculations over a wide range of energies and nuclei.

CHAPTER VI

TOTAL AND PARTIAL CROSS SECTIONS

Before discussing the importance of total and partial cross section calculations as a test of the optical potential it is useful to define these quantities. The total cross section σ_T , the cross section for any kind of interaction to occur, can be divided into two pieces due to elastic scattering and to all other processes,

$$\sigma_{\mathsf{T}} = \sigma_{\mathsf{E}1} + \sigma_{\mathsf{R}}$$
, (VI-1)

where σ_{E1} is the differential cross section integrated over angles. The reaction cross section σ_R can again be divided into two parts, due to true pion absorption, σ_A , in which there is no pion in the final state, and to quasielastic scattering, σ_{QE} , which includes all processes with a pion in the final state. Note that in this discussion the charge exchange cross section, σ_{CX} , is included in σ_{OE} . Thus

$$\sigma_{\mathsf{T}} = \sigma_{\mathsf{E}1} + \sigma_{\mathsf{A}} + \sigma_{\mathsf{QE}} \tag{VI-2}$$

gives the various partial cross sections to be discussed in this chapter.

The total cross section and the partial cross sections σ_A and σ_{QE} are important because they are sensitive to parts of the optical potential that the differential elastic cross section may not be. In particular, σ_A and σ_{QE} are sensitive to the imaginary parts of the absorption and single nucleon parameters respectively and can provide information about the relative strength of these two parts of the potential which cannot be obtained from elastic scattering. Unfortunately the total and partial cross sections are difficult to measure, and the data are sparse. It is also not clear how to divide the calculated reaction cross section into its absorptive and quasielastic pieces in the model considered here. Thus the analysis can yield only tentative conclusions at present.

The first section of this chapter gives a discussion of the methods used in extracting total cross sections and forward nuclear amplitudes from the data and of the theoretical quantities to which these numbers correspond. In Section 2 the calculations of the total cross sections and nuclear amplitudes are compared to the data. The third section includes possible techniques for calculating the partial cross sections. Calculations of σ_{A} and σ_{QE} are compared to the experimental data in Section 4.

1. Extraction of Total Cross Sections and Scattering Amplitudes

Before calculations can be made the term total cross section must be redefined for any problem which involves the Coulomb interaction, because the total Coulomb cross section is infinite. A

quantity must be defined which has this Coulomb cross section subtracted, and which can be extracted from some set of experimental data. Two experimental groups have defined and measured such a quantity, Carroll et al. (78) and Jeppesen et al. (79). Their choices will be described in the discussion given below. Both begin with data obtained in a transmission experiment, in which the beam flux is measured before striking the target, and the flux of particles within a solid angle Ω centered on the beam axis is measured after the target. The difference can be expressed in terms of a cross section $\sigma(\Omega)$. Several cross sections can be defined relative to this. (This discussion follows that of Cooper and Johnson (80).)

One cross section which can be extracted from transmission data is the reaction cross section. Define

$$\sigma_{\mathbf{R}}(\Omega) = \sigma(\Omega) - \int_{>\Omega} d\Omega' \frac{d\sigma_{\mathbf{E}1}}{d\Omega'}$$
 (VI-3)

That is, the flux lost due to reactions other than elastic scattering is the total flux lost minus the flux that went into elastic processes with angle greater than Ω . The reaction cross section is the limit of $\sigma_R(\Omega)$ as Ω goes to zero. The calculation of the reaction cross section for $\sigma(\Omega)$ requires either a model for the elastic scattering or measured differential elastic cross sections at all angles.

The cross section usually referred to as the total cross section, also called the removal cross section, is defined as the limit of

$$\sigma_{\mathsf{T}}(\Omega) = \sigma(\Omega) - \int_{>\Omega} d\Omega' |f_{\mathsf{C}}|^2 - 2\mathsf{Re} \left[\int_{>\Omega} d\Omega' f_{\mathsf{C}}^{\star} f_{\mathsf{N}} \right]$$
 (VI-4)

as $\Omega \to 0$. This is the quantity extracted by Carroll et al. (78). Here the scattering amplitude has been separated into a Coulomb and a nuclear part,

$$f(\theta) = f_{N}(\theta) + f_{C}(\theta)$$
 (VI-5)

where

$$f_{C}(\theta) = -\frac{\eta_{C}}{2k \sin^{2} \frac{\theta}{2}} \exp \left\{2i\left[\sigma_{0} - \eta_{C}\ln(\sin \frac{\theta}{2})\right]\right\}$$
 (VI-6)

with

$$\eta_{\mathbf{C}} = \mathbf{Z} \varepsilon_{\mathbf{\pi}} \alpha \, \frac{\omega}{\mathbf{k}} \tag{VI-7}$$

and

$$f_{N}(\theta) = \frac{1}{ik} \sum_{\alpha} (2\ell + 1)e^{2i\sigma_{\ell}} \left[\frac{e^{2i\delta_{\ell}} - 1}{2} \right] P_{\ell}(\cos \theta) \qquad (VI-8)$$

Note that the nuclear amplitude cannot be completely separated from the Coulomb; f_N still contains the Coulomb phase shifts σ_{ℓ} . The removal cross section measures flux lost to reaction processes and the $|f_N|^2$ part of the elastic scattering. The extraction of σ_T is difficult because one needs not only $|f_C|^2$ which is calculable,

but also $\text{Re}(f_{C}^{*}f_{N})$, for which a model of f_{N} is required. It can be shown (80) that the cross section σ_{T} defined in equation VI-4 can be related to the scattering phase shifts by

$$\sigma_{T} = \frac{4\pi}{k} \operatorname{Im}[\tilde{f}_{N}(0)] \tag{VI-9}$$

where

$$\tilde{f}_{N}(\theta) = \frac{1}{ik} \sum_{\ell} (2\ell + 1) \left[\frac{e^{2i\delta_{\ell}} - 1}{2} \right] P_{\ell}(\cos \theta) \qquad (VI-10)$$

Note that $\tilde{\mathbf{f}}_N$ differs from \mathbf{f}_N in the absence of the Coulomb phase shift factor.

The quantity extracted by Jeppesen et al. (79) is $\sigma_N(\Omega)$, defined and discussed by Cooper and Johnson (80)

$$\sigma_{N}(\Omega) = \sigma(\Omega) - \int_{>\Omega} d\Omega' |f_{C}|^{2}$$
 (VI-11)

The advantage of this definition is that only the known function $f_{\mathbb{C}}$ is required; no model is necessary for the full pion nucleus interaction. Cooper and Johnson show that the limit of $\sigma_{\mathbb{N}}(\Omega)$ as $\Omega \to 0$ is given by

$$\sigma_{\mathbf{N}} = \frac{4\pi}{k} \operatorname{Im}[f_{\mathbf{N}}(0)] \tag{VI-12}$$

The quantity $\sigma_{\rm N}$ has no direct physical significance, and in fact is not always positive. If equation VI-11 is rearranged and a

polynomial expansion in Ω is made for the various terms, the following form results,

$$\sigma_{N}(\Omega) = (\sigma_{N} + \sum_{n} A_{n} \Omega^{n}) \cos W + \left[\frac{4\pi}{k} \operatorname{Re}[f_{N}(0)] + \sum_{n} B_{n} \Omega^{n}\right] \sin W$$

$$+ \sum_{n} C_{n} \Omega^{n} \qquad (VI-13)$$

where

$$W = \gamma \log (\Omega/4\pi) - 2\sigma_0 \qquad (VI-14)$$

with

$$\gamma = \frac{Ze^2}{hv}$$
 (VI-15)

for positive pions. Here v is the pion velocity. The quantity f_N is given in equation VI-8. Thus if sufficient data exists at small enough Ω so that the sums have only a few terms, the parameters σ_N , $\text{Re}[f_N(0)]$, A_n , B_n , and C_n can be determined. For large Z the cos W and sin W terms can be distinguished and both $\text{Re}[f_N(0)]$ and $\text{Im}[f_N(0)]$ (from σ_N) can be derived. For small nuclei only $\text{Im}[f_N(0)]$ is determined. A model for elastic scattering can be used as an aid to extracting $f_N(0)$; the number of fitted parameters can thereby be reduced. The role of the model in this analysis is much less important than in the extraction of σ_T , however. The chief difficulty in the approach of Cooper and Johnson is the problem

of interpreting the results, as f_N includes the Coulomb phase $2i\sigma_{\ell}$ factors e

This completes the description of the two experimental quantities related to the total cross section, σ_T and $f_N(0)$, and their relation to the calculated pion-nuclear phase shifts. Theoretical calculations of these quantities are compared to these data in the next section.

2. Total Cross Section and Scattering Amplitude Calculations

In this section two sets of calculations are presented for σ_T and $f_N(0)$, corresponding to the two sets of parameters discussed in Section 5 of the previous chapter. These are the theoretical set including the absorption parameters of Riska, shown in the figures as solid curves, and the set in which $\operatorname{Im}(B_0)$ and $\operatorname{Im}(C_0)$ are extrapolated from pionic atom fits, shown as dashed curves.

The first set of data to be considered is that of Carroll et al. (78), who have extracted σ_T , as defined in the previous section, from data on natural Li, C, Al, Fe, Sn, and Pb at energies from about 65 to 250 MeV. For the quantity f_N required in their analysis they used an optical model calculation with a first order Laplacian potential and parameters from π -N phase shifts. They adjusted the energy and width of the (3,3) resonance contribution, however, to fit the position and width of the peak in the total cross section as a function of energy.

A comparison of the experimental and calculated total cross sections is given in Figure 28. Although the calculations reproduce the data for the light nuclei, there are significant discrepancies for the larger nuclei, especially for π^+ . The calculations show a much greater difference between π^+ and π^- total cross sections at the lower energies than is seen in the data. It is to be noted that the calculated cross sections are insensitive to differences in the absorption parameters of the size to be found in the two parameter sets.

It is difficult to draw conclusions from this data, as the effect on the experimental cross sections of the model used in their extraction is unknown. The dashed curves of Figure 3 give the result of calculations with the first order Laplacian model with parameters from π -N phase shifts. As can be seen, the fits are somewhat random, being reasonable for 16 0 but not for 208 Pb. The effect of the variations made in the parameters in the fitting of the total cross section peak is not clear. Thus no definite conclusions can be drawn until the accuracy of the data has been assessed.

The second set of data to be discussed is that of Jeppesen et al. (79). The data are from targets of Al, 40 Ca, Cu, Sn, Ho, and Pb and pion energies from 63 to 215 MeV. Although their analysis is less model dependent, the interpretation of the trend in energy or A of the quantity $f_N(0)$ that they extract is complicated by the Coulomb phase, as noted in the previous section.

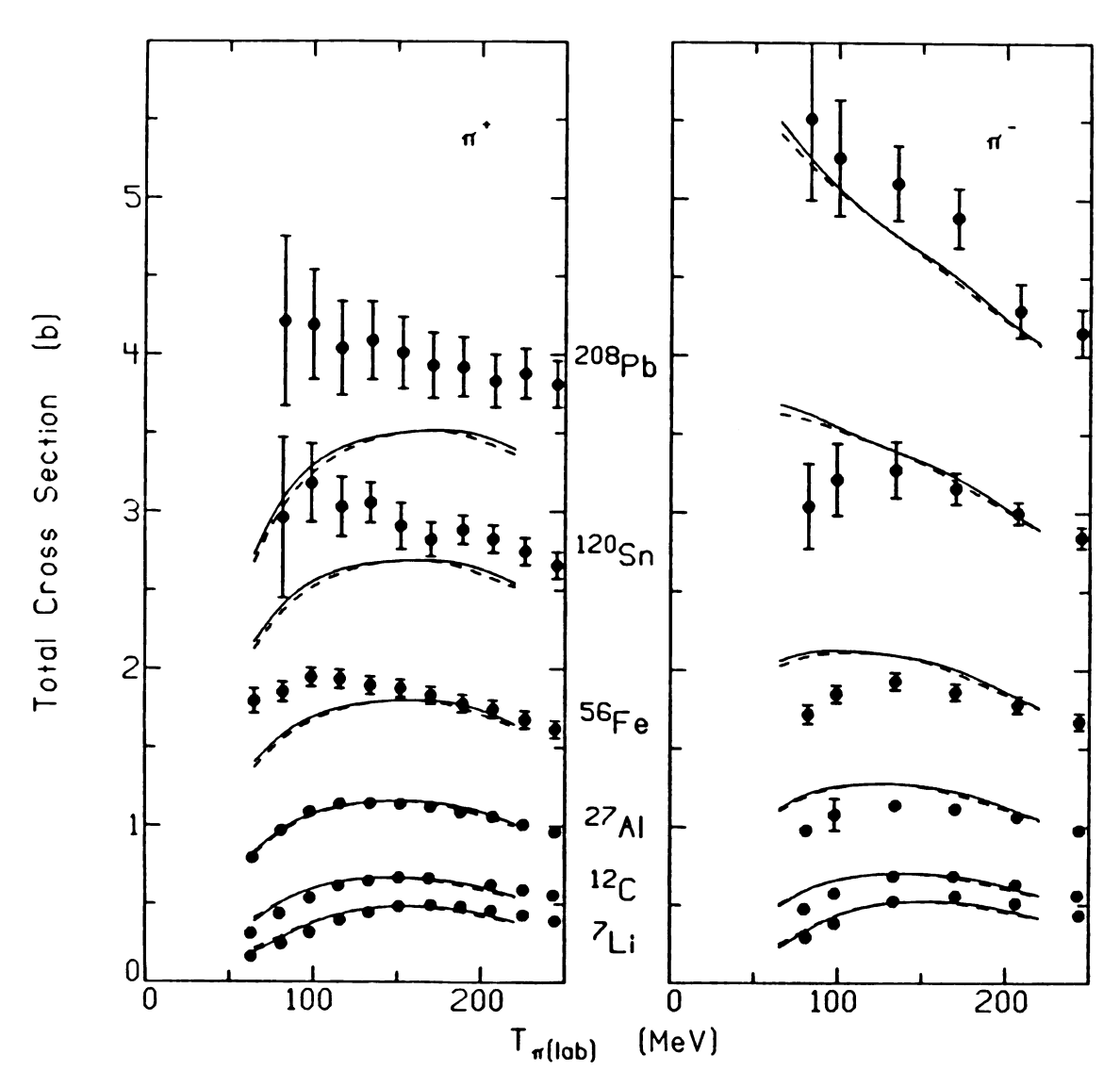


Figure 28. Total cross section calculations using the absorption parameters of Ref. 50 (solid curves) and extrapolated pionic atom parameters (dashed curves) compared to the data of Carroll et al. (78).

The experimental and calculated values of $f_N(0)$, defined in equation VI-8, are compared in Figures 29-31. Figures 29 and 30 illustrate the energy dependence of $f_N(0)$ for $^{27}\mathrm{Al}$ and $^{207}\mathrm{Pb}$ respectively; Figures 31 show the A dependence at 165 MeV. In each case the data for π^+ are indicated by circles, for π^- by X's. Although the general features of the data are well described, there are again problems with details. The poor quality of the fits to the data for ^{207}Pb may be due in part to the neglect of the V_{C}^{2} term in the potential, and its absence in the calculation of $\sigma_{\mbox{\scriptsize L}}$ and the Coulomb wavefunctions. The A dependence of the data at 165 MeV is quite well reproduced, suggesting that the large discrepancies between theory and the Carroll data seen for π^+ on the large nuclei may be exaggerated. A more detailed comparison of the two data sets is difficult, due to the fundamental differences between the quantities $\sigma_{\mbox{\scriptsize T}}$ and $f_{\mbox{\scriptsize N}}(0)\,.$ As in the case of the resonance region elastic scattering, the poor quality of the fits and the insensitivity to moderate parameter changes demand a closer scrutiny of the optical potential itself.

3. Theoretical Expressions for the Partial Cross Sections

Measurements have recently been made of the components of the reaction cross section: the quasielastic, charge exchange, and absorption cross sections, both as a function of energy for one nucleus and as a function of A at a particular energy (81).

Although the reaction cross section can be calculated from the simple expression (82)

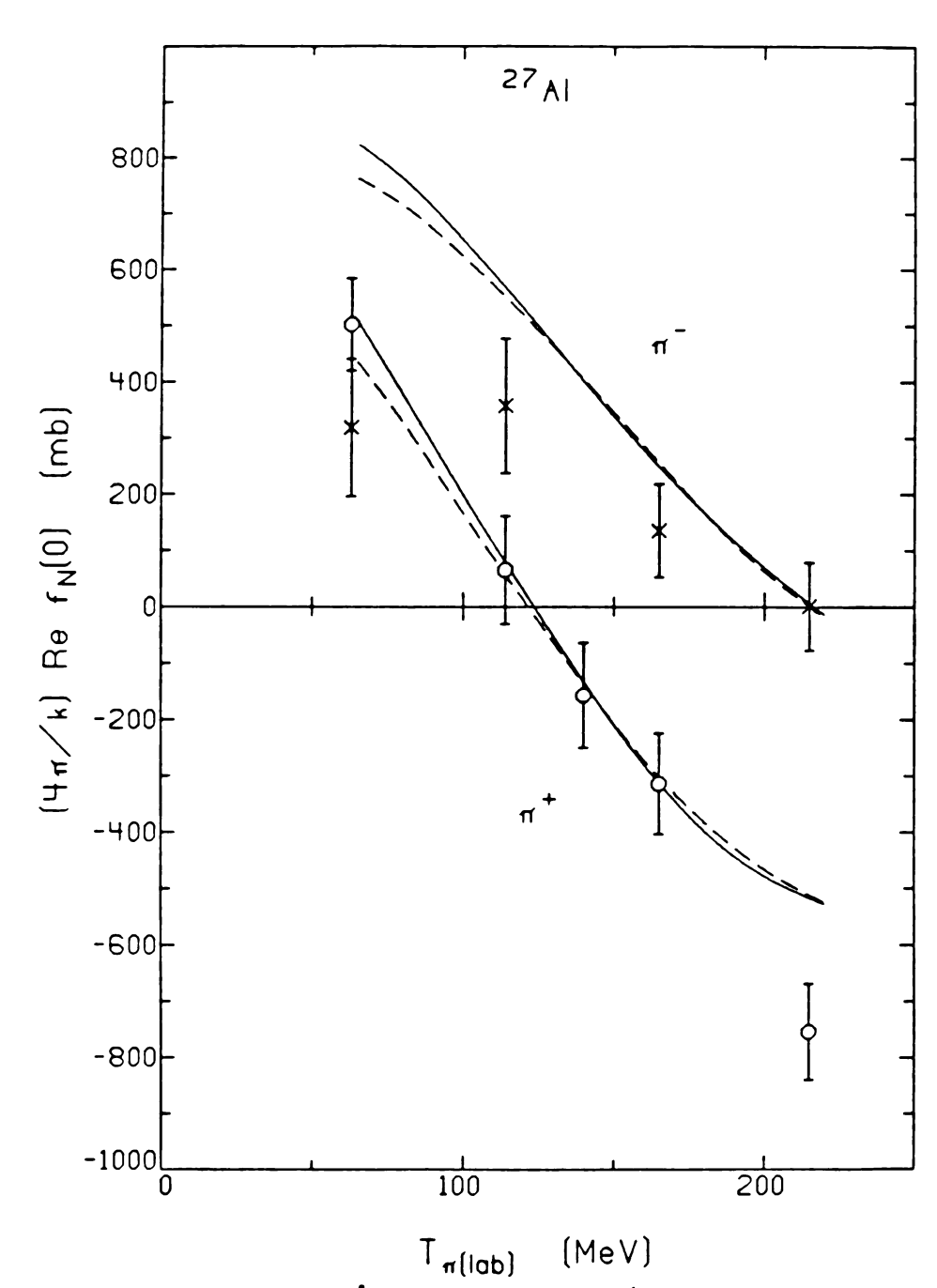
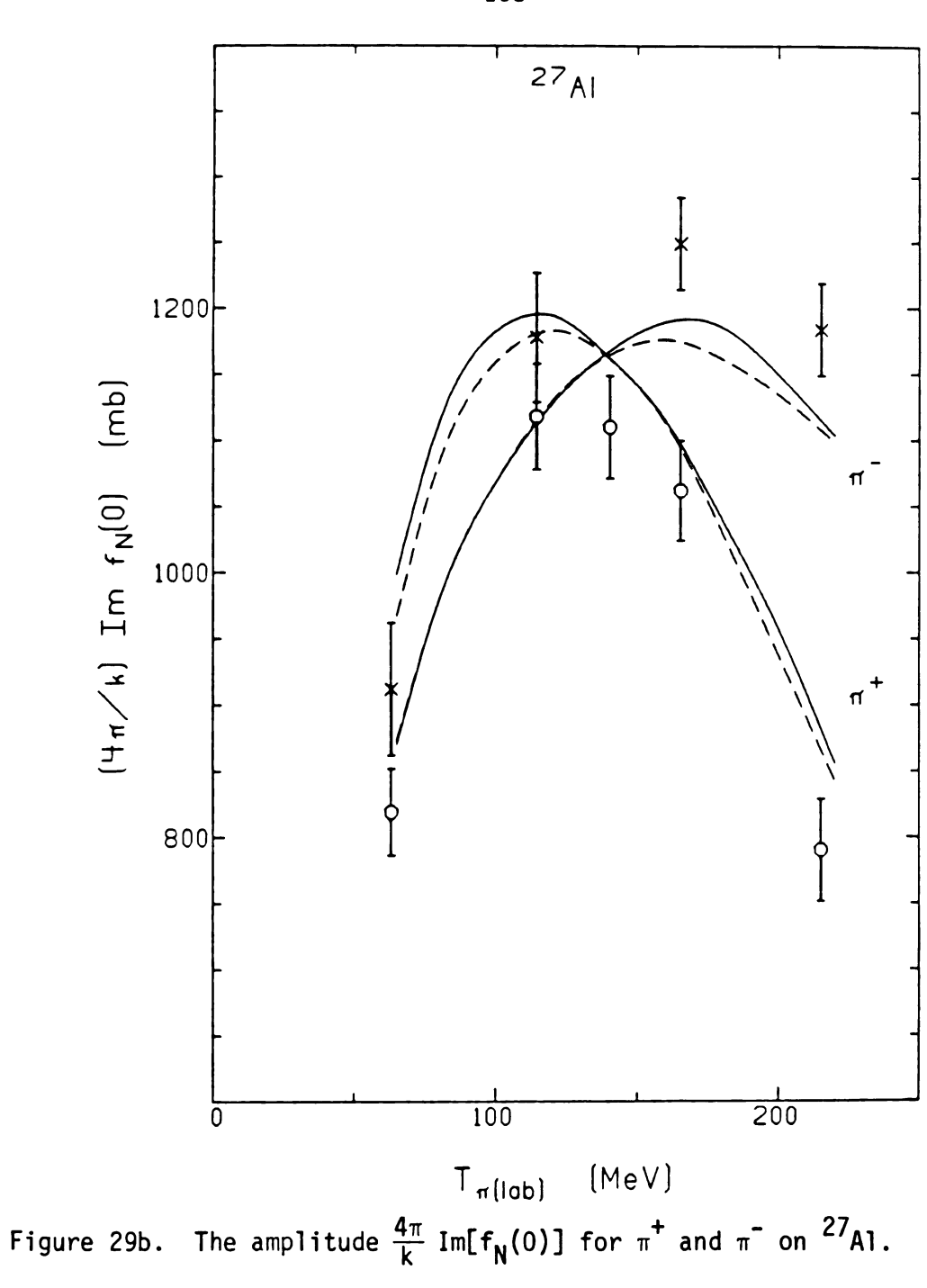


Figure 29a. The amplitude $\frac{4\pi}{k}$ Re[f_N(0)] for π^+ (circles) and π^- (x's) on 27 Al, as a function of energy. Curves are same as in Figure 28. Data are from Jeppeson et al. (79).



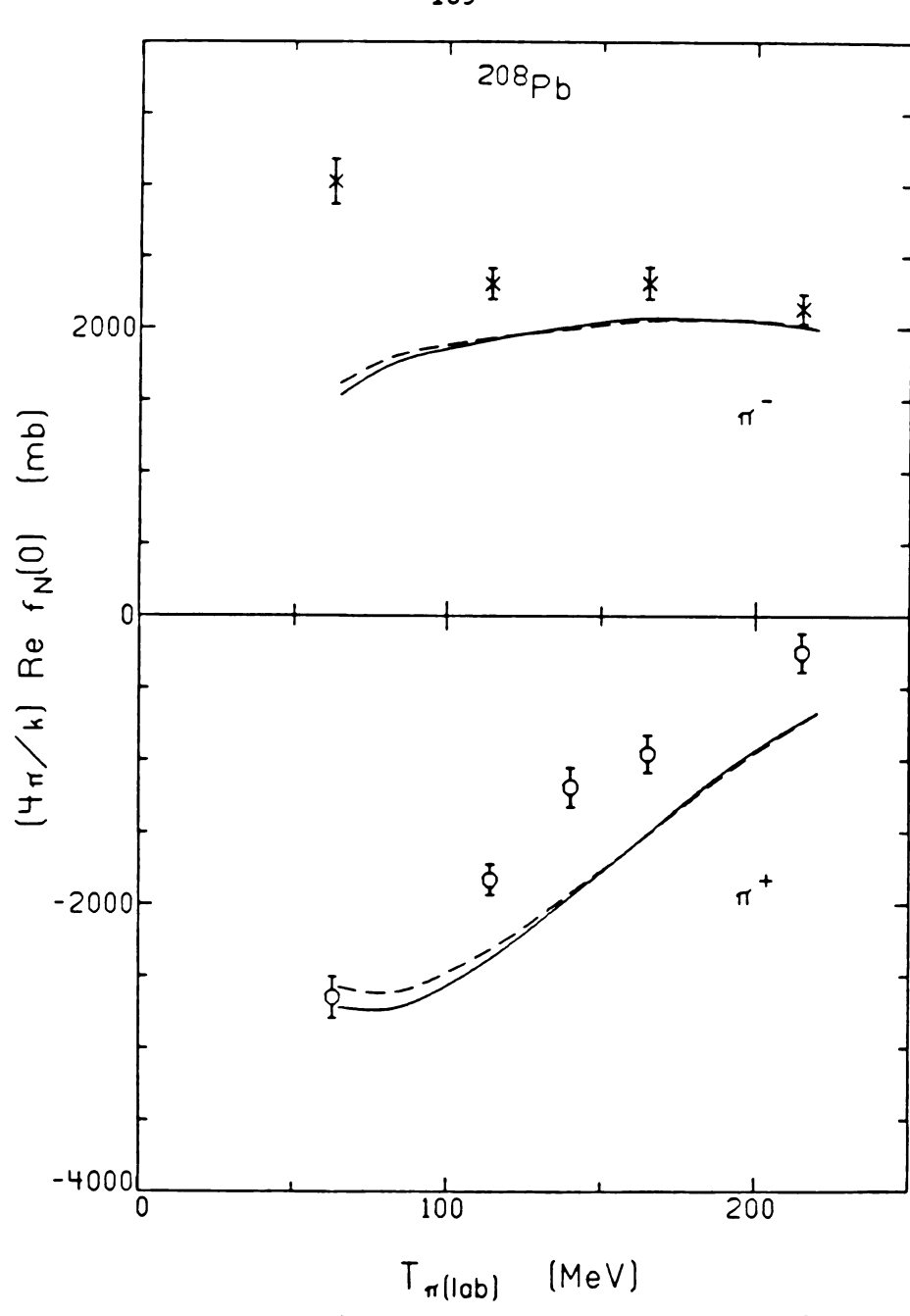


Figure 30a. The amplitude $\frac{4\pi}{k}$ Re[f_N(0)] for π^+ and π^- on 208 Pb. Curves are same as in Figure 28. Data are from Ref. 79.

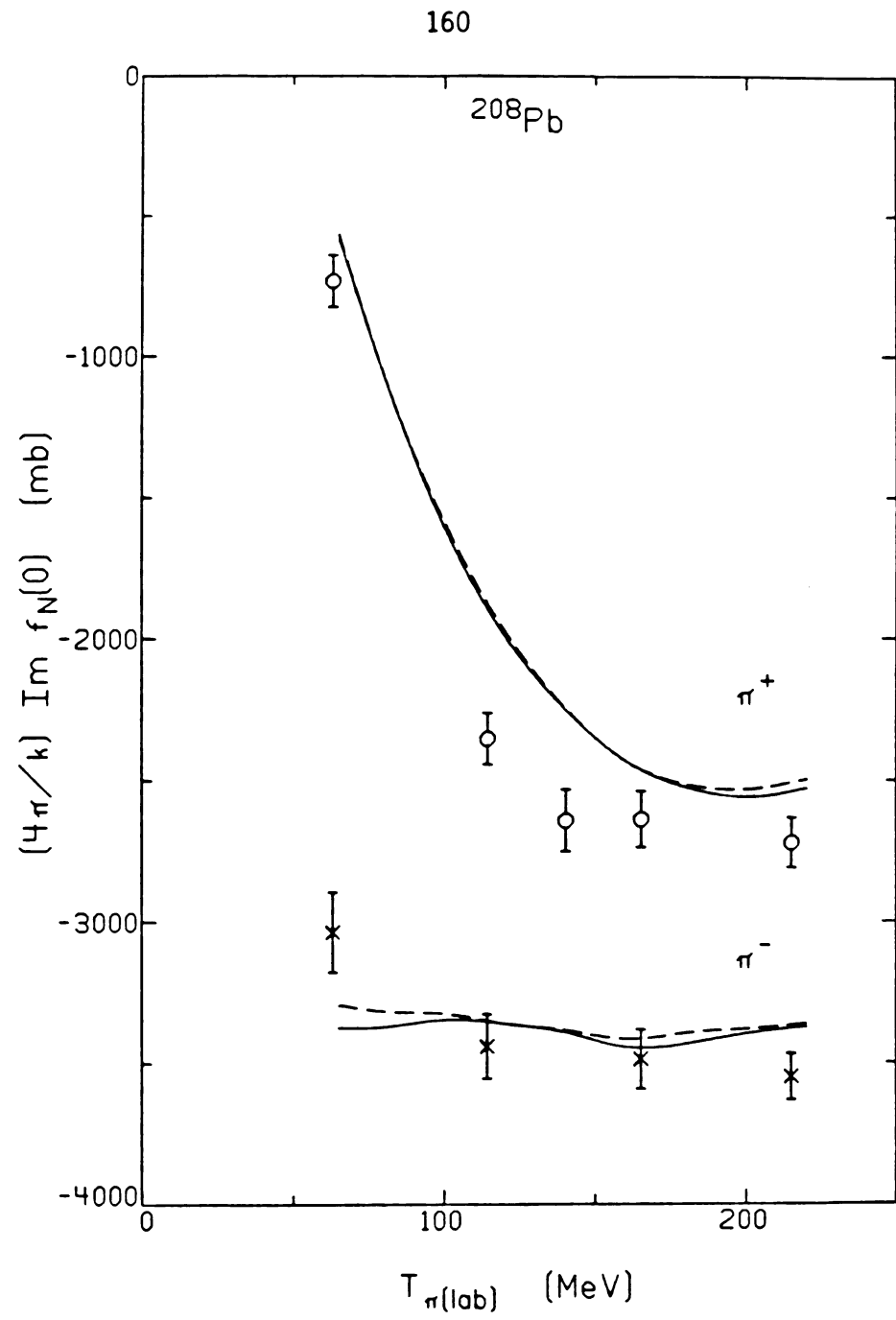


Figure 30b. The amplitude $\frac{4\pi}{k}$ Im[f_N(0)] for π^+ and π^- on 208 Pb.

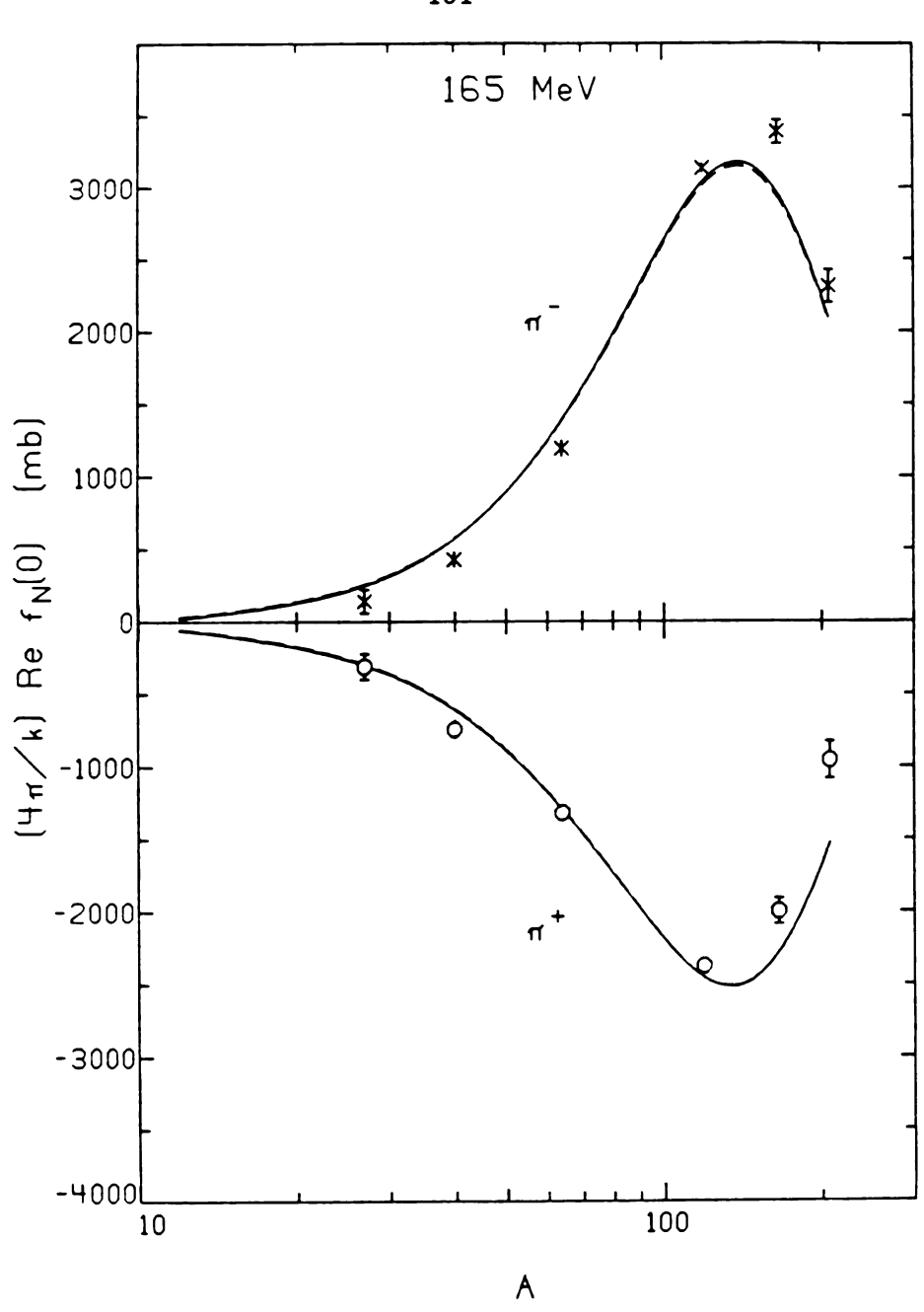
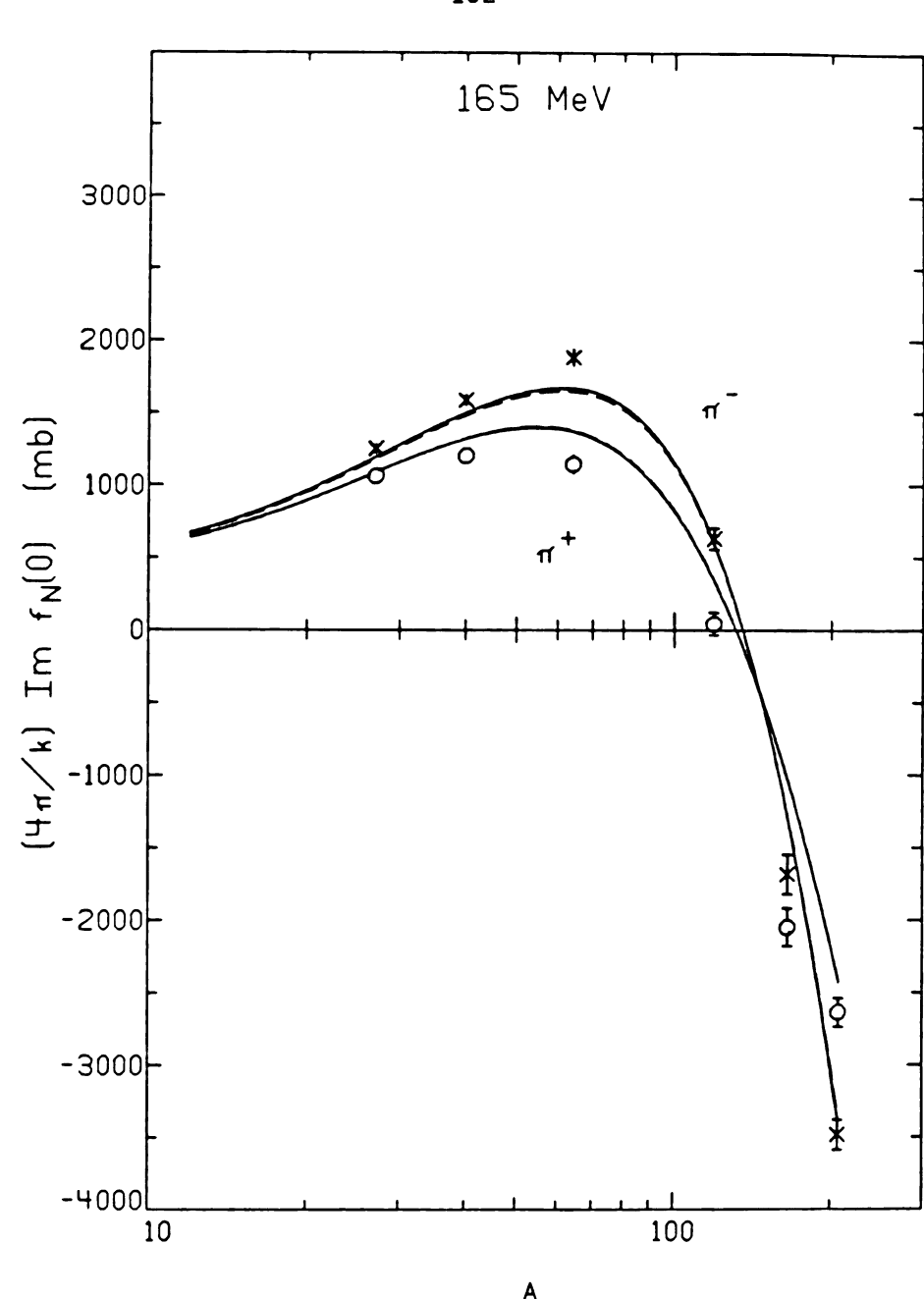


Figure 31a. The amplitude $\frac{4\pi}{k}$ Re[f_N(0)] for π^+ and π^- as a function of A at 165 MeV. Curves are same as in Figure 28. Data are from Ref. 79.



\$A\$ Figure 31b. The amplitude $\frac{4\pi}{k}$ Im[f_N(0)] as a function of A.

$$\sigma_{R} = -\frac{1}{k} \int \phi^{*}(\underline{r}) Im[2\overline{\omega}U_{opt}(\underline{r})] \phi(\underline{r}) d^{3}r , \qquad (VI-16)$$

where $\phi(r)$ is the distorted pion wavefunction, there is no well defined prescription for calculating the various components of σ_R within the framework of the optical model. Thus some approximate means of calculating σ_{OE} and σ_A must be devised.

As the optical potential can be divided into single nucleon and absorption terms, a first guess at the form of the partial cross sections is

$$\sigma_{QE} = -\frac{1}{k} \int \phi^{\star}(\underline{r}) Im[2\overline{\omega} U_{opt}^{sn}(\underline{r})] \phi(\underline{r}) d^{3}r \qquad (VI-17)$$

and

$$\sigma_{A} = -\frac{1}{k} \int \phi^{*}(r) \operatorname{Im}[2\overline{\omega}U_{\text{opt}}^{A}(r)] \phi(r) d^{3}r \qquad (VI-18)$$

This technique is perhaps reasonable in the low energy region, where the absorption terms dominate. It is not a good prescription in the resonance region, where the imaginary single nucleon and absorption parameters are both large. The reason is that the two processes are not equivalent; a pion which scatters quasielastically can still be absorbed, but an absorbed pion cannot later scatter. This problem was considered in Glauber theory (14), which is a good approximation in the limit of high energy, projectile wavelength short compared to the nuclear size, and strong forward scattering. The Glauber result can be recast in the form of equations VI-17 and

VI-18. The result is that only the imaginary absorptive terms should be used in calculating the distorted wavefunctions in the expression for σ_{Δ} ,

$$\sigma_{A} = -\frac{1}{k} \int \phi_{A}^{\star}(\underline{r}) \operatorname{Im}[2\overline{\omega} U_{\text{opt}}^{A}(\underline{r})] \phi_{A}(\underline{r}) d^{3}r . \qquad (VI-19)$$

That is, the ϕ_A satisfy a wave equation with an optical potential in which the imaginary parts of the single nucleon parameters are set equal to zero. The quasielastic cross section is then the difference between the reaction cross section from equation VI-16 and σ_A ,

$$\sigma_{OF} = \sigma_{R} - \sigma_{A} . \qquad (VI-20)$$

The Glauber theory result can also be derived in a simple semiclassical transport theory, as noted by Koltun and Schneider (83). This theory is expected to be a good approximation in the same limit as for Glauber theory provided phases are not important, i.e., the real parts of the optical potential are small. These conditions are all reasonably well satisfied near the resonance energy. They consider a pion traveling through the nucleus with impact parameter b. The change with x in the probability $P_S(x)$ that the pion is in a particular state S at a horizontal distance x can be related to the probabilities for processes which feed or rob the state S. The possible states of the pion are the elastic channel, with

probability P_0 , a quasielastic scattering state, with probability P_{QE} , and nonexistence due to absorption, with probability P_A . The quasielastic scattering and absorption processes are characterized by mean free paths, λ_S and λ_A . The transport equations, which describe the change in the probability of a given state with position, can be written

$$\frac{dP_0}{dx} = -\frac{P_0}{\lambda_S} - \frac{P_0}{\lambda_A}$$

$$\frac{dP_{QE}}{dx} = \frac{P_0}{\lambda_S} - \frac{P_{QE}}{\lambda_A}$$

$$\frac{dP_A}{dx} = \frac{P_0}{\lambda_A} + \frac{P_{QE}}{\lambda_A}$$
(VI-21)

Positive terms on the right-hand side refer to processes which feed into the channel being considered, negative terms to processes which rob the channel. The small terms due to quasielastic processes feeding back into the elastic channel have been neglected. The boundary conditions for the probabilities are

$$P_{0}(0) = 1$$

$$P_{QE}(0) = 0 \qquad (VI-22)$$

$$P_{A}(0) = 0 ,$$

where x = 0 is the edge of the nucleus at which the pion enters, with x increasing across the nucleus. The solutions to equations VI-21 with these boundary conditions are

$$P_{0} = e^{-x/\lambda}$$

$$P_{QE} = e^{-x/\lambda}A(1 - e^{-x/\lambda}S)$$

$$P_{A} = 1 - e^{-x/\lambda}A$$
(VI-23)

where λ is defined by

$$\frac{1}{\lambda} = \frac{1}{\lambda_{A}} + \frac{1}{\lambda_{S}} \tag{VI-24}$$

The cross sections for these processes are obtained by integrating the probabilities at the end of the pion path through the nucleus over all impact parameters and angles,

$$\sigma_{QE} = 2\pi \int b \, db \, e^{-L(b)/\lambda} A (1 - e^{-L(b)/\lambda} S)$$

$$\sigma_{A} = 2\pi \int b \, db (1 - e^{-L(b)/\lambda} A)$$
(VI-25)

where L(b) is the length of the path through the nucleus at impact parameter b, L(b) = $2\sqrt{R^2 - b^2}$. Here R is the radius of the nucleus, taken to have a uniform matter distribution. The reaction cross section is just the sum of these two expressions,

$$\sigma_{R} = 2\pi \int b \ db(1 - e^{-L(b)/\lambda})$$
 (VI-26)

with λ given by equation VI-24. Comparison of the expressions for σ_A and σ_R indicates the Glauber result, that the absorption cross section is calculated in the same way as the reaction cross section, but with only absorptive processes taken into account.

The transport calculation just described can itself be used to give the quasielastic and absorption cross sections, with the mean free paths estimated from the optical potential. The results, however, give the wrong ratio of quasielastic and absorption cross sections and the wrong A dependence of the quasielastic cross sections. Various improvements to the transport theory are possible (83); however, these will not be discussed here. The transport theory result is used only as an approximate justification for equations VI-19 and VI-20.

Partial Cross Section Calculations

In this section the calculations of σ_{QE} and σ_{A} are compared to the data of Navon et al. (81). The two approximations discussed in the last section are adopted in their respective energy domains: equations VI-17 and VI-18 are employed for energies through 50 MeV, equations VI-19 and VI-20 in the resonance region, 160-220 MeV. No reliable method is known for extracting σ_{QE} and σ_{A} between 50 and 160 MeV. The limitations of the model should be kept in mind when comparisons of calculations and data are made.

In Figure 32 calculations of partial cross sections, using the two parameter sets described in Section 2, are compared with the data for π^+ on 12 C as a function of pion energy. Note that smooth curves have been drawn to connect the low energy and resonance regions. The reaction cross sections are well described by the calculations. The differences between the results of the two parameter sets for $\sigma_{\mathbf{p}}$ at low energies are due almost entirely to differences between $\sigma_{\!A}$ for the two sets; the quasielastic cross sections are about the same. The calculated absorption cross sections mirror to some extent the differences between the p-wave absorption parameters of the two sets, with the extrapolated pionic atom parameters giving much higher absorption cross sections at low energies, peaking earlier, and falling faster than the calculations with the Riska parameters. It is clear that both sets of calculations overestimate the absorptive and underestimate the quasielastic pieces of the reaction cross section. The absorption cross section has the correct shape, peaking near the resonance and falling off at higher energies. The data are not yet precise enough to determine the energy at which $\sigma_{\!\Delta}$ peaks, thus little can be said of the relative merits of the two parameter sets. The calculated quasielastic cross section appears to rise too slowly between 50 and 150 MeV; however, as the curves are pure interpolation in this region no conclusions can be drawn from this. Insufficient evidence exists at present to determine whether the overestimated absorption cross sections are due to the strength of the absorption parameters themselves or to



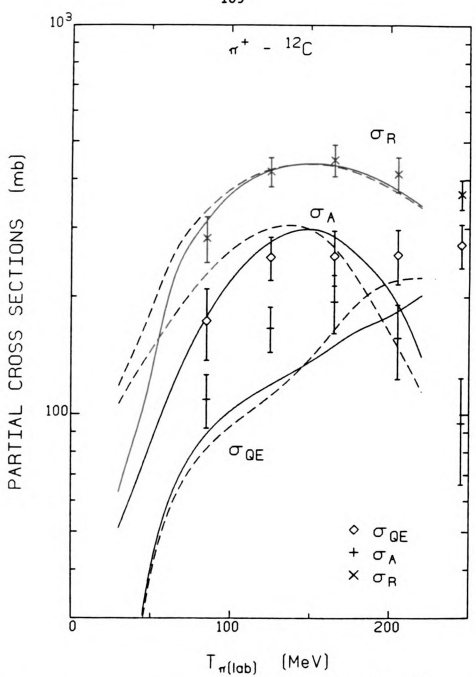
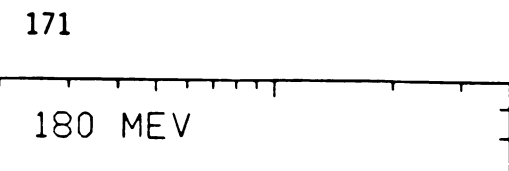


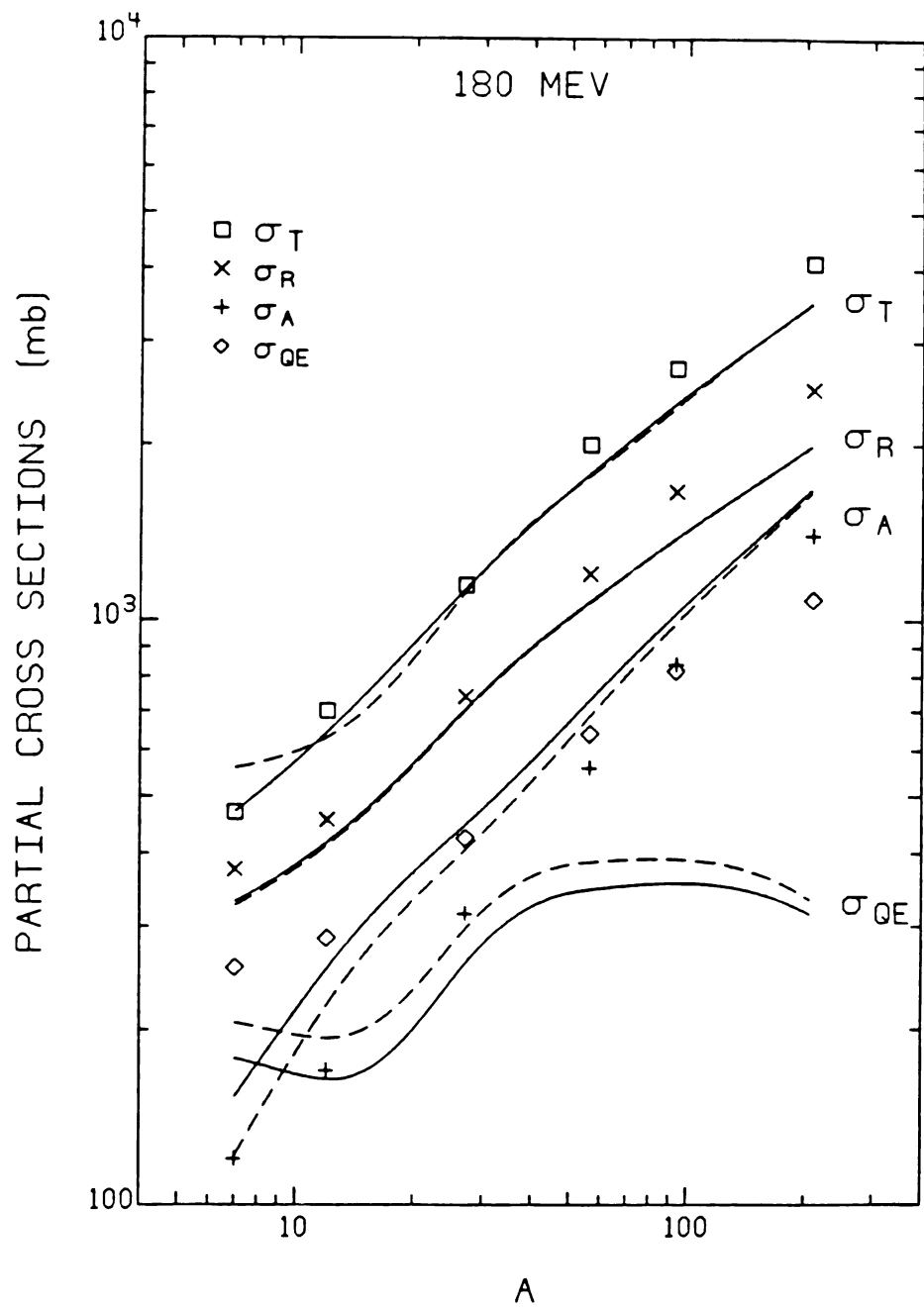
Figure 32. Partial cross section calculations for π^{+} on ^{12}C as a function of energy compared to the data of Navon et al. (81). Curves are same as in Figure 28.

the method of calculating the cross sections. It should be noted that calculations of σ_A using equation VI-17, that is, with the fully distorted wavefunctions, produce much smaller absorption cross sections. The true value may lie between these two calculations.

Figure 33 shows comparisons of calculated and experimental partial cross sections as a function of A. The data were taken at 165 MeV; however, the calculations are done at the resonance energy, 180 MeV, where the conditions required for the transport theory to be a good approximation are best met. The differences between cross sections at 165 and 180 MeV are presumed small. The solid and dashed curves are the optical potential calculations with the two parameter sets previously described. Note that the data are preliminary and have not been assigned errors as yet. The reaction and total cross sections are well reproduced by both sets of calculations. Although the calculated absorption cross section has about the right A dependence, it is too large in comparison with the data. The calculated quasielastic cross section is much too small and exhibits a flattening or saturation effect at large A which is not seen in the data. Part of this effect may be due to noise in the calculation, as σ_{OE} is the difference of two large terms. Again, the uncertainties in the method of determining $\sigma_{\mbox{\scriptsize OE}}$ and $\sigma_{\!A}$ preclude any definite conclusions about the optical potential at this stage.

It is possible that the problem of separating the reaction cross section into absorptive and quasielastic pieces could be solved





Partial cross section calculations as a function of A for π^+ at 165 MeV, compared to the data of Ref. 81. Curves are same as in Figure 28. Figure 33.

by a different approach. The quasielastic cross section can perhaps be calculated directly, as was done for nucleon scattering by Bertsch and Tsai (84). Studies of charge exchange reactions indicate that the quasielastic scattering, of which charge exchange is assumed representative, looks like quasi-free scattering in energy and angle dependence, but with an effective number of nucleons $N_{\rm eff}$ which is less than A (85). Thus the quasielastic scattering is a simple process, and could be calculated by summing the distorted wave impulse approximation results to all final states, using the full optical potential to distort the incoming wave and the optical potential with only absorptive imaginary parts for the outgoing wave, as suggested by Koltun (83). A great deal of work remains to be done on this subject.

CHAPTER VII

CONCLUSIONS

The focus of this work has been the construction and testing of a pion-nucleus optical potential which is simple in form but which includes the important physics. In this chapter the main features of the model are reviewed and its accuracy in reproducing the relevant experimental data is summarized. Unsolved problems and areas for further study are also discussed.

The optical potential was constructed from the experimentally determined pion-nucleon transition amplitude using the Watson multiple scattering series. The off-shell form of the T matrix was taken to be of Kisslinger type, without form factors. This form is convenient because it leads to a coordinate space potential which is local (although velocity dependent), making calculations much simpler. The kinematic transformation of the T matrix was treated in an approximate way, expanding in ω/M and keeping only zero and first order terms. The second order s-wave term of the multiple scattering series as calculated in low energy approximation was included, as was a sum of the p-wave series in the same approximation. True pion absorption was represented by terms quadratic in the nuclear density, for which an approximate theoretical justification exists. Pauli blocking was roughly included, and an energy

shift due to the Coulomb potential was incorporated. The parameters for the various terms in the optical potential were taken from the experimental πN phase shifts and from various theoretical calculations (47,48,50). An alternative set of parameters was derived from fits to pionic atom level shifts and widths with suitable energy extrapolation.

This method of constructing the optical potential has several weaknesses. The first is that the starting point contains insufficient information; the πN data can only give the on-shell behavior of the T matrix (unless a separable form is assumed (37)). A fundamental theory of the πN interaction is necessary to give the correct off-shell dependence. Such a theory, if fully relativistic, would provide the proper kinematics for the problem as well as the necessary framework for treating the higher order multiple scattering and absorption terms consistently. No completely satisfactory πN theory exists, although some form of Chew-Low description (86) is probably adequate. To carry out this program of optical model construction is an impossibly complicated task; a proper first order calculation in a finite nucleus would be very difficult. The complicated dependence of the full T matrix on the nucleon momenta requires the use of realistic nucleon wavefunctions in the integral over the ground state, limiting the resulting potential to one nucleus as well as one energy. It must be hoped that such a complete calculation can be used to justify approximations which lead back to an optical potential of sufficient simplicity to be used in

practical calculations. The success of the simple potential presented here suggests that this hope is not groundless.

The second weakness in the derivation of the potential given here is the number and severity of approximations required. Some of these are necessary to keep the potential form simple; others are required to make calculation of a given term feasible. Most of the approximations are easily justified for low pion energies but are not obviously valid in the resonance region. Fortunately they are also less important there, as the scattering calculations are not as sensitive to the terms in question.

It should be noted that knowledge of the experimental phase shifts is vital for studies of pion-nucleus processes, whether incorporated directly, as in the present study, or used as a test of the fundamental πN theory which generates the pion-nucleus interaction. The resonance region phase shifts are fairly well determined; however, the low energy phase shifts are difficult to measure and not well known at present. This is a serious problem, as the low energy scattering calculations are quite sensitive to these numbers.

The validity of a model such as the one presented here rests ultimately on its ability to reproduce the experimental results.

The initial comparisons at low energies were somewhat disappointing. The pionic atom level shifts and widths indicated too little s and p-wave absorptive strength in the potential at zero energy and too little s-wave repulsion. The problem of the absorption parameters

is not serious, as the calculation of these parameters is still subject to uncertainty. The missing real s-wave strength is more disturbing, since it is not clear what mechanism could provide the required repulsion. This problem appears also in the low energy scattering, for which the potential gives a good description provided the s-wave repulsion is increased. A reasonable fit is also given by the potential with parameters extrapolated from the pionic atom fit. These two potentials have quite different absorptive strengths; the elastic scattering data at low energies are not very sensitive to the imaginary part of the optical potential. Unfortunately, there is as yet no low energy absorption cross section data, which would provide more information about the absorption parameters. Thus the form of the potential gives an excellent framework for studying the systematics of the low energy data; however, the theoretically derived parameters do not satisfactorily reproduce the experimental quantities.

The optical potential does reasonably well in the resonance region. The general features of the elastic scattering and total cross sections are reproduced over a wide range of energies and nuclei. No attempt has been made to improve the fit by parameter searches, as the Coulomb energy shifts incorporated in the potential would necessitate a separate search for each nucleus at each energy. The results of such a study would be very difficult to correlate. The evidence from the absorption cross section measurements cannot be interpreted unambiguously because of the uncertainties

inherent in the calculation of the absorption cross sections within the context of the present theory.

Thus much work needs to be done, both experimentally and theoretically. Studies of more complicated pion-nucleus processes offer new tests of the simple optical potential concept, while microscopic calculations can give new insight into the appropriate form and approximations for the problem.

APPENDIX A

THE PION-NUCLEON SCATTERING AMPLITUDE

APPENDIX A

THE PION-NUCLEON SCATTERING AMPLITUDE

In this Appendix a review is given of the origin of the form of the scattering amplitude used to describe pion-nucleon scattering. The expansion of the scattering amplitude in terms of the phase shifts is given, and the terms of this expansion which are important for the pion-nucleon interaction are expressed in simple form with the parameters related to the relevant phase shifts.

The scattering amplitude can be expanded (3) in terms of isospin I, orbital angular momentum L, and total angular momentum J,

$$f(k,k') = \sum_{I,L,J} Q_I P_{LJ} (2L+1) \alpha_{2I,2J}^{L} P_{L} (\cos \theta)$$
 (A-1)

where

$$\alpha_{2I,2J}^{L} = \frac{\exp(2i\delta_{2I,2J}^{L}) - 1}{2i k_{cm}}$$
 (A-2)

is the scattering amplitude for the (I,L,J) partial wave, and $\mathbf{Q}_{\mathbf{I}}$ and $\mathbf{P}_{\mathbf{L},\mathbf{J}}$ are projection operators projecting onto states of given I or L and J,

$$Q_{1/2} = \frac{1}{3}(1 - t \cdot \tau)$$

$$Q_{3/2} = \frac{1}{3}(2 + t \cdot \tau)$$

$$P_{L,J} = L - \frac{1}{2} = \frac{L - \sigma \cdot \ell}{2L + 1}$$

$$P_{L,J} = L + \frac{1}{2} = \frac{L + 1 + \sigma \cdot \ell}{2L + 1}$$
(A-3)

Here $\frac{\ell}{2}$ is the relative angular momentum operator, which acts on the Legendre polynomials in equation A-1,

$$\underset{\sim}{\ell} P_{\ell}(\cos \theta) = \underset{\sim}{r} \times (-i \nabla) P_{\ell}(\cos \theta)$$

$$= -i \hat{r} \times \hat{\theta} \frac{\partial}{\partial \theta} P_{\ell}(\cos \theta) .$$
(A-4)

Note that the plane defined by \hat{r} and $\hat{\theta}$ is the same as that defined by k_{CM} and k_{CM}^{I} ,

$$-\hat{\mathbf{r}} \times \hat{\boldsymbol{\theta}} = \frac{\overset{\mathbf{k}_{ccm}}}{\overset{\mathbf{k}_{ccm}}{\overset{\mathbf{k}_{ccm}}{\overset{\mathbf{k}_{ccm}}{\overset{\mathbf{k}_{ccm}}}{\overset{\mathbf{k}_{ccm}}{\overset{\mathbf{k}_{ccm}}}}{\overset{\mathbf{k}_{ccm}}}{\overset{\mathbf{k}_{c$$

Thus

$${\underset{\sim}{\ell}} P_{\ell}(\cos \theta) = \hat{\ln} P_{\ell}(\cos \theta) .$$
 (A-6)

The important terms in the pion-nucleon amplitude for the energies considered here are the L=0 and L=1 terms of equation A-1. The L=0 terms are

$$Q_{1/2}P_{0,1/2}\alpha_{11}^{0}P_{0}(\cos\theta) + Q_{3/2}P_{0,1/2}\alpha_{31}^{0}P_{0}(\cos\theta)$$

$$= \frac{1}{3}(1 - t \cdot \tau)\alpha_{11}^{0} + \frac{1}{3}(2 + t \cdot \tau)\alpha_{31}^{0} = b_{0} + b_{1}t \cdot \tau$$
(A-7)

where

$$b_0 = \frac{1}{3}(\alpha_{11}^0 + 2\alpha_{31}^0)$$

$$b_1 = \frac{1}{3}(-\alpha_{11}^0 + \alpha_{31}^0) . \tag{A-8}$$

The p-wave terms are

$$\begin{split} &3[P_{1,1/2}(Q_{1/2}\alpha_{11}^{1}+Q_{3/2}\alpha_{31}^{1})+\\ &+P_{1,3/2}(Q_{1/2}\alpha_{13}^{1}+Q_{3/2}\alpha_{33}^{1})]P_{1}(\cos\theta)\\ &=[(Q_{1/2}\alpha_{11}^{1}+Q_{3/2}\alpha_{31}^{1})+2(Q_{1/2}\alpha_{13}^{1}+Q_{3/2}\alpha_{33}^{1})]\cos\theta\\ &+[-(Q_{1/2}\alpha_{11}^{1}+Q_{3/2}\alpha_{31}^{1})+(Q_{1/2}\alpha_{13}^{1}+Q_{3/2}\alpha_{33}^{1})]ig\cdot\hat{n}\sin\theta \ . \end{split}$$

Noting that $|\mathbf{k}_{cm}| = |\mathbf{k}_{cm}'| \equiv \mathbf{k}_0$ for elastic scattering, the functions of θ can be written

$$\cos \theta = \frac{k_{\text{cm}} \cdot k'_{\text{cm}}}{k_{0}^{2}}$$
 (A-10)

and

$$\hat{n} \sin \theta = \frac{1}{k_0^2} k_{\text{cm}} \times k_{\text{cm}}'. \tag{A-11}$$

Therefore the p-wave terms are

$$(c_0 + c_1 t \cdot \tau) k_{cm} \cdot k'_{cm} + (s_0 + s_1 t \cdot \tau) \sigma \cdot (k_{cm} \times k'_{cm}) , \qquad (A-12)$$

where

$$c_{0} = \frac{1}{k_{0}^{2}} \frac{1}{3} [(\alpha_{11}^{1} + 2\alpha_{31}^{1}) + 2(\alpha_{13}^{1} + 2\alpha_{33}^{1})]$$

$$c_{1} = \frac{1}{k_{0}^{2}} \frac{1}{3} [(-\alpha_{11}^{1} + \alpha_{31}^{1}) + 2(-\alpha_{13}^{1} + \alpha_{33}^{1})]$$

$$s_{0} = \frac{1}{k_{0}^{2}} \frac{1}{3} [-(\alpha_{11}^{1} + 2\alpha_{31}^{1}) + (\alpha_{13}^{1} + 2\alpha_{33}^{1})]$$

$$s_{1} = \frac{1}{k_{0}^{2}} \frac{1}{3} [-(-\alpha_{11}^{1} + \alpha_{31}^{1}) + (-\alpha_{13}^{1} + \alpha_{33}^{1})].$$

APPENDIX B

DETAILS OF THE DERIVATION OF THE MULTIPLE SCATTERING SERIES

APPENDIX B

DETAILS OF THE DERIVATION OF THE MULTIPLE SCATTERING SERIES

In this Appendix two results are derived which are required in the development of the optical potential formalism given in Chapter III. These are:

(1) Let A, B, C, D, and F be operators in an arbitrary space. If

$$A = B + BCA \tag{B-1}$$

and

$$D = B + BFD (B-2)$$

then

$$D = A + A(F - C)D$$
 (B-3)

(2) Let A, B be many particle operators and $\alpha_{\pmb{i}}$, $\beta_{\pmb{i}}$ one particle operators. If

$$A = \sum_{i} \alpha_{i} + \sum_{i} \alpha_{i} BA$$
 (B-4)

and

$$A = \sum_{i} A_{i}$$
 (B-5)

then

$$A = \sum_{i} \beta_{i} + \sum_{j} \beta_{i} B \sum_{j \neq j} A_{j}$$
 (B-6)

where

$$\beta_{i} = \alpha_{i} + \alpha_{i}B\beta_{i} \tag{B-7}$$

To prove the first result, rewrite equation B-1,

$$B = A(1 + CA)^{-1}$$
 (B-8)

and substitute for B in equation B-2

$$D = A(1 + CA)^{-1}(1 + FD) . (B-9)$$

By writing 1 = 1 + CA - CA this becomes

$$D = A(1 + CA)(1 + CA)^{-1}(1 + FD) + ACA(1 + CA)^{-1}(1 + FD)$$

$$= A(1 + FD) - ACB(1 + FD)$$
(B-10)

where equation B-8 was used in the last step. The second term can be simplified using equation B-2, giving

$$D = A + AFD - ACD (B-11)$$

or

$$D = A + A(F - C)D$$
 (B-12)

This proves the first result.

For the second result, equations B-4 and B-5 imply

$$A_{i} = \alpha_{i} + \alpha_{i}BA = \alpha_{i} + \alpha_{i}B \sum_{j} A_{j}. \qquad (B-13)$$

Grouping the A_i terms gives

$$(1 - \alpha_{\mathbf{i}} B) A_{\mathbf{i}} = \alpha_{\mathbf{i}} + \alpha_{\mathbf{i}} B \sum_{\mathbf{j} \neq \mathbf{i}} A_{\mathbf{j}}$$
 (B-14)

or

$$A_{i} = (1 - \alpha_{i}B)^{-1}\alpha_{i}(1 + B\sum_{j \neq i}A_{j})$$
 (B-15)

Equation B-7 can be written

$$\beta_{i} = (1 - \alpha_{i}B)^{-1}\alpha_{i}$$
 (B-16)

and substituted in equation B-15, yielding

$$A_{i} = \beta_{i} (1 + B \sum_{j \neq i} A_{j})$$
 (B-17)

Summing both sides over i gives the second result,

$$A = \sum_{i} \beta_{i} + \sum_{j} \beta_{i} B \sum_{j \neq i} A_{j} . \qquad (B-18)$$

APPENDIX C

INTEGRATION OVER NUCLEON MOMENTA

APPENDIX C

INTEGRATION OVER NUCLEON MOMENTA

The derivation of the optical potential requires the integration of several one and two particle operators over the coordinates (or momenta) of the nucleons in the ground state nucleus. In this Appendix the required integrals are performed. The Fourier transforms of the two common momentum space forms for the optical potential are also given. As mentioned in the text, the momentum of the nucleus as a whole is ignored in the evaluation of the ground state terms.

The one particle operators to be evaluated are

$$I_1^{(1)} = A<0|(2\pi)^3\delta(k' + p'_i - k - p_i)(a_0 + a_1t\cdot\tau_i)|0>$$
, (C-1)

$$I_1^{(2)} = A<0|(2\pi)^3\delta(k' + p'_i - k - p_i)(a_0 + a_1t\cdot\tau_i)P_i|0>$$
, (C-2)

and

$$I_{1}^{(3)} = A<0 | (2\pi)^{3} \delta(k' + p'_{i} - k - p_{i})(a_{0} + a_{1} \tilde{\tau}_{i}) p_{i} \cdot p'_{i} | 0>.$$
(C-3)

Let

$$A(\tau_i) = a_0 + a_1 \overset{t}{\sim} \overset{\tau}{\sim} i$$

$$O^{(1)}(p_i,p_i) = 1$$

$$O^{(2)}(p_{i},p'_{i}) = p_{i} \equiv \frac{p_{i} + p'_{i}}{2}$$

$$O^{(3)}(p_{i},p'_{i}) = p_{i} \cdot p'_{i}$$
(C-4)

Then expressions C-1, C-2, and C-3 can be written

$$I_{1}^{(n)}(\underline{q}) = A \int \psi^{\star}(\underline{p}_{1} - \underline{q}, \underline{p}_{2} \dots \underline{p}_{A})A(\tau_{1})O^{(n)}(\underline{p}_{1} - \underline{q}, \underline{p}_{1})$$

$$\times \psi(\underline{p}_{1}, \underline{p}_{2} \dots \underline{p}_{A}) \prod_{j} \frac{d^{3}p_{j}}{(2\pi)^{3}} \qquad (C-5)$$

where q = k' - k. The i = 1 term has been chosen and the spin and isospin variables suppressed to simplify notation. Transforming to coordinate space gives

$$I_{1}^{(n)}(\underline{r}) = A \int \psi^{*}(\underline{r}_{1},\underline{r}_{2} \dots \underline{r}_{A})\psi(\underline{r}_{1},\underline{r}_{2} \dots \underline{r}_{A})A(\underline{\tau}_{1})$$

$$\times O^{(n)}(\underline{p}_{1} - \underline{q},\underline{p}_{1})e^{i(\underline{p}_{1} - \underline{q})\cdot\underline{r}_{1}'}e^{-i\underline{p}_{1}\cdot\underline{r}_{1}}e^{i\underline{q}\cdot\underline{r}}\frac{d^{3}\underline{p}_{1}}{(2\pi)^{3}}\frac{d^{3}\underline{q}}{(2\pi)^{3}}$$

$$\times d^{3}\underline{r}_{1}' \underline{\Pi} d^{3}\underline{r}_{j} \qquad (C-6)$$

The operator $O^{(n)}(\underline{p}_1 - \underline{q}, \underline{p}_1)$ can be replaced by $O^{(n)}(\frac{1}{i} \nabla_1^i, -\frac{1}{i} \nabla_1)$ acting on the exponentials, allowing the momentum integrals to be performed

$$I_{1}^{(n)}(\underline{r}) = A \int \psi^{\star}(\underline{r}_{1}^{\prime}, \underline{r}_{2} \dots \underline{r}_{A}) \psi(\underline{r}_{1}, \underline{r}_{2} \dots \underline{r}_{A})$$

$$\times \left[O^{(n)}(\frac{1}{i} \nabla_{1}^{\prime}, -\frac{1}{i} \nabla_{1}) \delta(\underline{r}_{1}^{\prime} - \underline{r}_{1}^{\prime})\right] d^{3}r_{1}^{\prime} \quad \underline{\Pi} \ d^{3}r_{j} \quad . \tag{C-7}$$

For n = 1 this becomes

$$I_{1}^{(1)}(\underline{r}) = A \int \psi^{\star}(\underline{r},\underline{r}_{2} \dots \underline{r}_{A})(a_{0} + a_{1}\underline{t}\cdot\underline{\tau}_{1})\psi(\underline{r},\underline{r}_{2} \dots \underline{r}_{A})$$

$$\times \prod_{j>1} d^{3}r_{j}$$
(C-8)

The a_0 term is just the nuclear density $\rho(r)$. As there is no change in the isospin projection for the nucleus, the only non-zero contribution from $t \cdot \tau_1$ is from $t_3 \tau_3$, where τ_3 is +1 for protons, -1 for neutrons. Expression C-8 is therefore

$$I_1^{(1)}(r) = a_0 \rho(r) + a_1 t_3 [\rho_p(r) - \rho_n(r)],$$
 (C-9)

where ρ is normalized to A, ρ_p to Z, and ρ_n to N. Expression C-1 is the Fourier transform of this,

$$I_1^{(1)}(q) = a_0 \rho(q) + a_1 t_3 [\rho_p(q) - \rho_n(q)]$$
 (C-10)

For the second expression, $\mathbf{O}^{(2)} = \frac{\nabla_1^t - \nabla_1}{2i}$, and integration by parts gives

$$I_{1}^{(2)}(\underline{r}) = \frac{1}{2i} A \int [\psi^{\star}(\underline{r},\underline{r}_{2} \dots \underline{r}_{A}) \nabla \psi(\underline{r},\underline{r}_{2} \dots \underline{r}_{A}) \\ - \nabla \psi^{\star}(\underline{r},\underline{r}_{2} \dots \underline{r}_{A}) \psi(\underline{r},\underline{r}_{2} \dots \underline{r}_{A})]A(\tau_{1}) \prod_{j\neq 1}^{\Pi} d^{3}r_{j}$$
(C-11)

This is, aside from the factor $A(\tau)$, the current density and is zero for a spherically symmetric nucleus. Assuming the neutron and proton distributions are spherically symmetric, expression C-2 is zero.

For n = 3, $O^{(3)} = \nabla_1 \cdot \nabla_1'$ and integration by parts twice gives $I_1^{(3)}(r) = a_0 A \int \nabla_1' (r, r_2 \dots r_A) \cdot \nabla_1' (r, r_2 \dots r_A) \int_{j>1}^{n} d^3r_j$ $= a_0 K(r)$

(C-12)

where $\kappa(r)$ is 2M times the kinetic energy density of the nucleons, and the isovector part of A(τ) has been dropped. The quantity $\kappa(r)$ is evaluated in the Thomas-Fermi approximation (41),

$$\kappa(r) = \frac{3}{5} (\frac{3}{2} \pi^2)^{2/3} \rho^{5/3}$$
 (C-13)

This completes the evaluation of the one-body operators.

The first two-particle operator to be evaluated is

$$I_2^{(1)} = A(A - 1) < 0 | (2\pi)^6 \delta(p_1' + k' - p_1 - k'') \delta(p_2' + k'' - p_2 - k)$$

$$\times (a_0 + a_1 t \cdot \tau_1)(a_0 + a_1 t \cdot \tau_2)|_{0} ,$$
 (C-14)

which can be written

$$I_{2}^{(1)}(k',k'',k) = A(A-1) \int \psi^{*}(p_{1}-(k'-k''),p_{2}-(k''-k),p_{3}...p_{A})$$

$$\times A(\tau_{1})A(\tau_{2})\psi(p_{1},p_{2},p_{3}...p_{A}) \prod_{j} \frac{d^{3}p_{j}}{(2\pi)^{3}}$$
(C-15)

This is only a function of the variables (k' - k'') and (k'' - k) and can be Fourier transformed resulting in a function of r and r',

$$I_{2}^{(1)}(\underline{r},\underline{r}') = A(A - 1) \int \psi^{*}(\underline{r},\underline{r}',\underline{r}_{3} \dots \underline{r}_{A}) \psi (\underline{r},\underline{r}',\underline{r}_{3} \dots \underline{r}_{A})$$

$$\times A(\tau_{1})A(\tau_{2}) \prod_{j>2}^{\Pi} d^{3}r_{j} . \qquad (C-16)$$

Without the isospin factors this is just the two particle density $\rho_2(r,r'), \text{ which can be written in terms of the two body correlation}$ function C(r,r'),

$$\rho_2(r,r') = [1 + C(r,r')]\rho(r)\rho(r') . \qquad (C-17)$$

In order to simplify expression C-16, assume that ψ can be expressed as an antisymmetrized product of single particle wavefunctions,

$$\psi = \frac{1}{\sqrt{A!}} \det \{\phi_i(r_j)\}$$
 (C-18)

Then expression C-16 becomes

$$I_{2}^{(1)}(\underline{r},\underline{r}') = \sum_{i,j} \phi_{i}^{\star}(\underline{r})\phi_{j}^{\star}(\underline{r}')A(\tau)A(\tau')[\phi_{i}(\underline{r})\phi_{j}(\underline{r}') - \phi_{i}(\underline{r}')\phi_{j}(\underline{r})]$$
(C-19)

The first term is just

$$[a_0 \rho(\underline{r}) + t_3 a_1 (\rho_p(\underline{r}) - \rho_n(\underline{r}))][a_0 \rho(\underline{r}') + t_3 a_1 (\rho_p(\underline{r}') - \rho_n(\underline{r}'))]$$
(C-20)

The spin and isospin dependence of the second term can be made explicit and factored out, replacing $\phi_k(r)$ by $\phi_k(r)\chi_m(\sigma)\eta_s(\tau)$ where χ and η are Pauli spinors in spin and isospin space. For this term the spin and isospin projection of the nucleus will be approximated as zero. Then the sum over states can be separated into sums over space, spin, and isospin states. The sum over spin dependent factors gives

$$\sum_{m,n=1,2} \chi_{m}^{+}(\sigma)\chi_{n}^{+}(\sigma')\chi_{n}(\sigma)\chi_{m}(\sigma') = 2.$$
 (C-21)

The sum over isospin factors gives

$$\sum_{s,t=1,2} \eta_s^{\dagger}(\tau) \eta_t^{\dagger}(\tau') (a_0 + a_1 t \cdot \tau) (a_0 + a_1 t \cdot \tau') \eta_s(\tau') \eta_t(\tau)$$

$$= 2(a_0^2 + 2a_1^2) .$$
(C-22)

The spatial sum can be evaluated in the Fermi gas model, in which

$$\phi_{i}(r_{j}) = e^{ik_{i} \cdot r_{j}}$$
 (C-23)

Then

$$-\sum_{i,j} \phi_{i}^{*}(\underline{r}) \phi_{j}^{*}(\underline{r}') \phi_{i}(\underline{r}') \phi_{j}(\underline{r})$$

$$= -\int \frac{d^{3}k_{i}}{(2\pi)^{3}} e^{i\underline{k}_{i} \cdot (\underline{r}' - \underline{r})} \int \frac{d^{3}k_{j}}{(2\pi)^{3}} e^{-i\underline{k}_{j} \cdot (\underline{r}' - \underline{r})}$$

$$= -\frac{1}{2\pi^{2}} \left[\frac{\sin(k_{F}|\underline{r}' - \underline{r}|)}{|\underline{r}' - \underline{r}|^{3}} - \frac{k_{F}\cos(k_{F}|\underline{r}' - \underline{r}|)}{|\underline{r}' - \underline{r}|^{2}} \right]^{2}$$
(C-24)

where k_F is the Fermi momentum, $k_F = 1.36 \text{ fm}^{-1}$. The density is a constant in the Fermi gas model,

$$\rho(r) = \rho(r') = \frac{2k_F^3}{3\pi^2}$$
 (C-25)

and can be factored out,

$$-\sum_{ij} \phi_{i}^{*}(\underline{r}) \phi_{j}^{*}(\underline{r}') \phi_{i}(\underline{r}') \phi_{j}(\underline{r}) = -\rho(\underline{r}) \rho(\underline{r}') \frac{1}{16} \left[\frac{3j_{1}(k_{F}|\underline{r}' - \underline{r}|)}{k_{F}|\underline{r}' - \underline{r}|} \right]^{2}$$
(C-26)

Combining equations C-19, C-20, C-21, C-22, and C-26 gives for expression C-14

$$I_{2}^{(1)}(\underline{r},\underline{r}') = [a_{0}\rho(\underline{r}) + t_{3}a_{1}(\rho_{p}(\underline{r}) - \rho_{n}(\underline{r}))]$$

$$\times [a_{0}\rho(\underline{r}') + t_{3}a_{1}(\rho_{p}(\underline{r}') - \rho_{n}(\underline{r}'))]$$

$$- (a_{0}^{2} + 2a_{1}^{2}) \frac{1}{4} \left[\frac{3j_{1}(k_{F}|\underline{r}' - \underline{r}|)}{k_{F}|\underline{r}' - \underline{r}|} \right]^{2} \rho(\underline{r})\rho(\underline{r}')$$
(C-27)

Note that the right hand side can be identified with equation C-17 for $a_0 = 1$, $a_1 = 0$, and

$$C(r,r') = \frac{1}{4} \left[\frac{3j_1(k_F|r'-r|)}{k_F|r'-r|} \right]^2.$$
 (C-28)

As it is derived in the Fermi gas model, equation C-27 provides a reasonable description of the long range correlations due to the Pauli principle. It does not, however, properly describe the short range correlations. One would expect $I_2^{(1)}(r,r) = 0$ for N = Z, since the short range repulsion keeps the nucleons apart. It is not zero here because the Fermi gas model does not, of course, include interactions between nucleons. For the second order s-wave term the long range Pauli correlations are most important, and the result given in equation C-27 will be used. In the derivation of the Ericson-Ericson effect for the p-wave only the r=r' part of the right hand side of equation C-27 survives, and will be taken to be zero.

The second two particle operator to be evaluated is much simpler. It is

$$I_{2}^{(2)}(\underline{k},\underline{k}') = \langle 0 | (2\pi)^{3} \delta(\underline{p}_{1} + \underline{p}_{2} + \underline{k} - \underline{p}_{1}' - \underline{p}_{2}' - \underline{k}') | 0 \rangle$$

$$= \int \psi^{*}(\underline{r}_{1}',\underline{r}_{2}',\underline{r}_{3} \dots \underline{r}_{A}) \psi(\underline{r}_{1},\underline{r}_{2},\underline{r}_{3} \dots \underline{r}_{A})$$

$$\times e^{i[\underline{p}_{1}',\underline{r}_{1}' + \underline{p}_{2}',\underline{r}_{2}' - \underline{p}_{1},\underline{r}_{1} - \underline{p}_{2},\underline{r}_{2}]} \qquad (c-29)$$

$$\times (2\pi)^{3} \delta(\underline{p}_{1} + \underline{p}_{2} + \underline{k} - \underline{p}_{1}' - \underline{p}_{2}' - \underline{k}') d^{3} \underline{r}_{1}' d^{3} \underline{r}_{2}' \underline{\Pi} d^{3} \underline{r}_{1}'$$

$$\times \frac{d^{3} \underline{p}_{1}'}{(2\pi)^{3}} \frac{d^{3} \underline{p}_{2}'}{(2\pi)^{3}} \frac{d^{3} \underline{p}_{2}}{(2\pi)^{3}} \frac{d^{3} \underline{p}_{2}}{(2\pi)^{3}} .$$

The integration over $\underline{\textbf{p}}_2^{\, \textbf{i}}$ gives

$$I_{2}^{(2)}(q) = \int \psi^{*}(\underline{r}_{1}',\underline{r}_{2}',\underline{r}_{3} \dots \underline{r}_{A})\psi(\underline{r}_{1},\underline{r}_{2},\underline{r}_{3} \dots \underline{r}_{A})$$

$$\times e^{i\underline{p}_{1}'\cdot(\underline{r}_{1}'-\underline{r}_{2}')}e^{-i\underline{p}_{1}\cdot(\underline{r}_{1}-\underline{r}_{2}')}$$

$$\times e^{-i\underline{p}_{2}\cdot(\underline{r}_{2}-\underline{r}_{2}')}e^{-i\underline{q}\cdot\underline{r}_{2}'}e^{-i\underline{q}\cdot\underline{r}_{2}'}d^{3}r_{1}'d^{3}r_{2}' \prod_{i} d^{3}r_{i}$$

$$\times \frac{d^{3}p_{1}'}{(2\pi)^{3}} \frac{d^{3}p_{1}}{(2\pi)^{3}} \frac{d^{3}p_{2}}{(2\pi)^{3}},$$
(C-30)

and the remaining momentum integrals lead to delta functions. The result is the Fourier transform of the two particle density $\rho_2(r,r)$,

$$I_{2}^{(2)}(q) = \int \psi^{*}(r,r,r_{3},...,r_{A})\psi(r,r,r_{3},...,r_{A})e^{-iq\cdot r}d^{3}r \prod_{i>2}d^{3}r_{i}$$
(C-31)

This completes the discussion of two-body operators.

The simple Kisslinger and Laplacian models for the optical potential include the momentum space terms

$$k \cdot k' \rho(q)$$
 (C-32)

and

$$q^2 \rho(q) \tag{C-33}$$

respectively. The Fourier transform of C-32 is

$$\int \underbrace{k \cdot k' \rho(k' - k)}_{= \infty} e^{i k \cdot r} e^{-i k' \cdot r'} \frac{d^3k}{(2\pi)^3} \frac{d^3k'}{(2\pi)^3}$$
 (C-34)

which can be written

$$\int \tilde{\nabla} \cdot \tilde{\nabla}' \rho(q) e^{i\tilde{K} \cdot \tilde{X}} e^{i\tilde{q} \cdot \tilde{R}} \frac{d^3 \kappa}{(2\pi)^3} \frac{d^3 q}{(2\pi)^3}$$
 (C-35)

where

$$K = \frac{k + k'}{2}$$
, $q = k' - k$, $R = \frac{r + r'}{2}$, $x = r - r'$.

The integrals over K and q give

$$\nabla \cdot \nabla' \left[\delta(r - r')\rho(\frac{r + r'}{2})\right]$$
 (C-36)

Note that this is an operator of the form < r' |O| r >. The gradients which act on the delta and density functions can be turned around to act on whatever functions of r and r' are to the right and left of O. This gives

$$\vec{\nabla}' \cdot \left[\delta(\underline{r} - \underline{r}')\rho(\frac{\underline{r} + \underline{r}'}{2})\right] \vec{\nabla}$$
 (C-37)

which can be written as a function of r only, due to the delta function. The first gradient can now be reversed again, giving

$$- \nabla \cdot [\rho(r)\nabla]$$
 (C-38)

where the gradients now act on everything to their right. The Fourier transform of C-33 is

$$\int q^{2} \rho(q) e^{i \frac{k \cdot r}{c}} e^{-i \frac{k' \cdot r'}{c}} \frac{d^{3}k}{(2\pi)^{3}} \frac{d^{3}k'}{(2\pi)^{3}}$$

$$= - \nabla_{R}^{2} \int \rho(q) e^{i \frac{k \cdot x}{c}} e^{-i \frac{q}{c} \cdot R} \frac{d^{3}K}{(2\pi)^{3}} \frac{d^{3}q}{(2\pi)^{3}}.$$
(C-39)

The integrations over $\begin{tabular}{c} K \\ \tilde{\begin{tabular}{c} \chi \end{tabular}}$ and $\begin{tabular}{c} \tilde{\begin{tabular}{c} \chi \end{tabular}}$ give

$$-\nabla^2_{\mathbf{R}}\rho(\mathbf{R})\delta(\mathbf{x})$$
, (C-40)

which can be written as a function of $\underset{\sim}{r}$ only,

$$- \nabla^2 \rho(r)$$
 . (C-41)

Note that in this case the ∇^2 acts only on $\rho(r)$.

APPENDIX D

RELATIVISTIC POTENTIAL THEORY

APPENDIX D

RELATIVISTIC POTENTIAL THEORY

Relativistic potential theory (39) is one of the methods that have been proposed (42) to deal with the problem of relativistic kinematics in a potential based theory. Unlike theories that are manifestly Lorentz covariant, this theory includes quantities which do not have definite transformation properties; among them is the transition matrix T. In this appendix only a few of the details and results of the theory will be given, taken from Heller, Bohannon, and Tabakin (40).

Define the canonical transformation from the momenta of two particles \underline{p}_1 and \underline{p}_2 to the center of mass and relative momenta \underline{P}_2 and k:

$$P = P_1 + P_2 \tag{D-1}$$

$$k_{\tilde{e}} = \frac{1}{2h_0(H_0 + h_0)} \left[(h_0^2 + 2E_2h_0 + m_2^2 - m_1^2)p_1 - (h_0^2 + 2E_1h_0 + m_1^2 - m_2^2)p_2 \right]$$
(D-2)

where

$$H_0 = E_1 + E_2, E_i = (m_i^2 + p_i^2)^{\frac{1}{2}}$$

and

$$h_0 = (H_0^2 - P^2)^{\frac{1}{2}} = \omega_1(k) + \omega_2(k) \equiv \omega(k)$$

with

$$\omega_{i}(k) = (m_{i}^{2} + k^{2})^{\frac{1}{2}}$$

(The notation of reference 40 will be used throughout this appendix and the conventions given in Chapter I will be ignored.) Equation D-2 can be shown to be identical to the Lorentz transformation from an arbitrary frame with particle momenta p_1 and p_2 to the center of mass frame with momenta k and k. Interaction can be introduced by defining

$$h \equiv h_0 + v(k) \text{ and } H \equiv (h^2 + P^2)^{\frac{1}{2}}$$
 (D-3)

where the potential is given by $V \equiv H - H_0$. Although H transforms as the fourth component of a four-vector, neither H_0 nor V separately have well defined transformation properties. Since the transition matrix is given by

$$T(E_{T}) = V + V \frac{1}{E_{T} - H_{O} + i\varepsilon} T(E_{T})$$
 (D-4)

 ${\sf T}$ must have the same transformation properties as ${\sf V.}$

Let g_1, g_2 be the initial particle momenta, g_1', g_2' the final particle momenta. Then matrix elements of T may be written

$$\langle \underline{q}_{1}', \underline{q}_{2}' | T(E_{T}) | \underline{q}_{1}, \underline{q}_{2} \rangle = (2\pi)^{3} \delta(\underline{Q}' - \underline{Q}) T(E_{T}; \underline{q}_{1}', \underline{q}_{2}', \underline{q}_{1}, \underline{q}_{2})$$
(D-5)

where $Q = Q_1 + Q_2$ and $Q' = Q_1' + Q_2'$. Changing variables,

$$T(E_{T}; \underline{q}'_{1}, \underline{q}'_{2}, \underline{q}_{1}, \underline{q}_{2}) = NT(E_{T}; \underline{Q}; \underline{q}', \underline{q})$$
(D-6)

where $\underline{q} = \underline{k}(\underline{q}_1,\underline{q}_2)$ and $\underline{q}' = \underline{k}'(\underline{q}_1',\underline{q}_2')$ with $k(\underline{p}_1,\underline{p}_2)$ given by equation D-2. The factor N which appears is due to the coordinate transformation $(\underline{q}_1,\underline{q}_2) \rightarrow (\underline{Q},\underline{q})$ and $(\underline{q}_1',\underline{q}_2') \rightarrow (\underline{Q},\underline{q}')$,

$$N = [\mathcal{A}(q_1, q_2) \mathcal{A}(q'_1, q'_2)]^{-\frac{1}{2}}$$
 (D-7)

where \mathcal{J} is the Jacobian,

$$\mathcal{A}(\underline{q}_1,\underline{q}_2) \equiv \left| \frac{\partial(\underline{q}_1,\underline{q}_2)}{\partial(\underline{Q},\underline{q})} \right| = \frac{E_1(\underline{q}_1)E_2(\underline{q}_2)}{E_1(\underline{q}_1) + E_2(\underline{q}_2)} \frac{\omega_1(q) + \omega_2(q)}{\omega_1(q)\omega_2(q)}$$
(D-8)

The quantity $T(E_T; Q; q',q)$ must now be expressed in terms of t(w; q',q) where

$$t(w; \underline{q}',\underline{q}) \equiv T(E_{T} = \underline{w}; 0; \underline{q}',\underline{q}) , \qquad (D-9)$$

i.e., t is the transition amplitude in the two particle center of mass. This relation is derived in reference 40, where the result is given as

$$T(E_{T}, \underline{Q}; \underline{q}', \underline{q}) = F(\underline{Q}; \underline{q}', \underline{q})t(\omega(q); \underline{q}', \underline{q})$$

$$+ \int \frac{d^{3}p}{(2\pi)^{3}} F(\underline{Q}; \underline{q}', \underline{p})F(\underline{Q}; \underline{q}, \underline{p})t(\omega(p); \underline{q}', \underline{p}) \qquad (D-10)$$

$$\times t^{*}(\omega(p); \underline{q}, \underline{p}) \left[\frac{F^{-1}(\underline{Q}; \underline{k}, \underline{p})}{\omega(k) - \omega(p) + i\varepsilon} - \frac{F^{-1}(\underline{Q}; \underline{q}, \underline{p})}{\omega(q) - \omega(p) + i\varepsilon} \right]$$

where

$$F(Q; Q', Q', Q) \equiv \frac{\omega(Q') + \omega(Q)}{E(Q, Q') + E(Q, Q)}$$

$$E(Q,q) \equiv (\omega^2(q) + Q^2)^{\frac{1}{2}} \equiv E_1(q_1) + E_2(q_2)$$

and k is defined by

$$\omega(k) = (E_T^2 - Q^2)^{\frac{1}{2}}$$
.

Also given are the first terms in an expansion of equation D-10 in factors of \mathbb{Q}^2 . The first two terms are

$$T(E_{T},Q; \underline{q}',\underline{q}) \cong t(\omega(k); \underline{q}',\underline{q})$$

$$+ \frac{Q^{2}}{2} \left[-\frac{t(\omega(q); \underline{q}',\underline{q})}{\omega(q')\omega(q)} + (\frac{1}{\omega(k)} - \frac{1}{\omega(q')} - \frac{1}{\omega(q)}) \right]$$

$$\times g(k; \underline{q}',\underline{q}) + \frac{1}{\omega(q')} g(q; \underline{q}',\underline{q}) + 0(Q^{4})$$

$$(D-11)$$

where

$$g(k; \underline{q}',\underline{q}) \equiv \int \frac{d^3p}{(2\pi)^3} \frac{1}{\omega(p)} \frac{t(\omega(p),q',\underline{p})t^*(\omega(p),\underline{q},\underline{p})}{\omega(k) - \omega(p) + i\varepsilon}$$

It is to be hoped that the terms in Q^2 and above are small, giving a manageable result for T. For the pion-nucleon system Heller states that the most important kinematic corrections arise from the appearance of the relativistic rather than the nonrelativistic relative momentum g, and the appearance of the factor N in equation D-6.

LIST OF REFERENCES

- 1. H.A. Bethe, Phys. Rev. 57, 1125 (1940).
- 2. S. Fernbach, R. Serber, and T.B. Taylor, Phys. Rev. <u>75</u>, 1352 (1949).
- 3. See Daniel S. Koltun, Advances in Nuclear Physics, vol. 3 (New York: Plenum Press, 1969).
- 4. H. Feshbach, C.E. Porter, and V.F. Weisskopf, Phys. Rev. <u>96</u>, 448 (1954).
- 5. K.M. Watson, Phys. Rev. 89, 575 (1953).
- 6. A.K. Kerman, H. McManus, and R.M. Thaler, Ann. Phys. <u>8</u>, 551 (1959).
- 7. L.S. Kisslinger, Phys. Rev. 98, 761 (1955).
- 8. H. Byfield, J. Kessler, and L.M. Lederman, Phys. Rev. <u>86</u>, 17 (1952).
- 9. K.A. Brueckner, Phys. Rev. <u>98</u>, 769 (1955).
- 10. M. Ericson and T.E.O. Ericson, Ann. Phys. <u>36</u>, 323 (1966).
- 11. F. Binon, P. Duteil, J.P. Garron, J. Gorres, L. Hugon, J.P. Peigneux, C. Schmit, M. Spighel, and J.P. Stroot, Nucl. Phys. B17, 168 (1970).
- 12. R.R. Silbar and M.M. Sternheim, Phys. Rev. Lett. <u>31</u>, 941 (1973).
- 13. C. Wilkin, Proceedings of the Spring School on Pion Interactions at Low and Medium Energies, Zuoz, Switzerland, April 1971, ed. M.P. Locher (Geneva: CERN, 1971), p. 289; H.K. Lee and H. McManus, Nucl. Phys. <u>A167</u>, 257 (1971).
- 14. R.J. Glauber, Lectures in Theoretical Physics, vol. 1, ed. W.E. Brittin and L.G. Dunham (New York: Interscience Publishers, 1959), p. 315; R.J. Glauber, High Energy Physics and Nuclear Structure, ed. G. Alexander (New York: John Wiley and Sons, 1967), p. 311.

- 15. C. Schmitt, Lett. Nuovo Cimento 4, 454 (1970); C. Wilkin, Lett. Nuovo Cimento 4, 491 (1970); K. Bjoernenak, J. Finjord, P. Osland, and A. Reitan, Nucl. Phys. B22, 179 (1970).
- 16. See, however, R. Mach, Nucl. Phys. <u>A205</u>, 56 (1973), who showed the importance of including proper kinematics in low energy scattering calculations.
- 17. J.F. Amann, P.D. Barnes, M. Doss, S.A. Dytman, R.A. Eisenstein, and A.C. Thomson, Phys. Rev. Lett. 35, 426 (1975).
- 18. M. Thies, Phys. Lett. 63B, 43 (1976).
- 19. See G.E. Brown and W. Weise, Phys. Rept. 22C, 280 (1975); L. Kisslinger and W. Wang, Ann. Phys. 99, 374 (1976); E.J. Moniz, Theoretical Methods in Medium-Energy and Heavy-Ion Physics, NATO Advanced Study Institute on Theoretical Nuclear Physics, University of Wisconsin, Madison, 1978, ed. K.W. McVoy and W.A. Friedman (New York: Plenum Press, 1978); M. Hirata, J.H. Koch, F. Lenz, and E.J. Moniz, Ann. Phys. 120, 205 (1979).
- 20. See, for instance, S.A. Dytman et al., Phys. Rev. Lett. <u>38</u>, 1059 (1977) and Refs. 32, 33, 68, and 70 of this thesis.
- 21. See Chapter IV.
- 22. G.R. Stephenson, private communication.
- 23. Proceedings of the 6th International Conference on High Energy Physics and Nuclear Structure, Sante Fe and Los Alamos, 1975, AIP Conf. Proc. 26, ed. D.E. Nagle and A.S. Goldhaber (New York: American Institute of Physics, 1975); Proceedings of the International Conference on Meson-Nuclear Physics, Carnegie-Mellon, 1976, AIP Conf. Proc. 33, ed. P.D. Barnes, R.A. Eisenstein, and L.S. Kisslinger (New York: American Institute of Physics, 1976); Proceedings of the 7th Conference on High Energy Physics and Nuclear Structure, Zurich, 1977, ed. M.P. Locher; Theoretical Methods in Medium-Energy and Heavy-Ion Physics, NATO Advanced Study Institute on Theoretical Nuclear Physics, University of Wisconsin, Madison, 1978, ed. K.W. McVoy and W.A. Friedman (New York: Plenum Press, 1978): Proceedings of the 2nd International Topical Conference on Meson-Nuclear Physics, Houston, 1979, AIP Conf. Proc. 54, ed. E.V. Hungerford III (New York: American Institute of Physics, 1979); Proceedings of the 8th Conference on High Energy Physics and Nuclear Structure, Vancouver, 1979, ed. D.F. Measday and A.W. Thomas.
- 24. K. Stricker, H. McManus, and J.A. Carr, Phys. Rev. C<u>19</u>, 929 (1979).

- 25. Glenn Rowe, Martin Salomon, and Rubin H. Landau, Phys. Rev. C18, 584 (1978).
- 26. Particle Data Group, Report No. UCRL-20030 (1970).
- 27. Marvin L. Goldberger and Kenneth M. Watson, <u>Collision Theory</u> (Huntington, NY: Robert E. Krieger Publishing Co., 1975), pp. 223,340.
- 28. B. Lippmann and J. Schwinger, Phys. Rev. 79, 469 (1950).
- 29. J.M. Eisenberg, Beyong Lowest Order Results in Pion-Nucleus Reactions, Lectures at the NATO Summer School, Banff, Alberta, Canada, August 1978.
- 30. See Morton M. Sternheim and Richard R. Silbar, Ann. Rev. of Nucl. Science 24, 249 (1974).
- 31. T.E.O. Ericson and F. Myhrer, Phys. Lett. 74B, 163 (1978).
- 32. S.A. Dytman, J.F. Amann, P.D. Barnes, J.N. Craig, K.G.R. Doss, R.A. Eisenstein, J.D. Sherman, W.R. Wharton, G.R. Burleson, S.L. Verbeck, R.J. Peterson, and H.A. Thiessen, Phys. Rev. C19, 971 (1979).
- 33. D.J. Malbrough, C.W. Darden, R.D. Edge, T. Marks, B.M. Preedom, R.L. Burman, M.A. Moinester, R.P. Redwine, F.E. Bertrand, T.P. Cleary, E.E. Gross, C.A. Ludeman, and K. Gotow, Phys. Rev. C17, 1395 (1978).
- 34. Preliminary data, LASL, ORNL, VPI + SU, Tel Aviv University, South Carolina Collaboration.
- 35. Q. Ingram, E. Boschitz, L. Pflug, J. Zichy, J.P. Albanese, and J. Arvieux, Phys. Lett. 76B, 173 (1978).
- 36. B. Zeidman, C. Olmer, D.F. Geesaman, R.L. Boudrie, R.H. Siemssen, J.F. Amann, C.L. Morris, H.A. Thiessen, G.R. Burleson, M.J. Devereaux, R.E. Segel, and L.W. Swenson, Phys. Rev. Lett. 40, 1539 (1978).
- 37. See, for example, L.L. Foldy and J.D. Walecka, Ann. Phys. <u>54</u>, 447 (1969); R.H. Landau and F. Tabakin, Phys. Rev. <u>D5</u>, 2746 (1972); J.T. Londergan, K.W. McVoy, and E.J. Moniz, Ann. Phys. 86, 147 (1974).
- 38. M.A.B. Beg, Ann. Phys. 13, 110 (1961).

- 39. B. Bakamjian and L.H. Thomas, Phys. Rev. <u>92</u>, 1300 (1953); R. Fong and J. Sucher, J. Math. Phys. <u>5</u>, 456 (1964); F. Coester, Helv. Phys. Acta 38, 7 (1965).
- 40. L. Heller, G.E. Bohannon, and F. Tabakin, Phys. Rev. C<u>13</u>, 742 (1976); Leon Heller, Proceedings of the International Topical Conference on Meson-Nuclear Physics, Carnegie-Mellon, 1976, AIP Conf. Proc. <u>33</u>, ed. P.D. Barnes, R.A. Eisenstein, and L.S. Kisslinger (New York: American Institute of Physics, 1976), p. 93.
- 41. G.E. Brown, B.K. Jennings, and V. Rostokin, Stony Brook Preprint.
- 42. See, for example, L. Celenza, L.C. Liu, and C.M. Shakin, Phys. Rev. C11, 1593 (1975).
- 43. M. Ericson, Compt. Rend. <u>258</u>, 1471 (1964).
- 44. See, for example, John David Jackson, <u>Classical Electrodynamics</u> (New York: John Wiley and Sons, 1962), p. 119.
- 45. M. Krell and T.E.O. Ericson, Nucl. Phys. <u>B11</u>, 521 (1969).
- 46. J.M. Eisenberg, J. Hüfner, and E.J. Moniz, Phys. Lett. <u>47B</u>, 381 (1973).
- 47. G.E. Brown, private communication; G. Baym and G.E. Brown, Nucl. Phys. A247, 395 (1975).
- 48. E. Oset and W. Weise, Nucl. Phys. A319, 477 (1979).
- 49. R. Rockmore, E. Kanter, and P. Goode, Phys. Lett. <u>77B</u>, 149 (1978).
- G.F. Bertsch and D.O. Riska, Phys. Rev. C<u>18</u>, 317 (1978); J. Chai and D.O. Riska, Phys. Rev. C<u>19</u>, 425 (1979); C.M. Ko and D.O. Riska, Nucl. Phys. <u>A312</u>, 217 (1978); J. Chai and D.O. Riska, Nucl. Phys. <u>A329</u>, 429 (1979).
- 51. A.E. Woodruff, Phys. Rev. <u>117</u>, 1113 (1960), D.S. Koltun and A. Reitan, Phys. Rev. <u>141</u>, 1413 (1966).
- 52. F. Hachenberg and H.J. Pirner, Ann. Phys. <u>112</u>, 401 (1978).
- 53. G.A. Miller, Phys. Rev. C16, 2325 (1977).
- 54. E. Oset, W. Weise, and R. Brockmann, Phys. Lett. <u>82B</u>, 344 (1979).
- 55. M.L. Goldberger, Phys. Rev. 74, 1270 (1948).

- 56. Rubin H. Landau and Malcolm McMillan, Phys. Rev. C8, 2094 (1973).
- 57. Landolt-Bernstein: Nuclear Radii, New Series, Group I, vol. 2, ed. H.R. Collard, L.R.B. Elton, and R. Hofstadter (Berlin: Springer, 1967).
- 58. Atomic Data and Nuclear Data Tables 14, 479 (1974).
- 59. L. Tauscher and W. Schneider, Z. Physik 271, 409 (1974).
- 60. C.J. Batty, S.F. Biagi, E. Friedman, S.D. Hoath, J.D. Davies, G.J. Pyle, and G.T.A. Squier, Phys. Rev. Lett. 40, 931 (1978).
- 61. J. Konjin, J.K. Panman, J.H. Koch, W. Van Doesburg, G.T. Ewan, T. Johansson, G. Tibell, K. Fransson, and L. Tauscher, Nucl. Phys. A326, 401 (1979).
- 62. Ryoichi Seki, Phys. Rev. C<u>5</u>, 1196 (1972).
- 63. See, for example, <u>Handbook of Mathematical Functions</u>, ed. Milton Abramowitz and Irene A. Stegun (New York: Dover, 1965).
- 64. D.O. Riska, private communication.
- 65. Pierre Marmier and Eric Sheldon, <u>Physics of Nuclei and Particles</u>, vol. 1 (New York: Academic Press, 1969), p. 536.
- 66. R.A. Eisenstein and G.A. Miller, Comput. Phys. Commun. 8, 130 (1974).
- 67. M.D. Cooper, R.H. Jeppeson, and Mikkel B. Johnson, Phys. Rev. C<u>20</u>, 696 (1979).
- 68. R.R. Johnson, T.G. Masterson, K.L. Erdman, A.W. Thomas, and R.H. Landau, Nucl. Phys. A296, 444 (1978).
- 69. M. Blecher, K. Gotow, D. Jenkins, F. Milder, F.E. Bertrand, T.P. Cleary, E.E. Gross, C.A. Ludemann, M.A. Moinester, R.L. Burman, M. Hamm, R.P. Redwine, M. Yates-Williams, S. Dam, C.W. Darden III, R.D. Edge, D.J. Malbrough, T. Marks, and B.M. Preedom, submitted to Phys. Rev. C.
- 70. M.A. Moinester, R.L. Burman, R.P. Redwine, M.A. Yates-Williams, D.J. Malbrough, C.W. Darden, R.D. Edge, T. Marks, S.H. Dam, B.M. Preedom, F.E. Bertrand, T.P. Cleary, E.E. Gross, C.A. Ludemann, M. Blecher, K. Gotow, D. Jenkins, and F. Milder, Phys. Rev. C18, 2678 (1978).

- 71. R.R. Johnson, B. Bassalleck, K. Erdman, B. Gyles, T. Marks, T. Masterson, D.R. Gill, and C. Sabev, Phys. Lett. <u>78B</u>, 560 (1978).
- 72. R.R. Johnson, T. Marks, T.G. Masterson, B. Bassalleck, K.L. Erdman, W. Gyles, D. Gill, and C. Sabev, Can. J. Phys. <u>57</u>, 775 (1979).
- 73. J.A. Carr, private communication.
- 74. J.P. Albanèse, J. Arvieux, E. Boschitz, C.H.Q. Ingram, L. Pflug, C. Wiedner, and J. Zichy, Phys. Lett. <u>73B</u>, 119 (1978).
- 75. J. Arvieux, J.P. Albanèse, J. Bolger, E. Boschitz, C.H.Q. Ingram, L. Pflug, J. Jansén, J. Zichy, E. Rost, and A.S. Rosenthal, Nucl. Phys. A312, 368 (1978).
- 76. G.R. Stephenson, private communication.
- 77. W. Weise, private communication.
- 78. A.S. Carroll, I.-H. Chiang, C.B. Dover, T.F. Kycia, K.K. Li, P.O. Mazur, D.N. Michael, P.M. Mockett, D.C. Rahm, and R. Rubinstein, Phys. Rev. C14, 635 (1976).
- 79. R.H. Jeppesen, M.J. Jakobson, M.D. Cooper, D.C. Hagerman, M.B. Johnson, R.P. Redwine, G.R. Burleson, K.F. Johnson, I. Halpern, L.D. Knutson, R.E. Marrs, and H.O. Meyer, Proceedings of the 2nd International Topical Conference on Meson-Nuclear Physics, Houston, 1979, AIP Conf. Proc. <u>54</u>, 521; Mikkel B. Johnson, private communication.
- 80. M.D. Cooper and Mikkel B. Johnson, Nucl. Phys. A260, 352 (1976).
- 81. I. Navon, D. Ashery, G. Azuelos, H.J. Pfeiffer, H.K. Water, and F.W. Schlepütz, Proceedings of the 8th Conference on High Energy Physics and Nuclear Structure, Vancouver, 1979, p. 48.
- 82. Marvin L. Goldberger and Kenneth M. Watson, <u>Collision Theory</u> (Huntington, NY: Robert E. Krieger Publishing Co., 1975). p. 786.
- 83. Daniel S. Koltun, Proceedings of the 2nd International Topical Conference on Meson-Nuclear Physics, Houston, 1979, AIP Conf. Proc. 54, p. 87; David M. Schneider, Ph.D. Dissertation, University of Rochester, 1979.
- 84. G.F. Bertsch and S.F. Tsai, Phys. Reports 18C, 125 (1975).

- 85. T. Bowles, D.F. Geesaman, R.J. Holt, H.E. Jackson, R.M. Laszewski, J.R. Specht, L.L. Rutledge, Jr., R.E. Segel, R.P. Redwine, and M.A. Yates-Williams, Phys. Rev. Lett. 40, 97 (1978); T. Bowles, D.F. Geesamen, R.J. Holt, H.E. Jackson, R.M. Laszewski, J.R. Specht, E.J. Stephenson, R.E. Segel, R.P. Redwine, M.A. Yates-Williams, and J. Julien, Proceedings of the 2nd International Topical Conference on Meson-Nuclear Physics, Houston, 1979, AIP Conf. Proc. 54, p. 271.
- 86. G.F. Chew and F.E. Low, Phys. Rev. 101, 1570 (1956).